REPORT DOCUMENTATION PAGE	*Form Approved* *OMB No. 0704-0188*

1. REPORT DATE *(DD-MM-YYYY)* 10-02-2012	**2. REPORT TYPE** Book Chapter	**3. DATES COVERED** *(From - To)*

4. TITLE AND SUBTITLE Dynamical Evaluation of Ocean Models Using the Gulf Stream as an Example	**5a. CONTRACT NUMBER**
	5b. GRANT NUMBER
	5c. PROGRAM ELEMENT NUMBER 0601153N
6. AUTHOR(S) Harley Hurlburt, E. Joseph Metzger, James Richman, E. Chassignet, Y. Drillet, M. Hecht, O. Galloudec, Jay Shriver, Xiaobiao Xu, Luis Zamudio-Lopez	**5d. PROJECT NUMBER**
	5e. TASK NUMBER
	5f. WORK UNIT NUMBER 73-5732-10-5
7. PERFORMING ORGANIZATION NAME(S) AND ADDRESS(ES) Naval Research Laboratory Oceanography Division Stennis Space Center, MS 39529-5004	**8. PERFORMING ORGANIZATION REPORT NUMBER** NRL/BC/7304-10-0266
9. SPONSORING/MONITORING AGENCY NAME(S) AND ADDRESS(ES) Office of Naval Research One Liberty Center 875 North Randolph Street, Suite 1425 Arlington, VA 22203-1995	**10. SPONSOR/MONITOR'S ACRONYM(S)** ONR
	11. SPONSOR/MONITOR'S REPORT NUMBER(S)

12. DISTRIBUTION/AVAILABILITY STATEMENT

Approved for public release, distribution is unlimited.

20120217369

13. SUPPLEMENTARY NOTES

14. ABSTRACT

The Gulf Stream is the focus of an effort aimed at dynamical understanding and evaluation of current systems simulated by eddy-resolving Ocean General Circulation Models (OGCMs), including examples with and without data assimilation and results from four OGCMs (HYCOM, MICOM, NEMO, and POP), the first two including Lagrangian isopycnal coordinates in the vertical and the last two using fixed depths. The Gulf Stream has been challenging to simulate and understand. While different non-assimilative models have at times simulated a realistic Gulf Stream pathway, the simulations are very sensitive to small changes, such as subgrid-scale parameterizations and parameter values. Thus it is difficult to obtain consistent results and serious flaws are often simulated upstream and downstream of Gulf Stream separation from the coast at Cape Hatteras. In realistic simulations, steering by a key abyssal current and a Gulf Stream feedback mechanism constrain the latitude of the Gulf Stream near 68.5° W.

15. SUBJECT TERMS

HYCOM, Gulf Stream, eddy-resolving Ocean General Circulation Models

16. SECURITY CLASSIFICATION OF:			**17. LIMITATION OF ABSTRACT**	**18. NUMBER OF PAGES**	**19a. NAME OF RESPONSIBLE PERSON**
a. REPORT	**b. ABSTRACT**	**c. THIS PAGE**			E. Joseph Metzger
Unclassified	Unclassified	Unclassified	UU	7	**19b. TELEPHONE NUMBER** *(Include area code)* 228-688-4762

Chapter 21

Dynamical Evaluation of Ocean Models Using the Gulf Stream as an Example

Harley E. Hurlburt, E. Joseph Metzger, James G. Richman, Eric P. Chassignet, Yann Drillet, Matthew W. Hecht, Olivier Le Galloudec, Jay F. Shriver, Xiaobiao Xu and Luis Zamudio

Abstract The Gulf Stream is the focus of an effort aimed at dynamical understanding and evaluation of current systems simulated by eddy-resolving Ocean General Circulation Models (OGCMs), including examples with and without data assimilation and results from four OGCMs (HYCOM, MICOM, NEMO, and POP), the first two including Lagrangian isopycnal coordinates in the vertical and the last two using fixed depths. The Gulf Stream has been challenging to simulate and understand. While different non-assimilative models have at times simulated a realistic Gulf Stream pathway, the simulations are very sensitive to small changes, such as subgrid-scale parameterizations and parameter values. Thus it is difficult to obtain consistent results and serious flaws are often simulated upstream and downstream of Gulf Stream separation from the coast at Cape Hatteras. In realistic simulations, steering by a key abyssal current and a Gulf Stream feedback mechanism constrain the latitude of the Gulf Stream near 68.5°W. Additionally, the Gulf Stream follows a constant absolute vorticity (CAV) trajectory from Cape Hatteras to ~70°W, but without the latitudinal constraint near 68.5°W, the pathway typically develops a northern or southern bias. A shallow bias in the southward abyssal flow of the Atlantic Meridional Overturning Circulation (AMOC) creates a serious problem in many simulations because it results in abyssal currents along isobaths too shallow to feed into the key abyssal current or other abyssal currents that provide a similar pathway constraint. Pathways with a southern bias are driven by a combination of abyssal currents crossing under the Gulf Stream near the separation point and the increased opportunity for strong flow instabilities along the more southern route. The associated eddy-driven mean abyssal currents constrain the mean pathway to the east. Due to sloping topography, flow instabilities are inhibited along the more northern routes west of ~69°W, especially for pathways with a northern bias. The northern bias occurs when the abyssal current steering constraint needed for a realistic pathway is missing or too weak and the simulation succumbs to the demands of linear dynamics for an overshoot pathway. Both the wind forcing and the upper ocean branch of

---

H. E. Hurlburt (✉)
Oceanography Division, Naval Research Laboratory
Stennis Space Center, Mississippi, MS, USA
e-mail: harley.hurlburt@nrlssc.navy.mil

A. Schiller, G. B. Brassington (eds.), *Operational Oceanography in the 21st Century*,
DOI 10.1007/978-94-007-0332-2_21,

the AMOC contribute to those demands. Simulations with a northern pathway bias were all forced by a wind product particularly conducive to that result and they have a strong or typical AMOC transport with a shallow bias in the southward flow. Simulations forced by the same wind product (or other wind products) that have a weak AMOC with a shallow bias in the southward limb exhibit Gulf Stream pathways with a southern bias. Data assimilation has a very positive impact on the model dynamics by increasing the strength of a previously weak AMOC and by increasing the depth range of the deep southward branch. The increased depth range of the southward branch generates more realistic abyssal currents along the continental slope. This result in combination with vortex stretching and compression generated by the data-assimilative approximation to meanders in the Gulf Stream and related eddies in the upper ocean yield a model response that simulates the Gulf Stream-relevant abyssal current features seen in historical in situ observations, including the key abyssal current near 68.5°W, a current not observed in the assimilated data set or corresponding simulations without data assimilation. In addition, the model maintains these abyssal currents in a mean of 48 14-day forecasts, but does not maintain the strength of the Gulf Stream east of the western boundary.

21.1 Introduction

Ocean models run with atmospheric forcing but without ocean data assimilation are useful in studies of ocean model dynamics and simulation skill. Models that give realistic simulations with accurate dynamics, when run without data assimilation, are essential for eddy-resolving ocean prediction because of the multiple roles that ocean models must play in ocean nowcasting and forecasting, including dynamical interpolation during data assimilation, representing sparsely observed subsurface ocean features from the mixed layer depth to abyssal currents, converting atmospheric forcing into ocean responses, imposing topographic and geometric constraints, performing ocean forecasts, providing boundary and initial conditions to nested regional and coastal models, and providing forecast surface temperature to coupled atmosphere and sea ice models. A wide range of ocean dynamics contribute to these different roles. Here we focus on evaluating and understanding the dynamics of mid-latitude ocean currents simulated by state-of-the-art, eddy-resolving ocean general circulation models (OGCMs), using the Gulf Stream as an example.

Dynamical understanding and evaluation of current systems simulated by OGCMs has been a challenge because of the complexity of the models and the current systems, a topic discussed in recent reviews by Chassignet and Marshall (2008) and Hecht and Smith (2008) in relation to the Gulf Stream and North Atlantic. In some regions greater progress has been made. Tsujino et al. (2006) investigated the dynamics of large amplitude Kuroshio meanders south of Japan. Usui et al. (2006) used the same model to make Kuroshio forecasts from a data-assimilative initial state, typically demonstrating 40 to 60-day forecast skill south of Japan. Usui et al. (2008a, b) also used the model in dynamical studies of a 1993–2004 data-assimilative hindcast. Hurlburt et al. (2008b) examined OGCM dynamics and their relation to the underlying topography in studying mean Kuroshio meanders east of Japan and mean currents in the southern half of the Japan/East Sea. The simulations were consistent with observations and with dynamics found in purely hydrodynamic models with lower vertical resolution and vertically-compressed but otherwise realistic topography confined to the lowest layer. Consistent with observations (Gordon et al. 2002), the same Japan/East Sea OGCM simulation modeled the dynamics of intrathermocline eddy formation in that region, as discussed in Hogan and Hurlburt (2006). These are dynamics that could not be simulated by the purely hydrodynamic model. Hurlburt et al. (2008b) also investigated OGCM dynamics in simulating the Southland Current system east of South Island, New Zealand, where the topography of the Campbell Plateau and the Chatham Rise intrude well into the stratified ocean so that the design of the low vertical resolution model did not apply. In that case an alternative approach was used to investigate the dynamics. Recent observational evidence was sufficient to provide strong support for the results of the study.

In dynamical evaluation of the Gulf Stream simulations by eddy-resolving global and basin-scale OGCMs, we adopt an augmented version of the approach used by Hurlburt et al. (2008b) for OGCM simulations of the Kuroshio and Japan/East Sea. Thus we build from an explanation of Gulf Stream separation from the western boundary and its pathway to the east in Hurlburt and Hogan (2008). This explanation was derived using results from a 5-layer hydrodynamic isopycnal model with vertically-compressed but otherwise realistic topography confined to the lowest layer. It was tested versus observational evidence and theory, parts of the latter contributing directly to the explanation. In Sect. 21.2 we discuss the explanation and related 5-layer model results, theory, and observational evidence. In Sect. 21.3 we evaluate Gulf Stream dynamics in eddy-resolving OGCM simulations by the HYbrid Coordinate Ocean Model (HYCOM) (Bleck 2002), the Miami Isopycnic Coordinate Ocean Model (MICOM) (Bleck and Smith 1990), the Nucleus for European Modelling of the Ocean (NEMO) (Madec 2008), as used in the French Mercator ocean prediction effort, and the Parallel Ocean Program (POP) (Smith et al. 2000). Both simulations with a realistic Gulf Stream and those with a variety of unrealistic features are assessed and specific deficiencies are identified. In Sect. 21.4 we assess the impacts of data assimilation on variables relevant to Gulf Stream dynamics that are sparsely observed, in some cases not observed at all in real time. Are realistic model dynamics maintained in data-assimilative models? Are unrealistic dynamics improved? What are the impacts of dynamics on Gulf Stream forecast skill?

21.2 Dynamics of Gulf Stream Boundary Separation and Its Pathway to the East

21.2.1 Linear Model Simulation of the Gulf Stream

As an initial step, we examine a linear equivalent barotropic solution with the same wind forcing and upper ocean transport for the Atlantic meridional overturning circulation (AMOC) as the nonlinear solutions discussed in Sect. 21.2. The model boundary is located at the shelf break and the resolution is comparable to that used in nonlinear solutions discussed later in this chapter. The spun up mean solution has a Sverdrup (1947) interior, Munk (1950) western boundary currents and is consistent with the Godfrey (1989) island rule, except that, unlike Munk (1950), the solution is obtained by running a numerical model with horizontal friction applied everywhere.

Figure 21.1 depicts the mass transport streamfunction from a 1/16° 1.5 layer linear reduced-gravity simulation (with the lower layer infinitely deep and at rest) forced by the smoothed Hellerman and Rosenstein (1983) wind stress climatology plus the northward upper ocean flow of a 14 Sv AMOC. In comparison to the overlaid mean IR northwall pathway that lies along the northern edge of the Gulf Stream, the linear solution gives two unrealistic pathways, a broad one centered near the observed separation latitude (35.5°N) that extends eastward and a second one with nearly the same transport extending northward along the western boundary. The eastward pathway is wind-driven (~22 Sv) and the northward pathway has a 14 Sv AMOC component plus an 8 Sv wind-driven component, but both pathways contribute to a situation where ~31 Sv out of 44 Sv (~70%) separate from the western boundary north of the observed separation latitude. From Fig. 21.1 it is easy to appreciate the challenge of simulating an accurate nonlinear Gulf Stream pathway

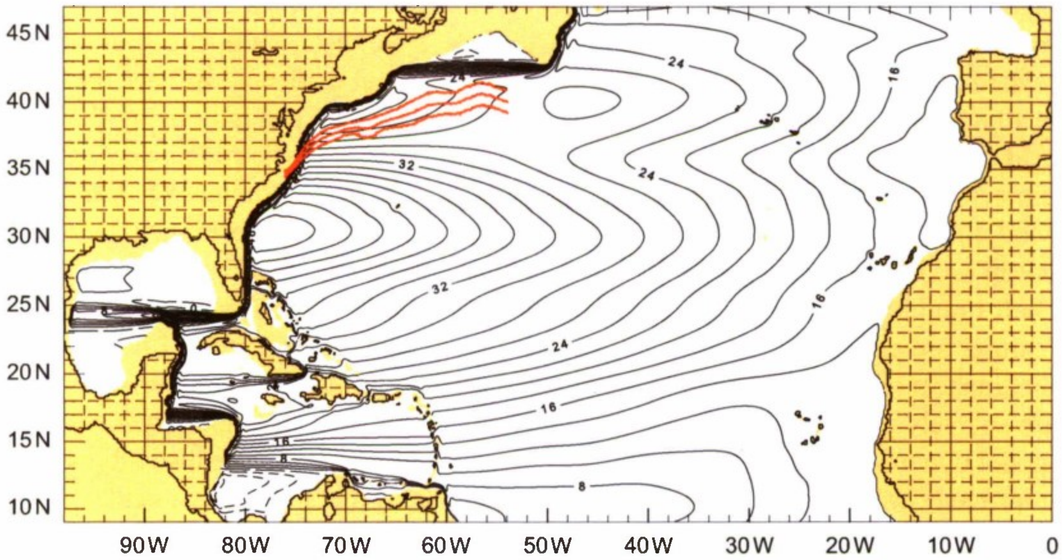

Fig. 21.1 Mean transport streamfunction (Ψ) from a 1/16°, 1.5-layer linear reduced-gravity simulation forced by the smoothed Hellerman and Rosenstein (1983) wind stress climatology and the northward upper ocean flow (14 Sv) of the Atlantic meridional overturning circulation (AMOC), forcing used for all of the simulations in Sect. 21.2. The contour interval is 2 Sv. A 15-year mean (1982–1996) Gulf Stream IR northwall pathway±1σ by Cornillon and Sirkes (unpublished) is overlaid. This pathway has 0.1° longitudinal resolution and is based on an average of 674 data points per 0.1° increment between 76° and 55°W. An earlier analysis of this frontal pathway and its variability (based on data from 1982–1989) is discussed in Lee and Cornillon (1996). The streamfunction shown here covers the 9–47°N model domain used by all the nonlinear simulations discussed in Sect. 21.2. (From Hurlburt and Hogan 2008, as adapted from Townsend et al. 2000)

in an ocean model. See Townsend et al. (2000) for linear solutions from 11 different wind stress climatologies.

21.2.2 *Impacts of the Eddy-Driven Abyssal Circulation and the Deep Western Boundary Current (DWBC) on Gulf Stream Boundary Separation and Its Pathway to the East*

It has been a popular theory, proposed by Thompson and Schmitz (1989), that the DWBC affects Gulf Stream separation from the western boundary as it passes underneath. To investigate this hypothesis Hurlburt and Hogan (2008) used a nonlinear 5-layer hydrodynamic isopycnal model covering the same domain shown in Fig. 21.1. They also used monthly climatological wind forcing and included a 14 Sv AMOC, the latter via inflow and outflow ports in the northern and southern boundaries. Figure 21.2 depicts the mean sea surface height (SSH) from six simulations.

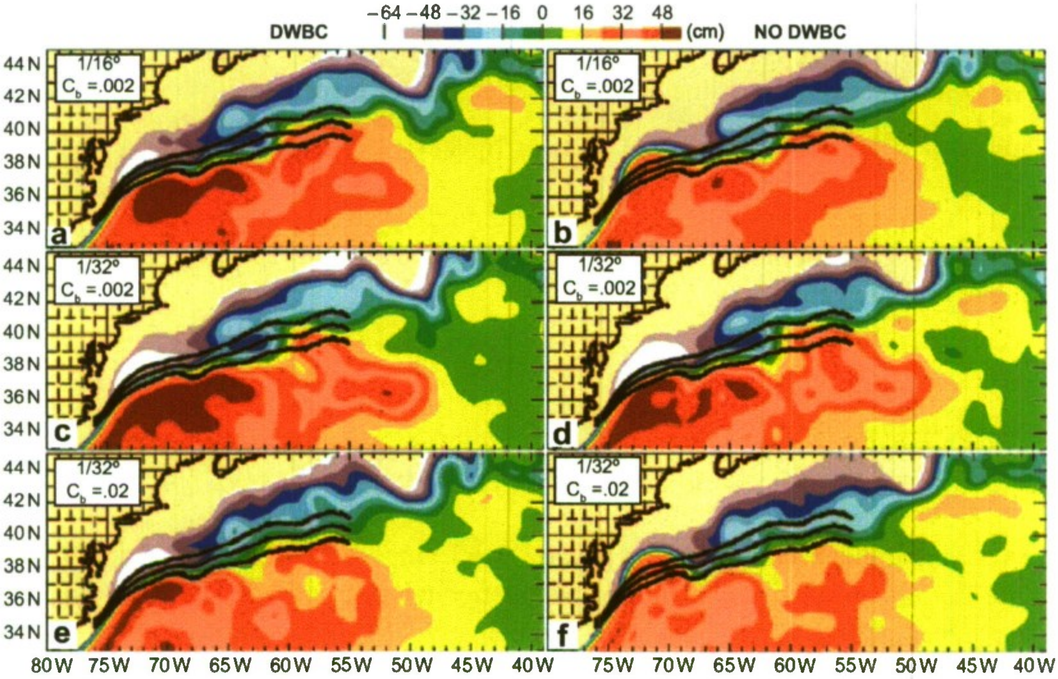

Fig. 21.2 Mean SSH from six 5-layer Atlantic Ocean simulations (9–47°N) zoomed into the Gulf Stream region between Cape Hatteras and the Grand Banks. The simulations depicted in **a**, **c** and **e** include a DWBC while those in **b**, **d** and **f** do not. **a** and **b** Depict results from 1/16° simulations. **c–f** From corresponding 1/32° simulations. **a–d** With a coefficient of quadratic bottom friction, $C_b=0.002$. **d** and **f** with a 10× increase to $C_b=0.02$. The northward upper ocean flow of the AMOC is included in all six simulations. The Laplacian coefficient of isopycnal eddy viscosity is A=20 (10) m^2/s for the 1/16° (1/32°) simulations. The SSH contour interval is 8 cm. The mean Gulf Stream IR northwall pathway $\pm 1\sigma$ by Cornillon and Sirkes is overlaid on each panel. For more information about the simulations used in Sect. 21.2, see Hurlburt and Hogan (2008). (From Hurlburt and Hogan 2008)

The northward upper ocean component of the AMOC resides in the top 4 layers and is always included, while the DWBC residing in the abyssal layer is included in the simulations in the left column of Fig. 21.2 and turned off in the simulations in the right column. Since the model is purely hydrodynamic, the DWBC can be turned off without altering the watermass characteristics. In the three rows of Fig. 21.2 the model resolution is varied in tandem with the horizontal friction and in the bottom row the bottom friction is increased 10-fold to damp the eddy-driven abyssal circulation. East of 68°W all of the simulations give similar, generally-realistic Gulf Stream pathways, except near 50°W, where the simulations with a DWBC exhibit two mean pathways (inner and outer meanders) at the location of the Gulf Stream transition to the North Atlantic Current as it rounds the southern tip of the Grand Banks, a phenomenon discussed dynamically in Hurlburt and Hogan (2008). All three of the simulations with a DWBC and one of the simulations without it exhibit a realistic mean Gulf Stream pathway west of 68°W, but the other two simulations without a DWBC exhibit pathways that overshoot the observed separation latitude in accord with the constraint of linear theory on the flow. These results indicate an abyssal current impact on the pathway west of 68°W.

To investigate the impacts of abyssal currents on the Gulf Stream pathway, we use a two-layer theory for abyssal current steering of upper ocean current pathways (Hurlburt and Thompson 1980; Hurlburt et al. 1996, 2008b). In a two-layer model with no diapycnal mixing, the continuity equation for layer 1 is

$$\mathrm{h}_{1t} + \mathbf{v}_1 \cdot \nabla \mathrm{h}_1 + \mathrm{h}_1 \nabla \cdot \mathbf{v}_1 = 0, \tag{21.1}$$

where h_1 is upper layer thickness, $_t$ is the time derivative and $\mathbf{v}_i$ is the velocity in layer i. The geostrophic component of the advective term in (21.1) can be related to the geostrophic velocity ($\mathbf{v}_{ig}$) in layer 2 by

$$\mathbf{v}_{1g} \cdot \nabla \mathrm{h}_1 = \mathbf{v}_{2g} \cdot \nabla \mathrm{h}_1, \tag{21.2}$$

because from geostrophy,

$$\mathbf{k} \times \mathrm{f}(\mathbf{v}_{1g} - \mathbf{v}_{2g}) = -\mathrm{g}'\nabla \mathrm{h}_1, \tag{21.3}$$

$\mathbf{v}_{1g}-\mathbf{v}_{2g}$ is parallel to contours of h_1. In (21.3) **k** is a unit vector in the vertical, $\mathrm{f}=2\omega\sin\theta$ is the Coriolis parameter, ω is the Earth's rotation rate, θ is latitude, $\mathrm{g}'=\mathrm{g}(\rho_2-\rho_1)/\rho_2$ is the reduced gravity due to buoyancy, g is the gravitational acceleration of the Earth, and ρ_i is the water density in layer *i*. Since geostrophy is typically a very good approximation outside the equatorial wave guide and normally near-surface currents are much stronger than abyssal currents, then usually $|\mathbf{v}_1| \gg |\mathbf{v}_2|$, making $\nabla \mathrm{h}_1$ a good measure of $\mathbf{v}_1$ under these conditions. From the preceding we see that abyssal currents can advect upper layer thickness gradients and therefore the *pathways* of upper ocean currents. Abyssal current advection of upper ocean current pathways is strengthened when strong abyssal currents intersect upper ocean currents at nearly right angles, but often the end result of this advection is near barotropy because the advection is reduced as $\mathbf{v}_1$ and $\mathbf{v}_2$ become more nearly parallel (or antiparallel).

This theory has proven useful in understanding the dynamics of ocean models with higher vertical resolution, when all of the following conditions are satisfied:

(a) the flow is nearly geostrophically balanced, (b) the barotropic and first baroclinic modes are dominant, and (c) the topography does not intrude significantly into the stratified ocean. Additionally, the interpretation in terms of near-surface currents applies when $|\mathbf{v}_{\text{near sfc}}| \gg |\mathbf{v}_{\text{abyssal}}|$. Note the theory does not apply at low latitudes because of (a) and (b), but should be useful in large parts of the stratified ocean, even where current systems are relatively weak, as seen in the well-stratified southern half of the Japan/East Sea (Hurlburt et al. 2008b). While abyssal currents driven by any means can steer upper ocean current pathways, baroclinic or mixed barotropic-baroclinic instability is an important source of abyssal currents because baroclinic instability is very effective in transferring energy from the upper to abyssal ocean. These eddy-driven abyssal currents are constrained to follow the geostrophic contours of the topography and in turn can steer the pathways of upper ocean currents, including their mean pathways. This upper ocean—topographic coupling via flow instabilities requires that the physics of baroclinic instability be very well resolved in order to obtain sufficient downward transfer of energy. As a result, this type of coupling is a key criterion in distinguishing between eddy-resolving and eddy-permitting ocean simulations, in regions where it occurs (Hurlburt et al. 2008b). Results from this model and ocean models discussed in Sect. 21.3 indicate that the upper ocean—topographic coupling requires the first baroclinic Rossby radius of deformation be resolved by at least 6 grid intervals and even higher resolution is required for realistic eastward penetration of inertial jets. This coupling also highlights the need for eddy-resolving ocean models in ocean prediction systems and in climate prediction models, as discussed in Hurlburt et al. (2008a, 2009).

Based on the preceding discussion, we look in Fig. 21.3 for abyssal currents west of ~68°W that may advect the simulated Gulf Stream pathways in Fig. 21.2. We start with the simulation shown in Figs. 21.2c and 21.3c because it has 1/32° resolution, the standard bottom friction, and a DWBC. In that simulation abyssal currents pass under the Gulf Stream near 68.5°W, 72°W, and the western boundary, all generally southward. The abyssal currents near 68.5°W and 72°W cross under at large angles and could clearly advect the Gulf Stream pathway, but the abyssal current adjacent to the western boundary is nearly antiparallel as it crosses under the Gulf Stream, a point noted by Pickart (1994) based on observations, and thus has a weak steering effect on the Gulf Stream pathway. The corresponding simulation without a DWBC (Figs. 21.2d and 21.3d) has nearly the same Gulf Stream pathway with an even stronger abyssal current crossing under it near 68.5°W. The two other simulations without a DWBC have only a weak mean abyssal current crossing under it at this longitude (<3 cm/s), while all of the simulations with realistic Gulf Stream separation have a more robust abyssal current passing under the Gulf Stream near 68.5°W (>4 cm/s). None of the simulations without a DWBC have an abyssal current crossing under near 72°W, while all of the simulations with a DWBC have one fed by two branches from the north side. The 1/32° simulations with a DWBC and standard (Figs. 21.2c and 21.3c) or high bottom friction (Figs. 21.2e and 21.3e) have nearly the same Gulf Stream pathway between the western boundary and 68°W, but in the simulation with high bottom friction the abyssal currents crossing under the Gulf Stream near 72°W are extremely weak. Thus, the abyssal current crossing under the Gulf Stream near 68.5°W is clearly the one that is essential for the model's simula-

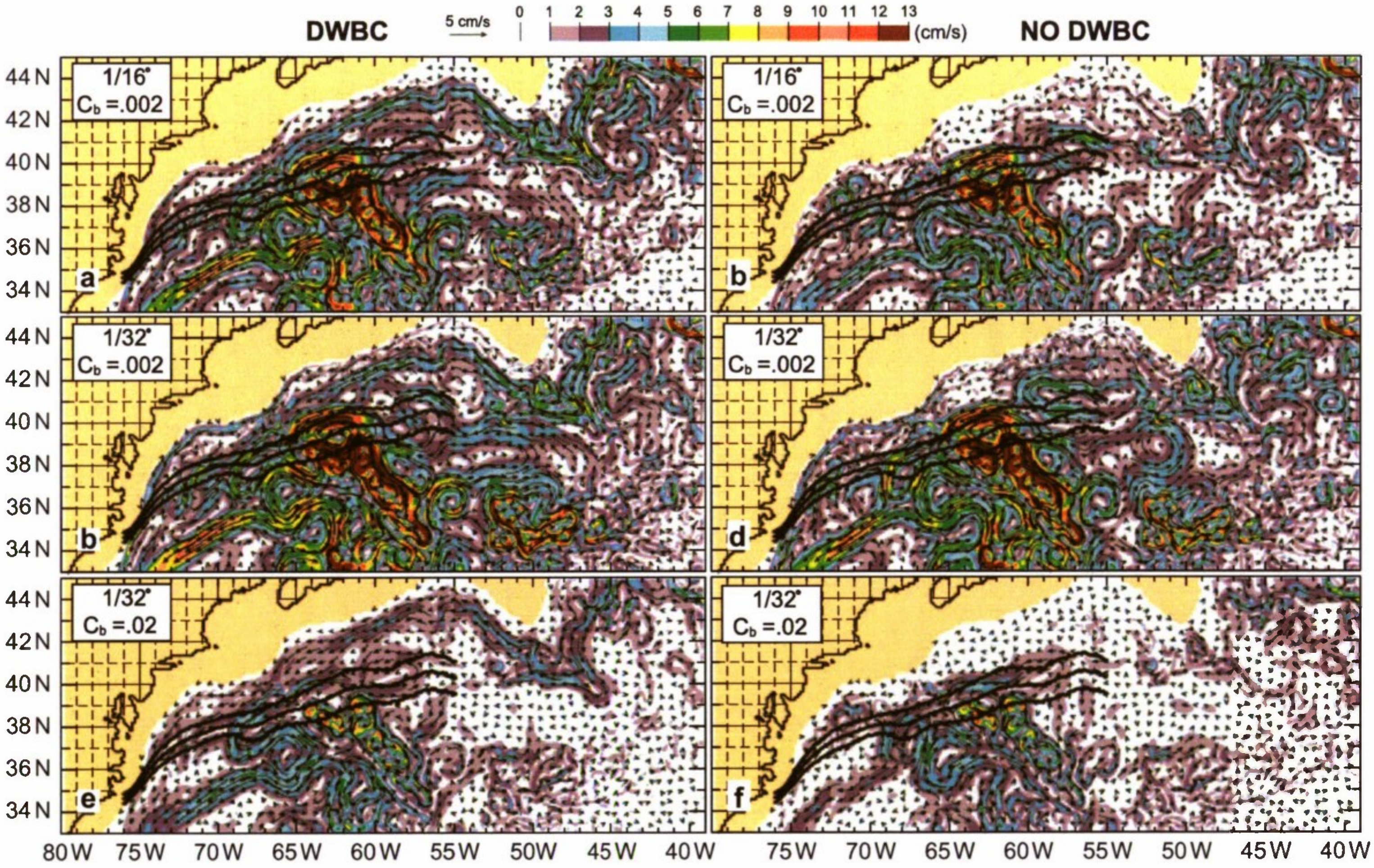

Fig. 21.3 Same simulations as Fig. 21.2 but depicting mean abyssal currents (arrows) overlaid on isotachs (in cm/s). The DWBC is most easily seen paralleling the northern model boundary north of 41°N between 65 and 51°W in panels (**a**, **c**, **e**). In the simulations with no DWBC (panels **b**, **d**, **f**) that current is not present. (From Hurlburt and Hogan 2008)

tion of a realistic Gulf Stream pathway between the western boundary and 68°W. Further, the DWBC is not necessary for simulation of a realistic Gulf Stream pathway, but it augments the key abyssal current sufficiently for that to occur in the two simulations with the weaker eddy-driven abyssal circulations.

The 1/32° simulation with standard bottom friction and a DWBC (Fig. 21.3c) is used in a zoom of the mean abyssal currents with the addition of topographic contours (Fig. 21.4a). The plotted contours are for the vertically-uncompressed (real) topography to facilitate comparisons between model and observed abyssal currents in relation to topographic features. Figure 21.4b depicts mean abyssal currents and uncompressed topography from a corresponding 1/8° eddy-permitting simulation over a larger region with the zoom region in Fig. 21.4a marked with a box. It should be noted that eddy-resolving and eddy-permitting OGCMs with higher vertical resolution and thermodynamics are typically characterized by their equatorial resolution, whereas the simulations in Sect. 21.2 are characterized by mid-latitude resolution. Thus, the corresponding equatorial resolution of the simulations in Fig. 21.4a, b would be 1/24 and 1/6°, respectively.

Unlike the 1/32° simulation (Fig. 21.4a), the abyssal circulation in the 1/8° model is dominated by the DWBC, which crosses under the observed location of the Gulf Stream near 72°W, and the eddy-driven abyssal circulation is extremely weak (Fig. 21.4b). In particular, the 1/8° model does not simulate the key abyssal current near 68.5°W. The DWBC augments this current in two of the simulations (Fig. 21.3a, e) because the DWBC and the eddy-driven abyssal circulation interact and become intertwined in the eddy-resolving simulations. The surface circulation in the 1/8° model is basically a wiggly version of the linear solution (Hurlburt and Hogan 2000, their Fig. 4a), who also present numerous model-data comparisons for the 1/16° simulation in Figs. 21.2a and 21.3a and the 1/32° simulation in Figs. 21.2c and 21.3c.

In addition to the abyssal current adjacent to the western boundary, abyssal currents are seen crossing under the Gulf Stream via three different pathways centered over different isobaths between the western boundary and 68°W. North of the Gulf Stream these pathways are centered over the 4,200, 3,700 and 3,100 m isobaths, the first crossing under near 68.5°W, the other two crossing under in a confluence near 72°W. All three abyssal currents cross isobaths to deeper depths while passing under the Gulf Stream. They do this to conserve potential vorticity in relation to the downward north to south slope of the base of the thermocline in accord with the theory of Hogg and Stommel (1985). The two currents over deeper isobaths retroflect toward the east and then take a variety of simple to complex pathways into the ocean interior (complex even in the mean, e.g. Fig. 21.3c). Ultimately all of these pathways emerge from the interior as a single strong abyssal current along a gentle escarpment. That current exits Fig. 21.4a near 72°W and rejoins the DWBC along the continental slope near 33°N. In contrast, the branch centered over the 3,100 m isobath north of the stream continues along the continental slope south of the stream (centered above the 3,700 m isobath). Each cross-under pathway is influenced by specific features of the topography and each also flows along one side of an associated eddy-driven abyssal gyre centered directly beneath the Gulf Stream. These gyres are located in regions where the slopes of the topography and the base of the thermocline are

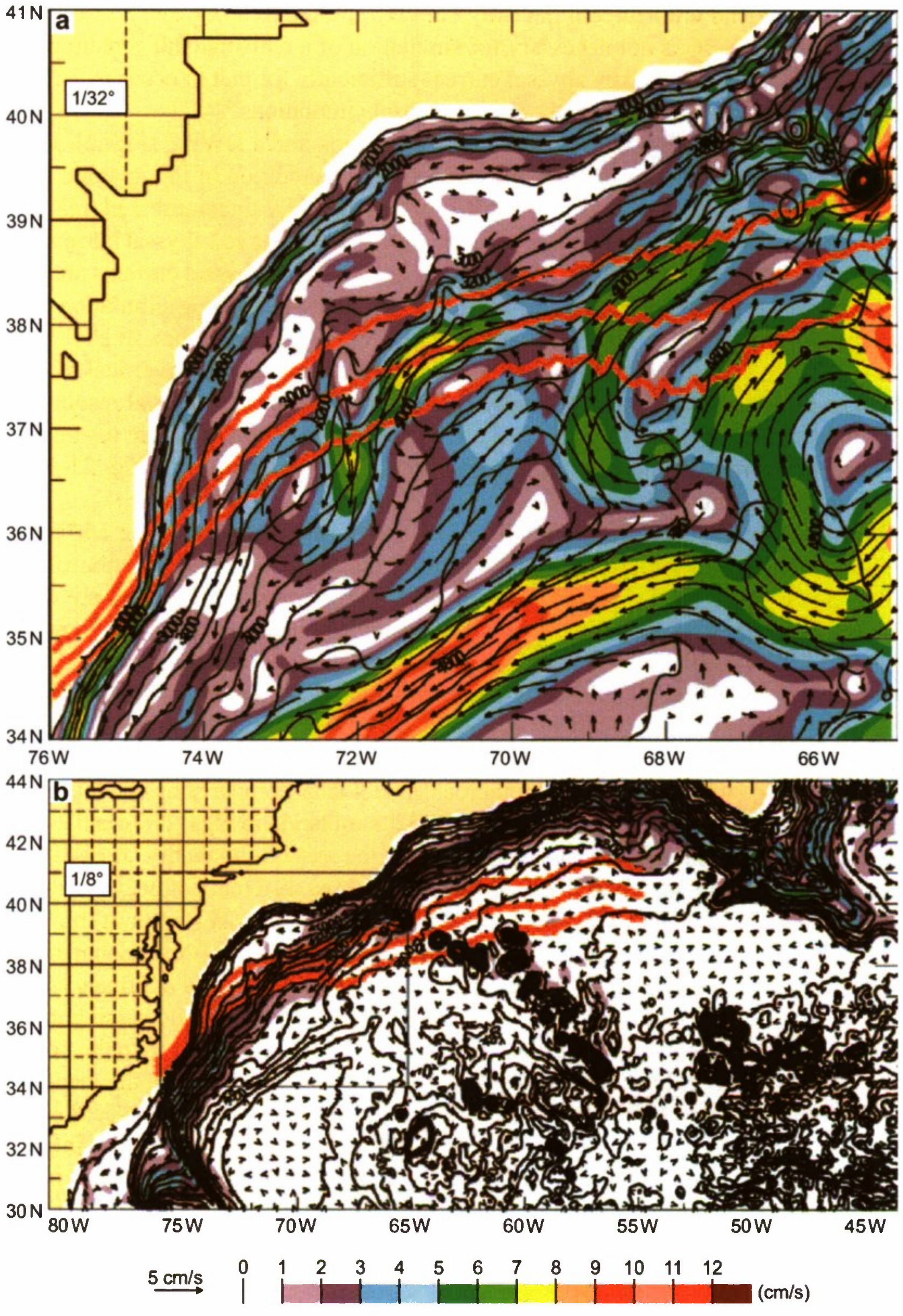

Fig. 21.4 **a** Zoom of Fig. 21.3c with (full amplitude, uncompressed) depth contours (in m) overlaid to facilitate geographical co-location in the model-data comparisons. **b** Same as **a** but covering a larger region from a corresponding 1/8° simulation overlaid with a box outlining the region covered by **a**. In the 1/8° simulation $A = 100\ m^2/s$ and $C_b = 0.002$. (From Hurlburt and Hogan 2008)

matched closely enough to create regions of quite uniform potential vorticity for abyssal currents, as shown in Hurlburt and Hogan (2008). The shallowest and westernmost gyre is anticyclonic, while the two associated with eastward retroflections into the interior are cyclonic, all three in accord with the sign of the relative vorticity generated due to topographic constraints on the pathways of the associated abyssal currents as they cross under the Gulf Stream (shown in Hurlburt and Hogan 2008).

21.2.3 Observational Evidence of Abyssal Currents in the Gulf Stream Region

Figure 21.5 (bottom) (from Johns et al. 1995) presents observational evidence for the key abyssal current crossing under the Gulf Stream near 68.5°W, including current speeds similar to the model, currents crossing isobaths to deeper depths beneath the Gulf Stream, and a closed cyclonic circulation. Additionally, the currents above the shallowest isobaths within the observational array flow along isobaths that would feed into the retroflecting abyssal current that crosses under the Gulf Stream near 72°W. Figure 21.6 (from Pickart and Watts 1990) provides a composite of historical abyssal current measurements 100–300 m above the bottom. It provides striking evidence of the complete cyclonic abyssal gyre centered near 37°N, 71°W with current speeds similar to the model. Another salient observation is the ~12.5 cm/s west-southwestward current near 34.5°N, 71.1°W that corroborates the strong abyssal current along the gentle escarpment in Fig. 21.4a (10.5 cm/s at the same location in the model).

Like the model (Fig. 21.4a), the observation-based abyssal current schematic of Schmitz and McCartney (1993, their Fig. 12a) depicts a retroflecting abyssal current pathway that later rejoins the DWBC, in addition to a pathway that continues along the continental slope. These two pathways are also consistent with Range and Fixing of Sound (RAFOS) float trajectories at 3,500 m depth discussed in Bower and Hunt (2000). RAFOS floats that crossed under the Gulf Stream west of ~71°W continued generally southward along a deeper isobath of the continental slope, while floats crossing under east of ~71°W retroflected into the interior, most of them taking complex eddying trajectories, but of the six retroflecting trajectories shown in Bower and Hunt (2000, their Fig. 7), the one that crossed under at the location of the key abyssal current (near 69°W) (their Fig. 7j) took an eddying trajectory en route to a small amplitude double retroflection, first to the east (at 36.7°N, 70.1°W) and then to the west (at 36.0°N, 68.4°W) before rapidly following a nearly straight-line trajectory along the gentle escarpment, an overall trajectory in good agreement with the model mean in Fig. 21.4a and one that provides additional evidence for the strong eddy-driven abyssal current along the gentle escarpment (seen in the southern part of Fig. 21.4a). This abyssal current (also seen in Fig. 21.6) is completely absent in the 1/8° eddy-permitting simulation (Fig. 21.4b), as are the observed cyclonic abyssal gyre centered near 37°N, 71°W (Fig. 21.6) and the abyssal current observed crossing under the Gulf Stream between 68° and 69°W (Fig. 21.5).

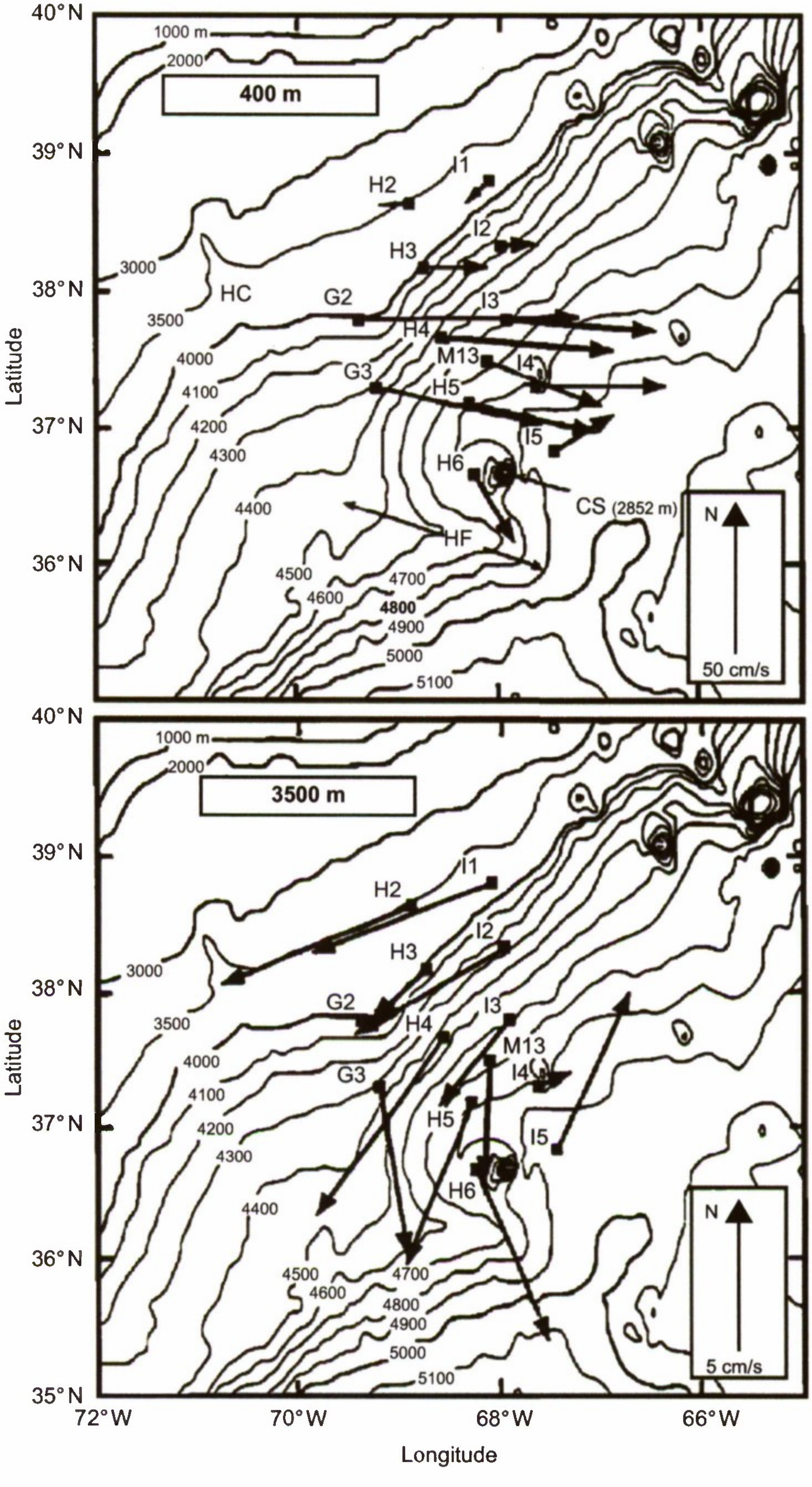

Fig. 21.5 Mean current meter velocities at 400 m (*top*) and 3,500 m (*bottom*) over the entire deployment, June 1988–August 1990. All of the vectors represent 26-month means except at sites H5 and M13, which are approximately 1-year means. (From Johns et al. 1995)

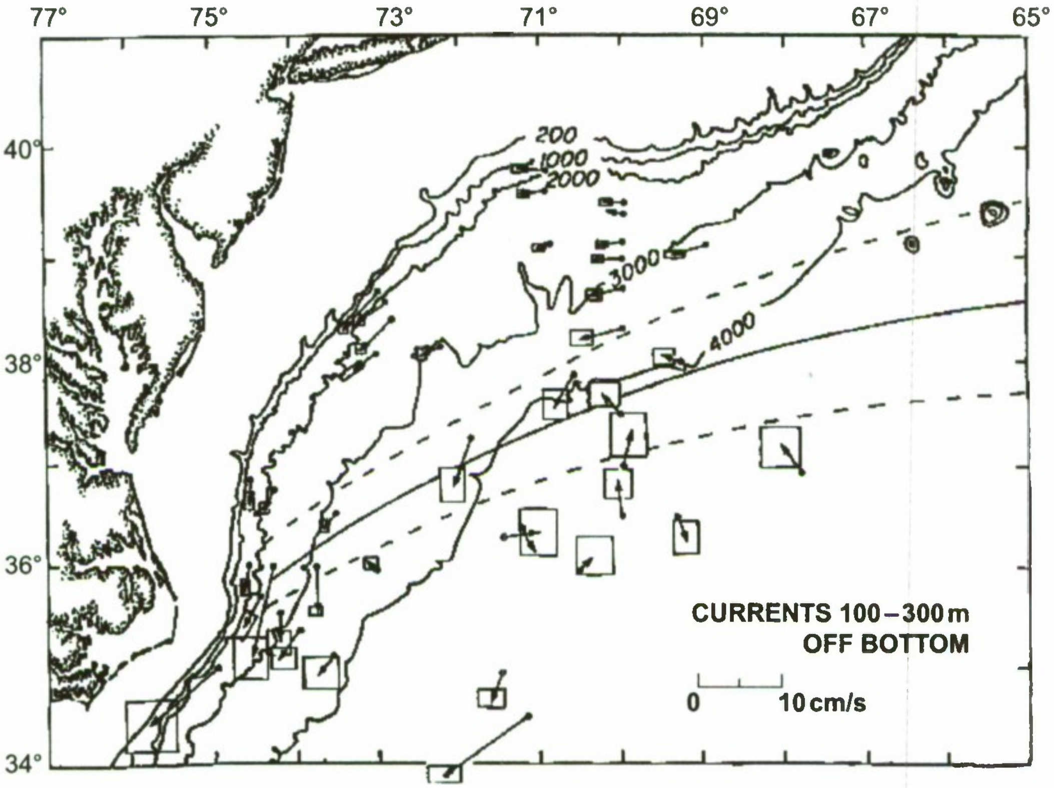

Fig. 21.6 Mean current meter velocities 100–300 m above the bottom from historical measurements collected in the middle Atlantic Bight. The record lengths of the measurements vary from 4 months to 2 years, and the box associated with each vector represents the uncertainty of the mean, typically 1–2 cm/s. (From Pickart and Watts 1990)

21.2.4 Gulf Stream Separation and Pathway Dynamics, Part I: Abyssal Current Impact

An eddy-driven abyssal current, the local topographic configuration, and a Gulf Stream feedback mechanism constrain the latitude of the Gulf Stream near 68.5°W. To help illustrate the steps explaining this statement, Fig. 21.7 depicts the mean depth of the base of the model thermocline overlaid with the same mean abyssal currents and topographic contours as Fig. 21.4a. The results are from the same 1/32° simulation with a DWBC shown in Figs. 21.2c, 21.3c, and 21.4a.

The steps in the explanation are (1) an eddy-driven abyssal current, possibly augmented by the DWBC, approaches from the northeast and advects the Gulf Stream pathway southward, i.e. prevents the overshoot pathway seen in Figs. 21.2b, f. (2) To conserve potential vorticity, the abyssal current crosses to deeper depths while passing under the Gulf Stream (Hogg and Stommel 1985), a feedback mechanism that allows the Gulf Stream to help determine its own latitude. (3) Due to the topographic configuration, the passage to deeper depths requires curvature toward the east and generation of positive relative vorticity. (4) Once the abyssal current becomes parallel to the Gulf Stream, further southward advection of the Gulf Stream

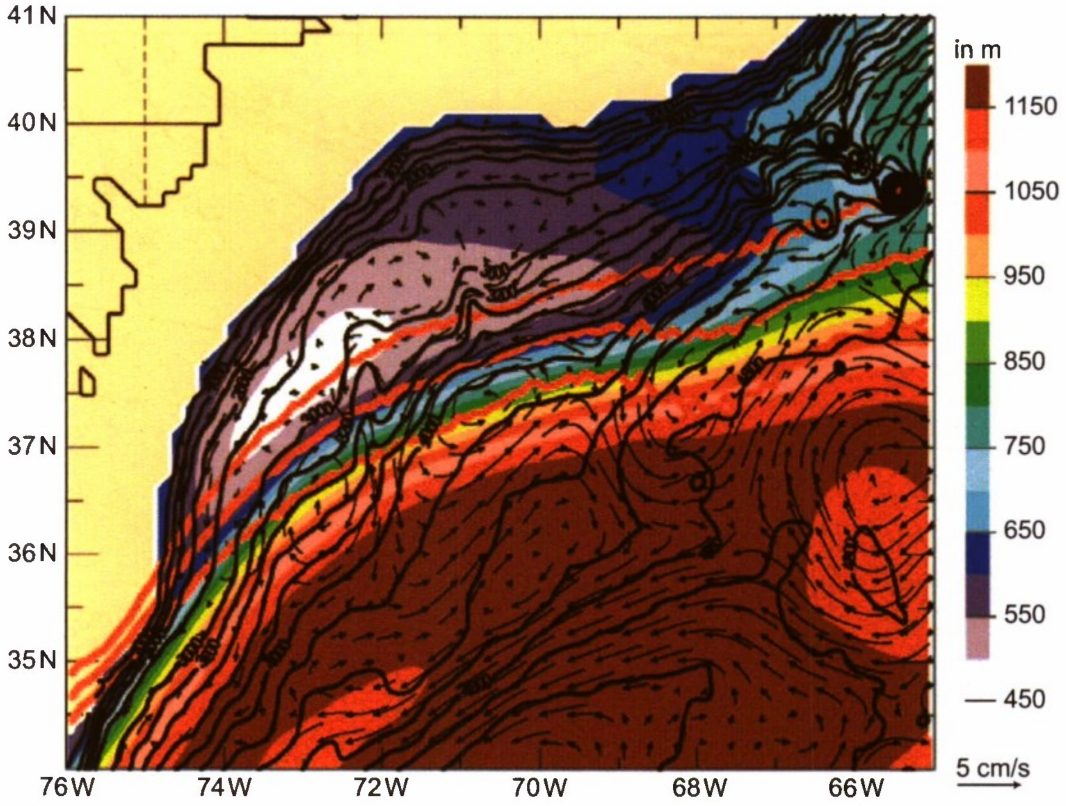

Fig. 21.7 Same as Fig. 21.4a but with isotachs (*in color*) replaced by the mean depth at the base of the model thermocline (*in m*) from the same simulation (*in color*), i.e. the mean depth of the interface between layer 4 and layer 5 (the abyssal layer) from the 1/32° simulation depicted in Figs. 21.2c and 21.3c. (From Hurlburt and Hogan 2008)

pathway is halted. (5) The local latitude of the Gulf Stream is determined by the northernmost latitude where the abyssal current can become parallel to the Gulf Stream. (6) Due to constraints of the local topographic configuration on this process, the resulting local Gulf Stream latitude is not very sensitive to the strength of the abyssal current, once it is sufficient to perform the advective role. However, the results of these dynamics would be sensitive to the location of abyssal currents in relation to the isobaths, the accuracy of the model in representing key topographic features, and the depth change in the base of the thermocline across the Gulf Stream.

Essentially the same explanation can be applied to the effects of the abyssal current crossing under the Gulf Stream near 72°W (when present and sufficiently strong) and to abyssal currents that develop either cyclonic or anticyclonic curvature and become either parallel or antiparallel to the Gulf Stream while crossing underneath. However, the response to the abyssal current near 72°W is minimal as evidenced in Figs. 21.2 and 21.3 and an impact is visible only in the 1/32° simulation with a DWBC and standard bottom friction ($C_b=0.002$) (Fig. 21.2c). In Fig. 21.2c there is a straightening of the Gulf Stream pathway over ~73–70°W not seen in the other figure panels. This phenomenon is also evident in the overlaid mean Gulf Stream IR northwall frontal pathway and in the Gulf Stream pathway as depicted by the 12°C isotherm at 400 m depth, the latter shown in Watts et al. (1995). An explanation for the slight impact of this abyssal current on this Gulf Stream simulation is discussed in the next subsection.

Additionally, it should be noted that the scale of the eddy-driven mean abyssal gyres beneath the Gulf Stream is similar to the width of the stream (Fig. 21.7) and related to regions of nearly uniform potential vorticity beneath the stream (Hurlburt and Hogan 2008), where slopes of topography and the base of the thermocline are quite well matched. These gyres are not related to mean meanders in the Gulf Stream. In contrast, the Kuroshio exhibits two mean northward meanders just east of where the Kuroshio separates from the coast of Japan, meanders that are dynamically related to eddy-driven mean abyssal gyres, as discussed in Hurlburt et al. (1996, 2008b).

21.2.5 *Gulf Stream Boundary Separation as an Inertial Jet Following a Constant Absolute Vorticity (CAV) Trajectory*

Constraint of the Gulf Stream latitude near 68.5°W is not a sufficient explanation of the Gulf Stream pathway between the western boundary and 69°W. Further, the abyssal current crossing under the Gulf Stream near 72°W demonstrated little effect on the pathway. Thus, there must be another essential contribution to Gulf Stream pathway dynamics over that longitude range.

Using along-track data from four satellite altimeters, Fig. 21.8 depicts only a narrow band of high SSH variability along the Gulf Stream west of 69°W, indicating a relatively stable pathway segment in that region. Thus, we test the relevance of a particular type of theoretical inertial jet pathway, namely a CAV trajectory (Rossby 1940; Haltiner and Martin 1957; Reid 1972; Hurlburt and Thompson 1980, 1982). In a nonlinear 1.5 layer reduced-gravity model, a CAV trajectory requires a frictionless steady free jet with the streamline at the core of the current following contours of constant SSH and layer thickness. The latter requires geostrophic balance so that conservation of potential vorticity becomes conservation of absolute vorticity along a streamline at the core of the current. Accordingly, the simulations in Fig. 21.2 were tested to see if (a) the mean path of the current core in the top layer of the model (black line in Fig. 21.9) overlaid an SSH contour (yellow-green line in Fig. 21.9) and (b) there was a narrow band of high SSH variability along the current core between the western boundary and 69°W (plotted in color in Fig. 21.9).

Following Reid (1972) and Hurlburt and Thompson (1980, 1982), the CAV trajectories were calculated from

$$\cos\alpha = \cos\alpha_o + 1/2\mathrm{y}^2/\mathrm{r}^2 - \mathrm{y}/\gamma_o, \qquad (21.4)$$

which is an integrated form of the differential equation that assumes the velocity at the core of the current, υ_c, is a constant and where $\mathrm{r} = (\upsilon_c/\beta)^{1/2}$, β is the variation of

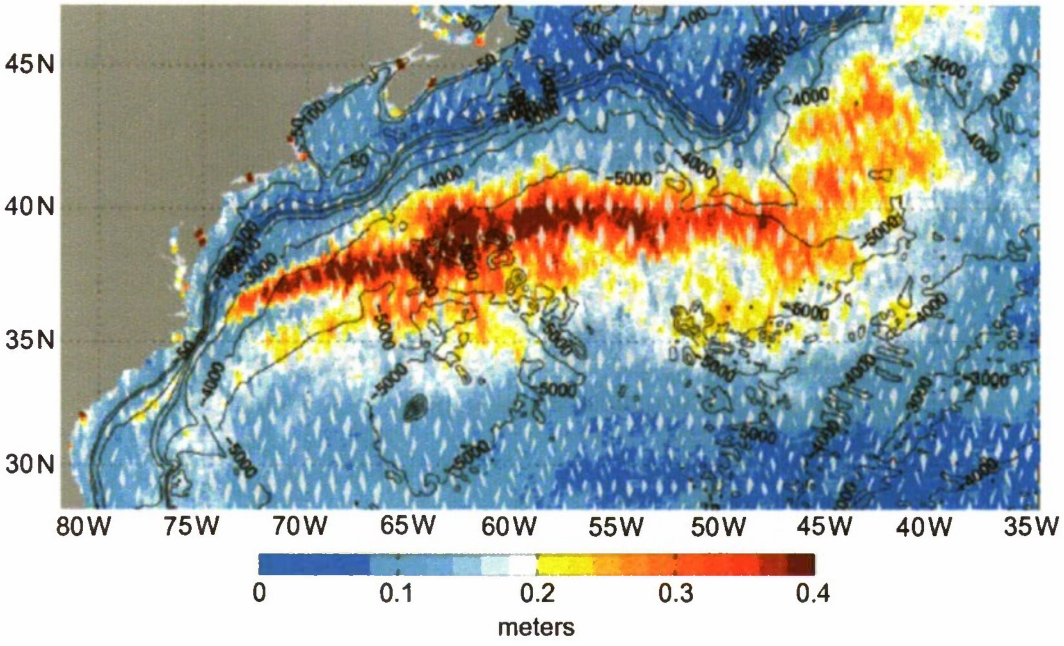

Fig. 21.8 Along-track SSH variability from quasi-contemporaneous satellite altimeter data in 4 different orbits overlaid on topographic contours (depth in m), Jason-1 over the period 15 Jan. 2002–18 Oct. 2007, GFO over 15 July 1999–12 Dec. 2007, Envisat over 24 Sept. 2002–29 Oct. 2007, and Topex in an interleaved orbit over 16 Sept. 2002–8 Oct. 2005. The tracks are overlaid in the following order from *top* to *bottom*: (1) Envisat, (2) GFO, (3) Jason-1, and (4) Topex interleaved. (Provided by Gregg Jacobs, NRL). (From Hurlburt and Hogan 2008)

the Coriolis parameter with latitude, α is the angle of the current with respect to the positive x-axis on a β-plane, y is the distance of the trajectory from the x-axis, γ is the trajectory radius of curvature, and the subscript $_0$ indicates values at the origin of the trajectory calculation (here at an inflection point where $\gamma_0 \rightarrow \infty$). The amplitude (b) (here the northernmost point) of the trajectory in relation to the inflection points can be calculated from

$$b = 2\mathrm{r} \sin 1/2\alpha_0. \tag{21.5}$$

In order for the Gulf Stream to separate from the western boundary as a free jet following a CAV trajectory, the CAV trajectory must be initialized with a trajectory inflection ($\gamma_0 \rightarrow \infty$) located at the separation point. Since the angle of separation (α_0) is north of due east, the CAV trajectory must subsequently develop curvature that is concave toward the south. If the simulation exhibits curvature to the north after separation, then it does not separate from the western boundary as a free jet, even through it may have one or more segments downstream that follow a CAV trajectory.

The calculated CAV trajectories are overlaid as red curves on Fig. 21.9. Details of the CAV trajectory calculations can be found in Table 2 of Hurlburt and Hogan (2008). The speed at the core of the current (υ_c) near separation from the western boundary is 1.6–1.7 m/s in the 1/16° simulations and 1.9–2.0 m/s in the 1/32°

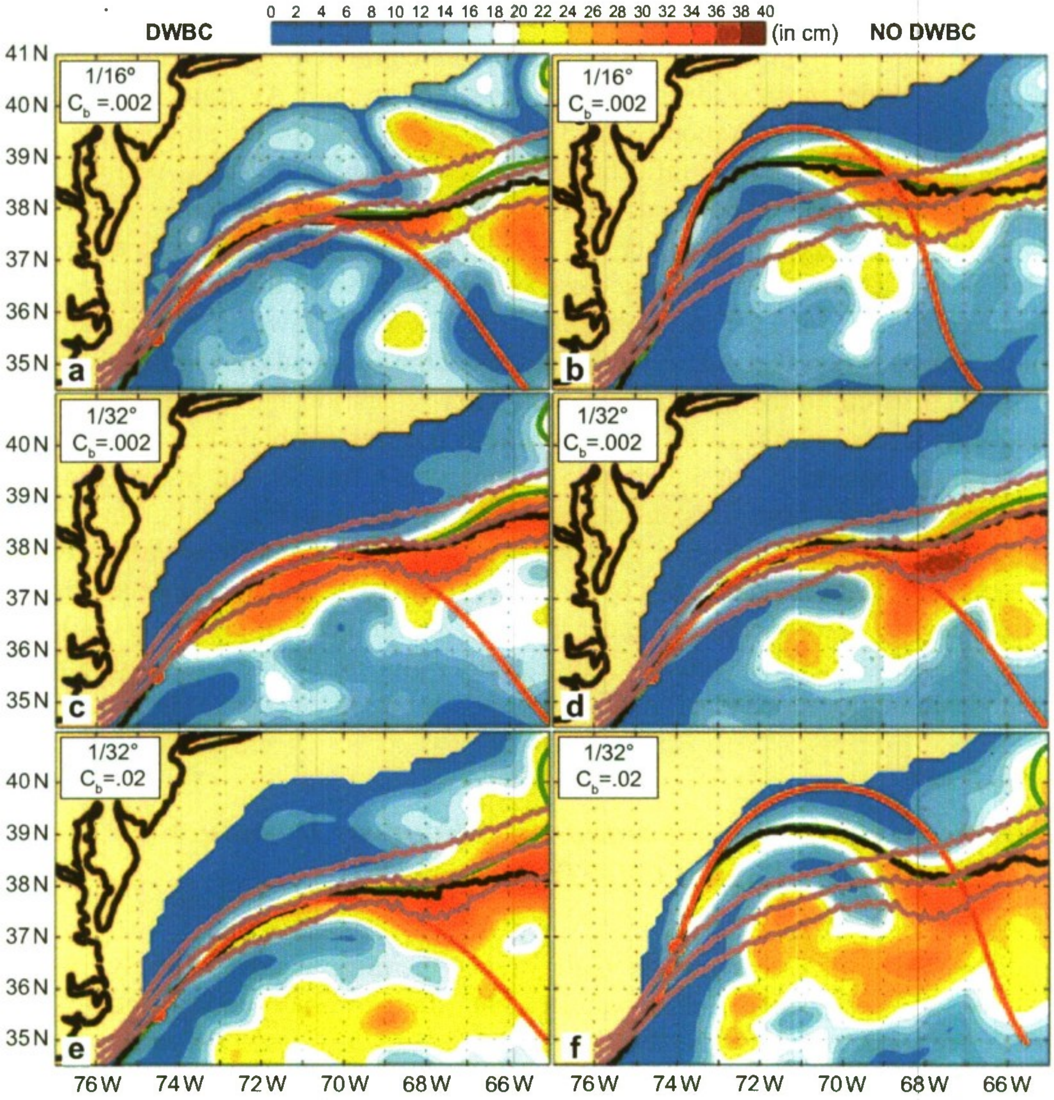

Fig. 21.9 CAV trajectory analysis for Gulf Stream pathways simulated by the six simulations illustrated in Fig. 21.2. The pathway of the maximum velocity at the core of the current (*black line*), the closest SSH contour (*yellow-green line*), the corresponding CAV trajectory (*red line with a dot* at the inflection point), the observed IR northwall frontal pathway ± std. dev. (*violet lines*), and the simulated SSH variability are overlaid on each panel. Due to the hierarchy of the overlaid lines (*light violet, red, black, yellow-green from top to bottom*), lines on the bottom tend to be obscured where close agreement occurs. That is particularly the case for the yellow-green SSH contour west of ~68°W, where the core of the current overlaying a single SSH contour is a prerequisite for the existence of a CAV trajectory. The SSH contour closest to the pathway of the velocity maximum is skewed toward the north side of the model Gulf Stream as depicted in SSH and is **a** –24 cm. **b** –16 cm. **c** –28 cm, and **d–f** –24 cm. See the corresponding panels in Fig. 21.2. Near the western boundary the Gulf Stream axis from Topex/Poseidon altimetry (Lee 1997) diverges from the IR frontal pathway in accord with the model simulations of panels a, c, d, and e (see Hurlburt and Hogan 2000, their Fig. 7). (From Hurlburt and Hogan 2008)

simulations, in line with observations of 1.6–2.1 m/s reported in Halkin and Rossby (1985), Joyce et al. (1986), Johns et al. (1995), Schmitz (1996), and Rossby et al. (2005). A model mean υ_c over 75–70°W was used in the CAV trajectory calculations. The angle of separation is 53±3° north of due east for the simulations with a realistic pathway and the inflection points used to initialize the CAV trajectory calculations are marked by red dots on the trajectories.

Between the western boundary and ~70°W, the four simulations with a realistic Gulf Stream pathway demonstrate close agreement between the model pathway, as represented by υ_c, and the corresponding CAV trajectory. However, the two simulations with pathways that overshoot the latitude of the observed Gulf Stream pathway exhibit curvature to the north immediately after separation and an inflection point (red dot) located northeast of separation from the western boundary. That means they do not separate from the western boundary as a free jet, but instead indicate a strong influence from the constraints of linear dynamics (Fig. 21.1). Thus, CAV trajectory dynamics alone are not sufficient to explain the Gulf Stream pathway between the western boundary and 69°W. However, they do explain the small impact of the abyssal current crossing under the Gulf Stream near 72°W (Fig. 21.4a), because the abyssal current and the CAV trajectory give nearly the same Gulf Stream latitude at that location (Fig. 21.9c).

21.2.6 Gulf Stream Separation and Pathway Dynamics, Part II: Role of CAV Trajectories

In the simulations with a realistic Gulf Stream, the mean pathway closely follows a CAV trajectory between its separation from the western boundary and ~70°W. The CAV trajectory depends on (1) the angle of boundary current separation (with respect to latitude), as largely determined by the angle of the shelf break prior to separation, (2) the speed at the core of the current, and (3) an inflection point located where boundary current separation occurs.

21.2.7 Gulf Stream Separation and Pathway Dynamics, Part III: The Cooperative Interaction of Abyssal Currents and CAV Trajectories

Neither abyssal currents nor CAV trajectories alone are sufficient to explain Gulf Stream separation from the western boundary and its pathway to the east. Abyssal current constraint of the Gulf Stream latitude near 68.5°W, in conjunction with the topographic configuration and a Gulf Stream feedback mechanism, is not a sufficient explanation of the Gulf Stream pathway between the western boundary and 68°W. Gulf Stream simulations with realistic speeds at the core of the current are not sufficiently inertial (a) to overcome the linear solution demand for an overshoot pathway and (b) to obtain realistic separation without assistance from the abyssal current near 68.5°W. Thus a CAV trajectory and the constraint on the latitude of the Gulf Stream near 68.5°W work together in simulation of a realistic Gulf Stream pathway between the western boundary and 68°W.

The eddy-driven abyssal circulation is sufficient to obtain the key abyssal current, which was not simulated without it. The DWBC is not necessary, but did augment the key abyssal current and did assist the eddy-driven abyssal circulation in effecting realistic Gulf Stream separation, when the latter was not strong enough by itself. The impact of the DWBC on Gulf Stream separation was resolution dependent, required at 1/16°, but not at 1/32° resolution.

Finally, the dynamical explanation is robust. As long as the speed at the core of the current was consistent with observations and the key abyssal current was sufficiently strong, the simulated Gulf Stream separation and its pathway to the east were in close agreement with observations despite differences in model resolution, bottom friction, strength of the abyssal circulation, and the presence or absence of a DWBC. Further, the explanation is consistent with a wide range of key observational evidence in the upper and abyssal ocean, including a 15-year mean Gulf Stream IR northwall pathway, the speed at the core of the current near Gulf Stream separation, the pattern of sea surface height variability from satellite altimetry, and mean abyssal currents. Hurlburt and Hogan (2000) present a large number of additional model-data comparisons for the simulations depicted in Fig. 21.2a, c.

21.3 Dynamical Evaluation of Gulf Stream Simulations by Eddy-Resolving Global and Basin-Scale OGCMs

Significant success has been achieved in simulating the Gulf Stream pathway in eddy-resolving basin-scale OGCMs with thermodynamics and higher vertical resolution (20–50 layers or levels) than the 5 layers used in the hydrodynamic model discussed in Sect. 21.2. However, the OGCM simulations have been very sensitive to changes, such as subgrid scale parameterizations and parameter values. Thus, it has been difficult to obtain consistent results and many simulations have exhibited serious flaws (Paiva et al. 1999; Smith et al. 2000; Bryan et al. 2007; Chassignet and Marshall 2008; Hecht and Smith 2008; Hecht et al. 2008). In this section we perform a dynamical evaluation of eddy-resolving global and basin-scale OGCM simulations of Gulf Stream separation and its pathway to the east. The immediate goals are to better identify and understand the sources of success and failure, and in Sect. 21.4 the impacts of data assimilation. So far, eddy-resolving global and basin-scale ocean prediction systems have demonstrated only 10–15 day forecast skill in the Gulf Stream region based on anomaly correlation >0.6 versus 30 days or more in some regions (Smedstad et al. 2003; Shriver et al. 2007; Hurlburt et al. 2008a; Chassignet et al. 2009; Hurlburt et al. 2009). Future goals are improved and more consistently realistic simulations of the Gulf Stream, increased ability to nowcast and forecast it on time scales up to a month, improved climate prediction in the Gulf

Stream region, and increased efforts to understand OGCM dynamics and dynamically evaluate their simulations in other regions.

A set of eddy-resolving global and basin-scale simulations from HYCOM, MICOM, NEMO, and POP is used in the evaluation (see Table 21.1). The resolution and model domain range from 1/10° Atlantic to 1/25° global. In addition to simulations with a realistic Gulf Stream pathway and dynamics consistent with observations, simulations with several types of flaws are evaluated, including (a) a realistic pathway with unrealistic dynamics, (b) overshoot pathways, (c) premature separation south of Cape Hatteras (the observed location), (d) pathways that separate at Cape Hatteras but have a pathway segment that is too far south east of the separation point, (e) pathways that bifurcate at or after separation, and (f) pathways impacted by unrealistic behavior upstream of the separation point, such as excessive variability or persistent large seaward loops east of the observed mean pathway. All four of the models used here have simulated a variety of Gulf Stream pathways, as illustrated here and in the references cited above.

To streamline the evaluation for the purpose of this discussion, we focus on the following: (1) To evaluate the mean path, mean SSH from the model is overlaid by the 15-year mean Gulf Stream IR northwall pathway$\pm 1\sigma$ (standard deviation) by Cornillon and Sirkes (unpublished). This frontal pathway has 0.1° longitudinal resolution and lies along the northern edge of the Gulf Stream. (2) SSH variability is used to look for a narrow band of high variability west of 69°W and, combined with abyssal eddy kinetic energy (EKE), it is used to identify regions of baroclinic instability. Thus these fields help identify the dynamics of Gulf Stream pathway segments and source regions for eddy-driven mean abyssal currents. (3) Mean speed at the core of the current is used to assess whether or not the simulated Gulf Stream inertial jet is consistent with observations near the western boundary. (4) The DWBC (a term used to identify mean abyssal currents that are clearly part of the AMOC) and eddy-driven mean abyssal currents are used to assess their impact in steering the Gulf Stream pathway and related upper ocean features. Depending on their strength and location in relation to the isobaths, abyssal currents have the potential to improve or increase the errors in the simulated pathways. (5) Both the strength and depth structure of the AMOC can affect the Gulf Stream pathway. Increasing the strength can make the simulated Gulf Stream more inertial, but can also increase the tendency for an overshoot pathway based on linear dynamics. The depth structure of the AMOC influences the depths of the isobaths followed by the DWBC and interactions between the DWBC and the eddy-driven abyssal circulation. (6) The basin-wide linear solution response to the mean wind stress forcing yields the constraints of linear dynamics on the strength and pathways of wind-driven currents in the Gulf Stream region. CAV trajectories were not calculated because there is sufficient proxy information to assess this from the mean pathway, the mean core speed near separation, and the characteristic narrow band of SSH variability along the Gulf Stream west of ~69°W.

In the dynamical evaluation we focus on a segment of the Gulf Stream that extends from 30°N, 80°W, upstream of the observed separation latitude near 35.5°N, 74.5°W, to about 68°W, and characterizations of accuracy refer to pathway segments

Table 21.1 Description of OGCM simulations and hindcasts used for dynamical analysis

Ocean Model[a]	Experiment number[a]	Horizontal Resolution[b]	Vertical Resolution	Years used	Comments
Section 21.3 Simulations					
Atlantic MICOM	1.0	1/12°	20 coordinate surfaces	1982–1983	
Atlantic NEMO	T46	1/12°	50 levels	2004–2006	
Global NEMO	T103	1/12°	50 levels	2004–2006	
Atlantic POP	14x	1/10°	40 levels	1998–2000	
Atlantic HYCOM	1.8	1/12°	32 coordinate surfaces	3–6 and 11–13	[c]Near twin of 1/12° global 18.0
Global HYCOM	9.4	1/12°	32 coordinate surfaces	12–15	
Global HYCOM	9.7	1/12°	32 coordinate surfaces	2004–2007	Twin of 1/12° 14.1 but no tides
Global HYCOM	14.1	1/12°	32 coordinate surfaces	2004–2007	[d]Twin of 1/12° 9.7 with tides
Global HYCOM	18.0	1/12°	32 coordinate surfaces	4–6 and 9–10	Near twin of 1/25° 4.0
Global HYCOM	4.0	1/25°	32 coordinate surfaces	3, 5–10	Near twin of 1/12° 18.0
Section 21.4 Simulations and hindcasts					
Global HYCOM	5.8	1/12°	32 coordinate surfaces	2004–2006	No data assimilation
Global HYCOM	60.5	1/12°	32 coordinate surfaces	2004–2006	[e]Cooper-Haines
Global HYCOM	19.0	1/12°	32 coordinate surfaces	6/2007–5/2008	No data assimilation
Global HYCOM	74.2	1/12°	32 coordinate surfaces	6/2007–5/2008	[e]MODAS synthetics

[a] *MICOM* Miami Isopycnic Coordinate Ocean Model, isopycnal coordinates on a C-grid, *NEMO* Nucleus for European Modelling of the Ocean, z-levels with terrain-following coordinates in shallow water on a C-grid, *POP* Parallel Ocean Program, z-levels on a B-grid; *HYCOM* HYbrid Coordinate Ocean Model, hybrid isopycnal/pressure levels/terrain-following in shallow water on a C-grid; [b] Resolution for each prognostic variable; [c] Twin of 1/12° global HYCOM-18.0 except for the model domain and relaxation to temperature (T) and salinity (S) climatology in buffer zones within 3° of the model boundaries at 28°S and 80°N, global HYCOM experiments are from the GLBa series and all HYCOM experiments use topography based on DBDB2 by D.S.K. (see http://www.7320.nrlssc.navy.mil/DBDB2_WWW); [d] Includes external and internal tides from 8 tidal constituents (Arbic et al. 2010); [e] Downward projection method for the SSH updates, i.e. Cooper and Haines (1996) or synthetic T&S profiles using the Modular Ocean Data Assimilation System (MODAS) (Fox et al. 2002). In both cases the Navy Coupled Ocean Data Assimilation (NCODA) system (Cummings 2005) was then used to assimilate all the data

and other features within this region, even though a larger region may be depicted in some figures. In Sect. 21.3.1 we present the mass transport streamfunction from linear simulations forced by wind stress products used in forcing the OGCM simulations discussed later. In Sect. 21.3.2 we discuss four simulations with a realistic Gulf Stream pathway and quite realistic Gulf Stream dynamics. In the remaining subsections we discuss simulations with different types of flaws, outlined earlier, including a simulation with a realistic Gulf Stream pathway but unrealistic separation dynamics. In each case one to four examples are used to help illustrate the range of simulated results and dynamics. None of the simulations in Sect. 21.3 include ocean data assimilation. Additionally, simulations in Sects. 21.2 and 21.3.1 are characterized by mid-latitude resolution (in °), whereas OGCMs in Sects. 21.3 and 21.4 are characterized by equatorial resolution, making 1/16° resolution in Sects. 21.2 and 21.3.1 approximately the same as 1/12° resolution for OGCMs in Sects. 21.3 and 21.4, ~7 km at mid-latitudes.

21.3.1 Linear model Gulf Stream Simulations from Wind Stress Products Used for OGCMs in Sects. 21.3 and 21.4

Linear barotropic solutions were obtained for the wind stress forcing products used by OGCM simulations discussed in Sects. 21.3 and 21.4. The solutions were obtained with the same model used in Sect. 21.2.1, but here excluding a contribution from the AMOC. Also, the model was run in barotropic, flat bottom mode rather than reduced gravity mode, which yields the same mean transport streamfunction. Figure 21.10 depicts the Atlantic mass transport streamfunction from 1/16° linear barotropic simulations forced by several different wind products, but only covering the latitude range of interest here. The wind stress products used to obtain the results in Fig. 21.10 are (a) an interim European Centre for Medium-Range Weather Forecasts (ECMWF) reanalysis mean over the years 2004–2006, (b) mean operational ECMWF over 2004–2006, (c) a 1978–2002 climatology derived using an ECMWF 40-year reanalysis (ERA-40) (Kallberg et al. 2004) and (d) a 2003–2008 climatology derived from the Navy Operational Global Atmospheric Prediction System (NOGAPS) (Rosmond et al. 2002). In both (c) and (d) the wind stress was calculated from 10 m winds using a bulk formula from Kara et al. (2005) and with the 10 m wind speeds corrected using a monthly QuikSCAT scatterometer climatology (Kara et al. 2009). For (e) an ERA-15 (Gibson et al. 1999) climatology was used and in (f) the ECMWF TOGA global surface analysis 1985-early 2001, based on operational

Fig. 21.10 Mean transport streamfunction (ψ) from 1/16° linear barotropic flat bottom simulations forced by monthly mean wind stress from **a** An interim ECMWF reanalysis over 2004–2006. **b** Operational ECMWF over 2004–2006. **c** A 1978–2002 climatology from ECMWF ERA-40 with wind speed corrected by a QuikSCAT scatterometer climatology. **d** NOGAPS over 2003–2008 also with the QuikSCAT correction. **e** An ECMWF ERA-15 climatology, and **f** An ECMWF TOGA global surface analysis over 1998–2000. The contour interval is 1 Sv

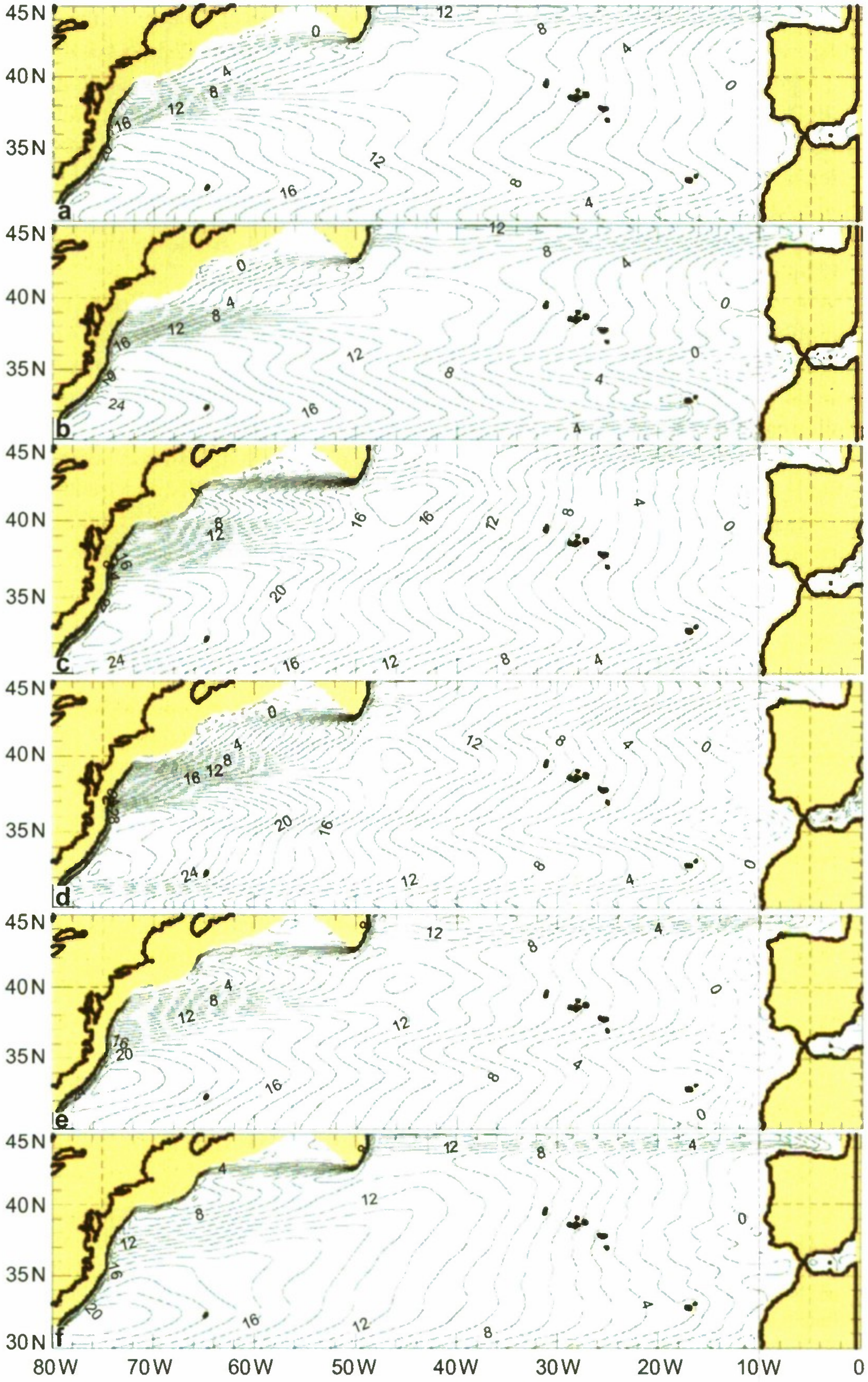
a
b
c
d
e
f
45N
40N
35N
30N
80W
70W
60W
50W
40W
30W
20W
10W
0
0
4
8
12
16
20
24

ECMWF products, was used (Smith et al. 2000; Bryan et al. 2007). In the latter 10 m winds were converted to surface stresses using the neutral drag coefficient of Large and Pond (1981). Note that 5 out of the 6 wind stress products are linked to ECMWF and one to NOGAPS. Although a temporal mean of the interannual wind products was used to force the linear simulations, otherwise the wind products listed above were used in forcing the simulations listed in Table 21.1: (a) 1/12° Atlantic NEMO, (b) 1/12° global NEMO, (c) all of the HYCOM simulations except as noted, (d) 1/12° global HYCOM 19.0 and 74.2, (e) 1/12° Atlantic MICOM and 1/12° global HYCOM 5.8 and 60.5, and (f) 1/10° Atlantic POP.

The resulting streamfunctions are all generally similar in the Gulf Stream region and quite different from that simulated using the smoothed Hellerman and Rosenstein (1983) wind stress climatology (Fig. 21.1). They separate from the western boundary with transports ranging from 20 to 27 Sv versus 30 Sv from smoothed Hellerman-Rosenstein. In all, a large majority of the streamfunction contours separate from the western boundary north of the observed Gulf Stream separation latitude (35.5°N) and at least 50% separate between 35° and 40°N and trend east-northeastward after separation. The two wind stress products with the QuikSCAT-corrected wind speeds give the strongest transports in Fig. 21.10 ((c) 26 Sv from ERA-40/QuikSCAT and (d) 27 Sv from NOGAPS/QuikSCAT). It is significant that almost all of the streamfunction contours driven by these two products leave the western boundary north of the observed Gulf Stream separation latitude. In the case of smoothed Hellerman-Rosenstein, 17 Sv leave the western boundary north of 35.5°N, suggesting an even stronger tendency for the wind stress products used in Fig. 21.10c, d to drive an overshoot pathway in the OGCM simulations.

21.3.2 *Simulations with a Realistic Gulf Stream Pathway*

Figure 21.11 presents mean SSH and Fig. 21.12 SSH variability from four simulations with a realistic Gulf Stream pathway in the segment of interest between separation from the western boundary and 68°W. These are 1/12° Atlantic MICOM (Figs. 21.11a, 21.12a), 1/12° global NEMO (Figs. 21.11b, 21.12b), 1/12° Atlantic HYCOM (Figs. 21.11c, 21.12c), and 1/25° global HYCOM (Figs. 21.11d, 21.12d). In the simulations, the mean IR northwall frontal pathway (in red) closely follows the northern edge of the simulated Gulf Stream over the segment of interest and the simulated pathway is generally realistic within the plot domain. In 1/12° Atlantic

Fig. 21.11 Mean SSH from simulations with a realistic Gulf Stream pathway: **a** 1/12° Atlantic MICOM over 1982–1983. **b** 1/12° global NEMO over 2004–2006. **c** 1/12° Atlantic HYCOM-1.8, years 3–6. **d** 1/25° global HYCOM-4.0, years 5–8 (see Table 21.1). The contour interval is 5 cm, a contour interval for SSH used throughout Sects. 21.3 and 21.4. The mean Gulf Stream IR northwall frontal pathway $\pm 1\sigma$ by Cornillon and Sirkes is overlaid in red on each panel and in red or black on many other panels. Sep v = mean speed at the Gulf Stream core near separation from the western boundary. Sep v is also given on other mean SSH and near surface current figure panels

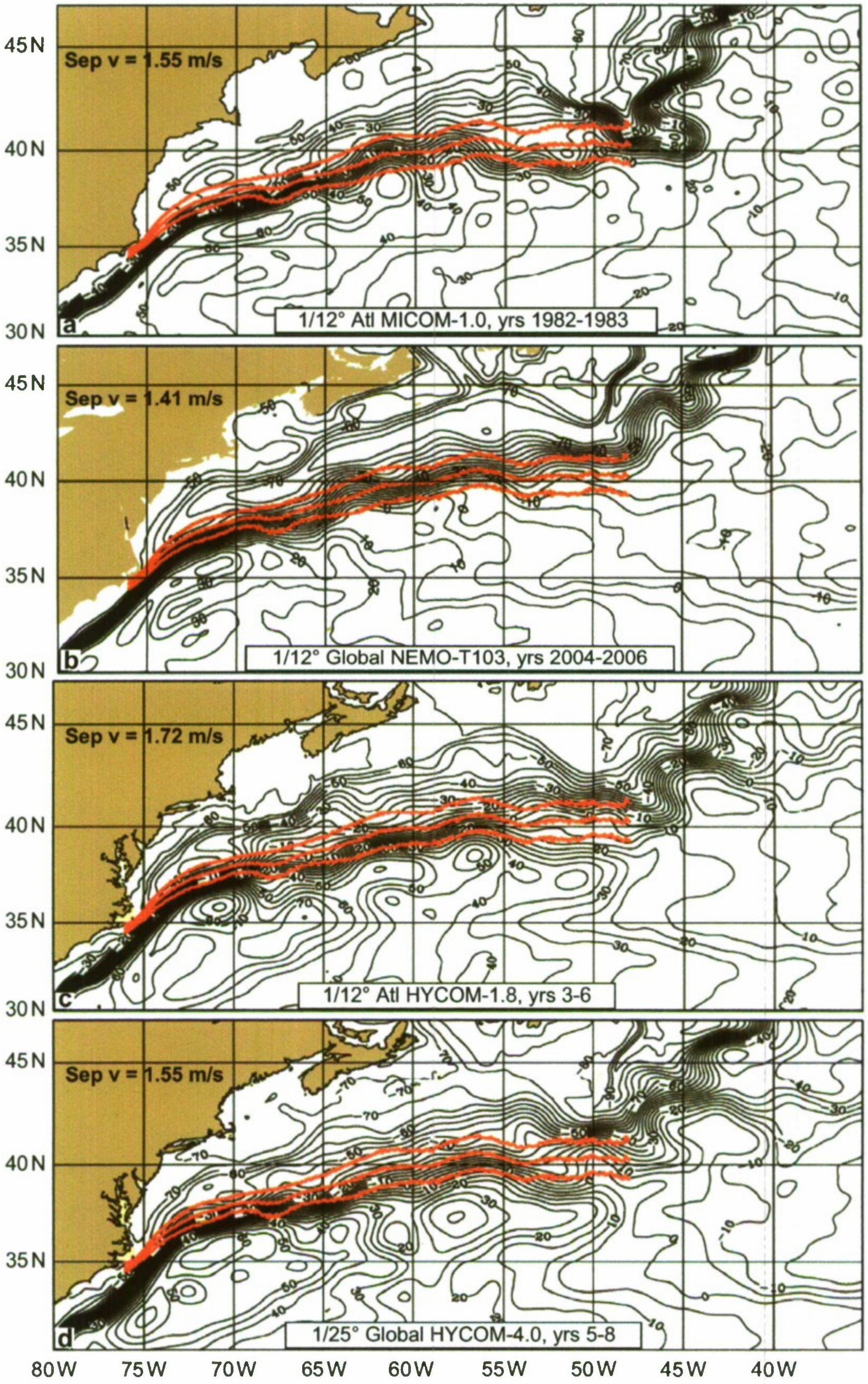
Sep v = 1.55 m/s
1/12° Atl MICOM-1.0, yrs 1982-1983
a
Sep v = 1.41 m/s
1/12° Global NEMO-T103, yrs 2004-2006
b
Sep v = 1.72 m/s
1/12° Atl HYCOM-1.8, yrs 3-6
c
Sep v = 1.55 m/s
1/25° Global HYCOM-4.0, yrs 5-8
d
45N
40N
35N
30N
80W
75W
70W
65W
60W
55W
50W
45W
40W

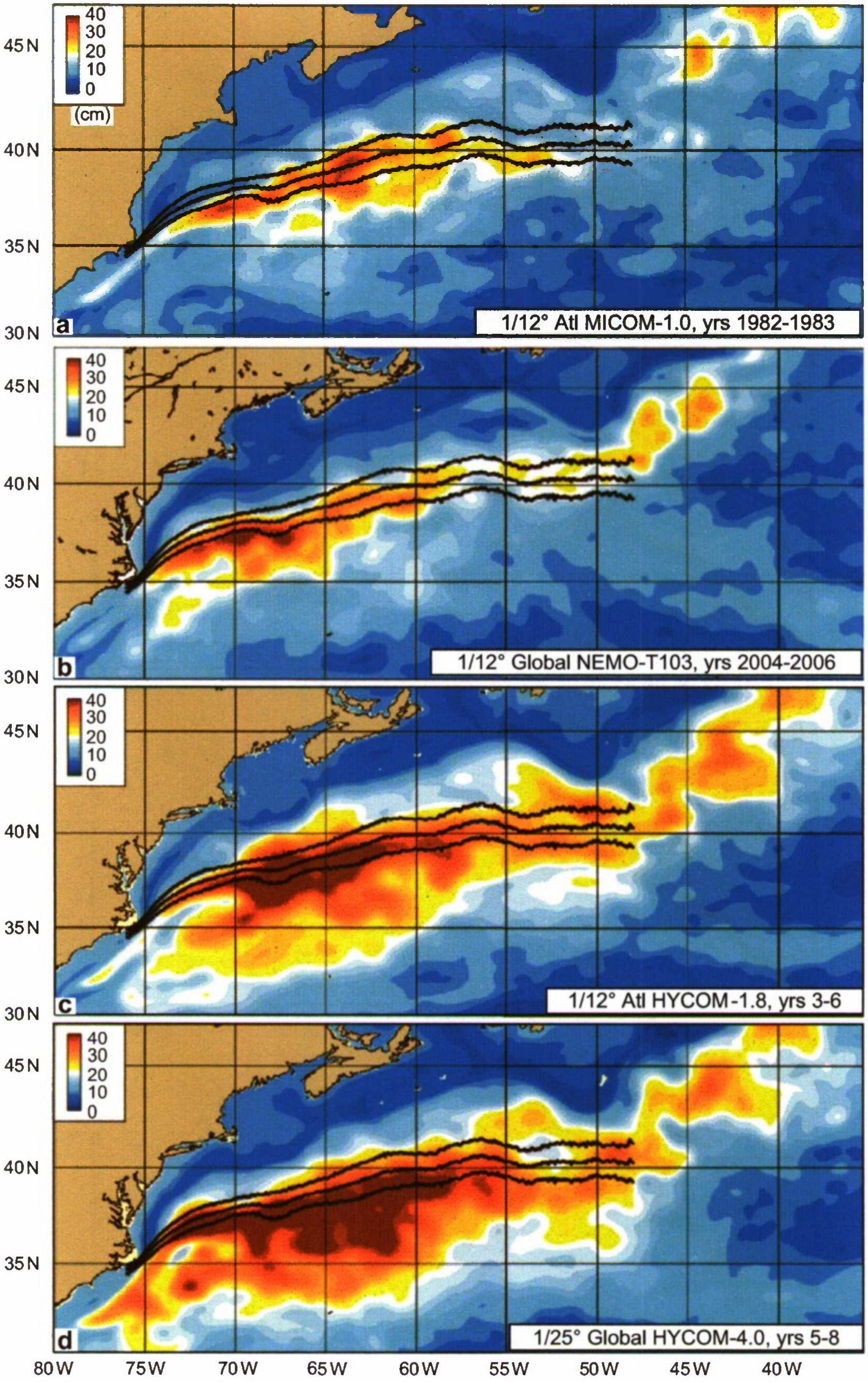

Fig. 21.12 Mean SSH variability from the same four simulations as Fig. 21.11. The contour interval is 2 cm with white spanning 18–20 cm on all SSH variability figure panels

MICOM (Fig. 21.12a) and HYCOM (Fig. 21.12c) there is an associated narrow band of high SSH variability west of 69°W, as observed (Fig. 21.8). In 1/12° global NEMO (Fig. 21.12b) and 1/25° global HYCOM (Fig. 21.12d) the band of SSH variability remains relatively narrow west of 69°W, but in 1/12° global NEMO there is a bulge in variability near 72°W and in 1/25° global HYCOM there is a broader band of high variability over the segment of interest and higher variability than observed south of the separation latitude. The blob of high variability near 72°W in 1/12° global NEMO (similar to that seen in Fig. 21.9c, but not in satellite altimetry) suggests that, as in the 1/32° simulation of Figs. 21.2c and 21.9c, the abyssal current cross-under near 72°W is slightly perturbing the simulated Gulf Stream pathway. As in Figs. 21.2c, 21.11b depicts a straightening of the pathway segment between 73° and 70°W in accord with the overlaid mean IR northwall pathway. In 1/25° global HYCOM (Fig. 21.12d) the broader band of variability is a consequence of small meanders generated south of the separation point that propagate into the segment of interest and a slight northward progression of the simulated pathway over the 4-year mean (years 5–8 after initialization from climatology). To assess the inertial character of the separating jet in relation to observational evidence, we use the Eulerian mean maximum speed at the core of the jet near the separation point, a relevant location where pathway variability is quite low in most simulations. In comparison to the observed range from 1.6 to 2.1 m/s, the 1/12° Atlantic HYCOM simulation is within the observed range at 1.72 m/s, 1/12° Atlantic MICOM and 1/25° global HYCOM are at the low end with 1.55 m/s, and 1/12° global NEMO is 12% below the range at 1.41 m/s.

Although all of the simulations exhibit a realistic Gulf Stream pathway over the segment of interest, overall, the 1/12° Atlantic MICOM simulation is in closest agreement with the relevant observational evidence. Therefore, the other three simulations are discussed in relation to that one and the observational evidence. In representing the mean abyssal currents, a depth average from ~3,000 m to the bottom is appropriate. Except for MICOM, approximately that depth range was used for all the simulations, but with bottom trapped currents often extended over slightly shallower depths. In MICOM layer 15 is very thick. Since MICOM is isopycnal, the layer interfaces vary in depth, but typically the top of layer 15 is ~2,000 m and the bottom ~3,600 m deep. Although depths this shallow in some OGCM simulations include features that are not bottom trapped (e.g. see Fig. 8 and related discussion in Hecht and Smith 2008), such features are not evident when layer 15 is included in the MICOM depth average over the abyssal layers (Fig. 21.13a). The current segments that cross under the Gulf Stream to deeper depths near 72 and 68.5°W are weaker by ~1 cm/s (one color contour) when layer 15 is included, but that is the most negative effect. Otherwise, adding layer 15 gives a broader picture of the MICOM abyssal circulation.

The mean abyssal circulation in MICOM (Fig. 21.13a) depicts the key abyssal current observed crossing under the Gulf Stream near 68.5°W (Fig. 21.5), the observed cyclonic gyre centered near 37°N, 71°W, and the strong current along the gentle escarpment observed at 34.5°N, 71.1°W (Fig. 21.6). It is also consistent with the RAFOS float trajectory in Bower and Hunt (2000, their Fig. 7j) and the

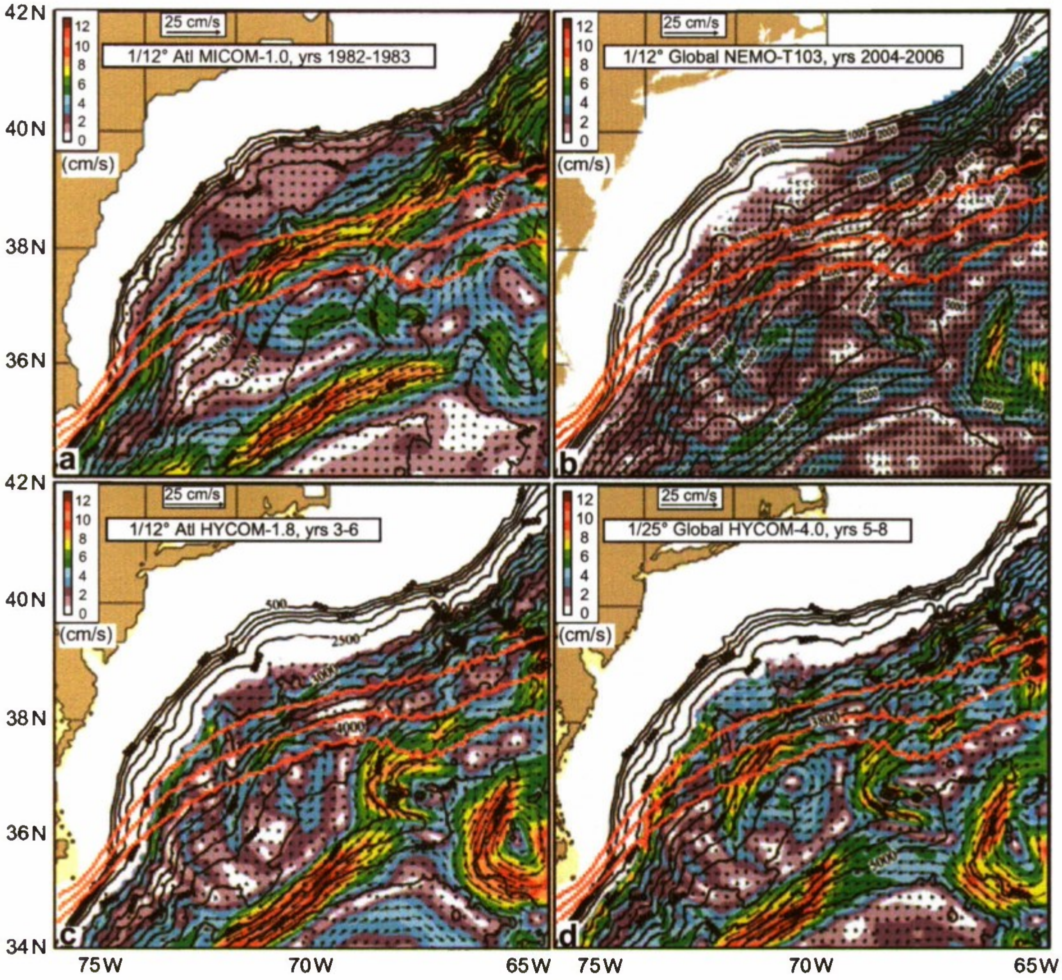

Fig. 21.13 Mean abyssal currents (*arrows*) overlaid on their isotachs (in color with a 1 cm/s contour interval and bathymetric depth contours at intervals of 200 (500) m at depths >(<) 3,000 m from the same four simulations as Fig. 21.11). The reference vector length for the currents is 25 cm/s (*black arrow over land*). All panels with mean abyssal currents are labeled the same way, except as noted

observation-based schematic in Schmitz and McCartney (1993, their Fig. 12a), both described in Sect. 21.2.3. These features in MICOM are very similar to those in Fig. 21.4a, including similar dual pathways approaching the Gulf Stream cross-under near 72°W. In both cases the eastern pathway crosses under and retroflects to the east, while the western one continues along the continental slope, the latter via different pathways in MICOM and Fig. 21.4a. In MICOM the western pathway follows a sharp westward turn in the 3,200 m isobath along the northern edge of the simulated Gulf Stream, while in Fig. 21.4a it crosses under the Gulf Stream and continues along the 3,600–4,000 m isobaths of the continental slope south of the stream. RAFOS float trajectories at ~3,500 m depth in Bower and Hunt (2000, their Fig. 7) support the existence of this deeper pathway along the continental slope, which is missing in the MICOM simulation.

All four of the simulations exhibit the cross-under pathway near 72°W, the dual pathways feeding into it from the north side, the associated cyclonic abyssal gyre, and west-southwestward flow along the gentle escarpment (Fig. 21.13). Except in MICOM, this cross-under flow is augmented by an anticyclonic abyssal gyre on the western side (also seen in Fig. 21.4a), most strongly in 1/12° global NEMO and progressively more weakly in 1/12° Atlantic HYCOM and 1/25° global HYCOM. Unlike the MICOM and NEMO simulations, 1/12° and 1/25° HYCOM simulate the observed continuation of flow along the continental slope from the southern end of the ~72°W cross-under, in addition to the retroflection to the east simulated by all four.

All but 1/12° global NEMO simulate the key abyssal current near 68.5°W (Fig. 21.5), most strongly in MICOM and with progressively weaker dual pathways feeding in from the north side in 1/25° and 1/12° HYCOM. As additional constraints on the modeled Gulf Stream pathway, 1/12° global NEMO, 1/12° Atlantic HYCOM, and 1/25° global HYCOM simulate abyssal Gulf Stream cross-under pathways near 67.5°W and 65.5°W not seen in MICOM and Fig. 21.4a. Before completely crossing under the simulated Gulf Stream, both turn to become roughly antiparallel to the model Gulf Stream in a west-southwestward direction along the 4,800–4,900 m isobaths in NEMO and the 4,600–4,800 m isobaths in the two HYCOM simulations. This abyssal current joins the observed pathway near 68.5°W, where it turns southward. In the process it advects the southern edge of the model Gulf Stream southward, forming the eastern edge of one lobe of the western nonlinear recirculation gyre on the south side of the Gulf Stream in NEMO (Fig. 21.11b) and two lobes in the two HYCOM simulations (Fig. 21.11c, d). This effect is not seen in the MICOM simulation (Fig. 21.11a) or the mean SSH (Fig. 21.2c) related to Fig. 21.4a. These two simulations do not exhibit the two eastern cross-unders or the resulting west-southwestward flow along the 4,600–4,900 isobaths between ~65.5°W and ~68.5°W. No observational evidence was found to confirm or dispute the existence of these abyssal currents.

At >30 Sv in the latitude range of Fig. 21.11, the AMOC in MICOM (Fig. 21.14a) is the strongest of all the simulations considered here, but at the same time the mean speed of the current core near separation is relatively weak, suggesting a relatively weak wind-driven contribution (Fig. 21.10e) and a strong contribution to the abyssal circulation from the AMOC. The depth range of the incoming DWBC (Fig. 21.13a) is conducive to the realistic abyssal current pathways simulated by MICOM. The other three simulations have a ~20 Sv AMOC (Fig. 21.14b–d) and a shallower southward abyssal limb.

21.3.3 Simulation with a Realistic Gulf Stream Pathway and Unrealistic Dynamics

In Sects. 21.2 and 21.3.2 it was evident that ocean models could simulate a realistic mean Gulf Stream pathway with generally realistic dynamics without exhibiting

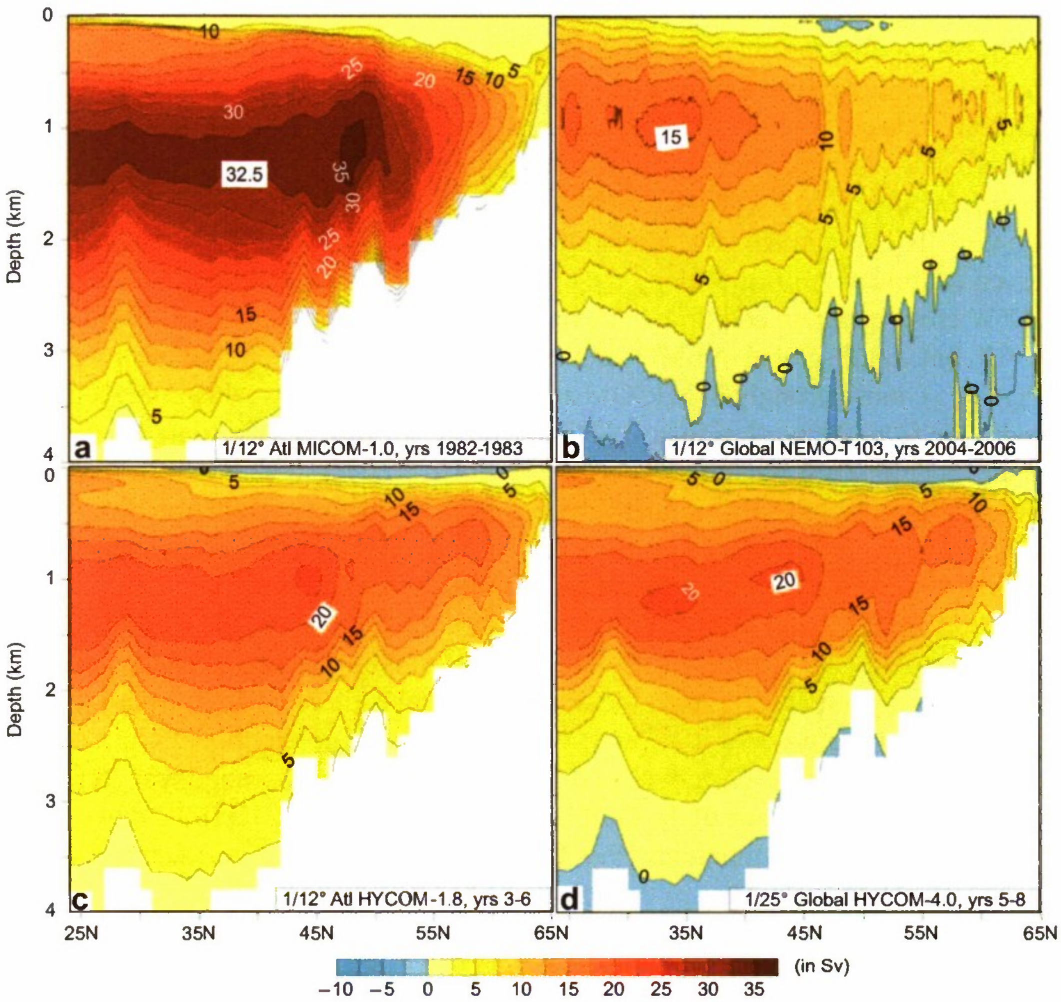

Fig. 21.14 Atlantic meridional overturning circulation (AMOC) streamfunction from the same four simulations as Fig. 21.11. An AMOC streamfunction contour interval of 2.5 Sv is used throughout. The AMOC is northward in the upper ocean and southward in the abyssal ocean

complete agreement with related observational evidence. Here we examine a simulation with a realistic Gulf Stream pathway comparable to the present state of the art. In our region of interest (the separation point to ~68°W) the mean pathway is only slightly too far south (Fig. 21.15a). At 1.34 m/s the mean core speed of the separating jet is 16% below the observed range of 1.6–2.1 m/s. The 12 Sv AMOC over 35–40°N is weaker than found in Sect. 21.3.2 and its southward abyssal flow is too shallow (not shown). As a result, abyssal currents along the continental slope (Fig. 21.15c) are weaker than in any of the simulations shown in Fig. 21.13. The abyssal current crossing under the Gulf Stream near 72°W is present, including the two branches feeding in from the north side, but it is relatively weak. Cross-unders farther to the east are extremely weak.

Then what are the dynamics of the separating jet? The large area of high SSH variability west of 68°W (Fig. 21.15b) is a strong indication that the separation is not associated with CAV trajectory dynamics. (1) The broad area of high SSH

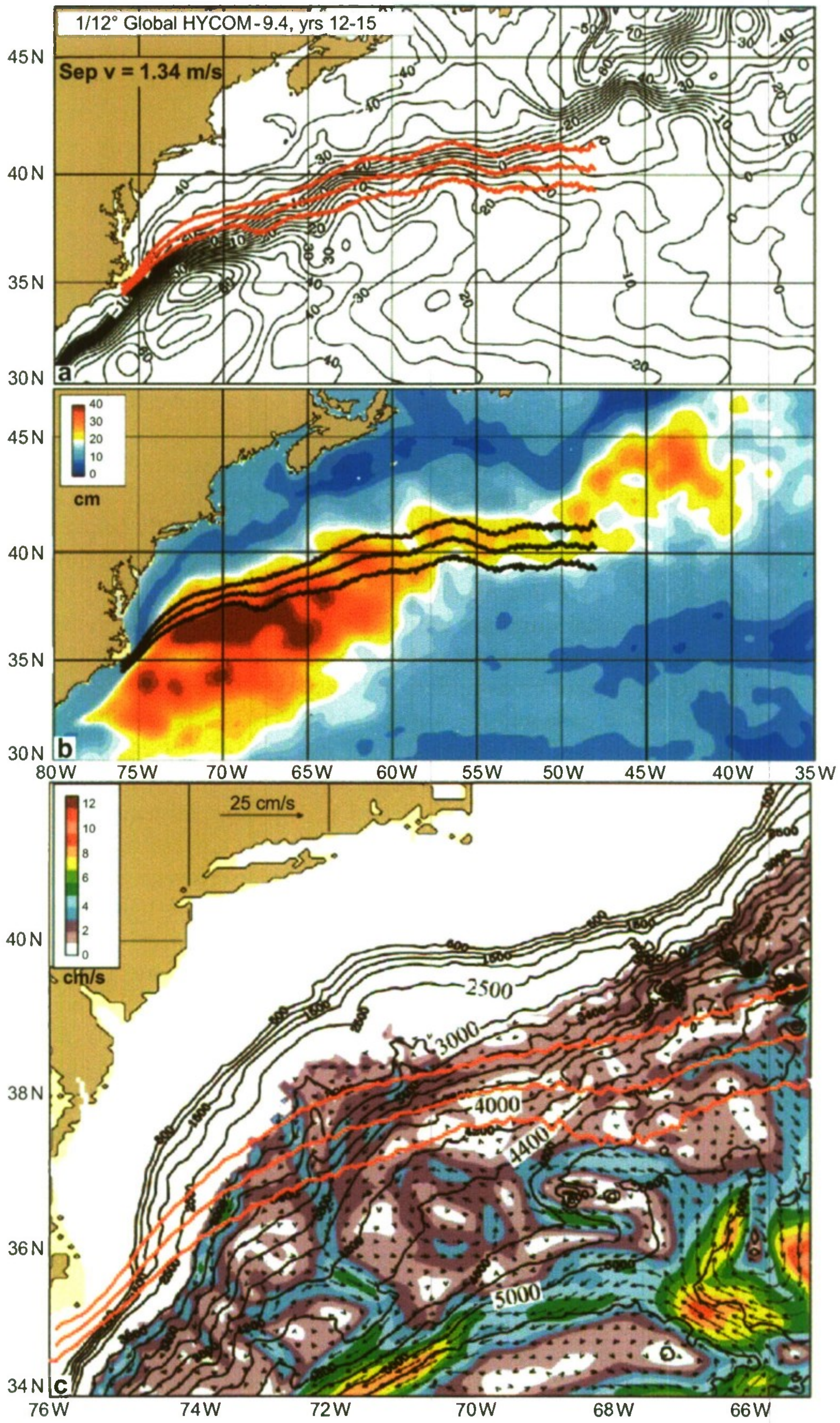

Fig. 21.15 Means from 1/12° global HYCOM-9.4, years 12–15 (Table 21.1), a simulation with a realistic mean Gulf Stream pathway but unrealistic dynamics: **a** SSH. **b** SSH variability, and **c** abyssal currents, isotachs, and depth contours. Sep v = 1.34 m/s, the mean speed at the Gulf Stream core near separation from the western boundary

variability extending north and south of the mean pathway, (2) the large amplitude southern recirculation gyre west of ~69°W (Fig. 21.15a), (3) the eddy-driven mean abyssal gyre (circling 35°N, 72°N in Fig. 21.15c) that is centered directly beneath the surface gyre, and (4) the associated high deep EKE (not shown) are evidence of strong baroclinic instability that encompasses the Gulf Stream and the strong southern recirculation gyre.

The separating Gulf Stream pathway lies along the northern edge of the southern recirculation gyre. The eddy-driven mean abyssal gyre lies over relatively flat topography located between regions of sloping topography to the northwest and southeast. The location of the eddy-driven mean abyssal gyre adjacent to the southern edge of the separating jet and the location of the northwesternmost flat topography suggest a topographic role in the pathway of the separating jet, because baroclinic instability and the eddy-driven abyssal gyre would be inhibited if positioned farther north or south over sloping topography. In Sects. 21.2 and 21.3.2 some mean abyssal gyres lie over sloping topography directly beneath the Gulf Stream, including examples of an anticyclonic abyssal gyre located northwest of the anticyclonic gyre just discussed (see Figs. 21.4a and 21.13b–d). In those simulations flow instabilities are limited to a narrow band of high variability along the Gulf Stream (as observed in Fig. 21.8) and the mean abyssal gyres form adjacent to Gulf Stream cross-unders in locations where the slopes of the Gulf Stream thermocline base and the topography are closely enough matched to permit regions of quite uniform potential vorticity. In flat bottom Gulf Stream simulations a barotropic relationship is expected between eddy-driven mean abyssal and upper ocean gyres with the mean Gulf Stream pathway along the northern (southern) edge of southern (northern) recirculation gyres, as discussed dynamically in Hurlburt and Hogan (2008), but in simulations with non-flat topography the relationship between such gyres is not necessarily barotropic, as illustrated in other subsections. Further, given the lack of abyssal current assistance east of 72°W, one might anticipate an overshoot pathway. The linear wind-driven simulation (Fig. 21.10c) gives the second strongest tendency for an overshoot pathway of all the linear solutions in Figs. 21.1 and 21.10 (nearly equal to the strongest tendency in Fig. 21.10d), but the 12 Sv AMOC is equal to the weakest of the nonlinear simulations studied here. Returning to the abyssal circulation, we see two relatively weak abyssal currents crossing southward under the Gulf Stream to deeper depths on the north side of the eddy-driven abyssal gyre. The western one crosses under the Gulf Stream between 73 and 74°W and retroflects to the east along the northern edge of the eddy-driven abyssal gyre and the boundary between the Gulf Stream and southern recirculation gyre. The second one near 72°W crosses under without retroflecting and continues southward along the eastern and southern edge of the eddy-driven abyssal gyre. Thus these abyssal currents tend to counteract tendencies for a northward displacement of the Gulf Stream and the adjacent southern recirculation gyre that lies between ~75 and 68°W.

The preceding discussion demonstrates that the simulated Gulf pathway between the western boundary and ~69°W lies in a region of strong baroclinic instability. Thus, while the 4-year mean Gulf Stream pathway in Fig. 21.15a is quite realistic, the dynamics of the separating jet are unrealistic. The simulation is inconsistent with the observed SSH variability and relevant abyssal current observations. The mean core speed near separation is below the range of observational evidence. The AMOC is too weak and its southward abyssal limb is too shallow.

21.3.4 Simulations with a Pathway That Overshoots the Observed Latitude

Pathways that overshoot the observed latitude of the Gulf Stream are more characteristic of eddy-permitting OGCMs (Barnier et al. 2006; Bryan et al. 2007), but they can also occur in eddy-resolving OGCMs, as shown in Barnier et al. (2006), Hecht and Smith (2008), and Fig. 21.16. In the discussion of overshoot pathways, the 1/12° Atlantic HYCOM simulation, shown in Figs. 21.16a, b and 21.17a, b, is used as the pivotal experiment and the two global HYCOM simulations are discussed in relation to this one. The 1/12° (Figs. 21.16e, f and 21.17e, f) and 1/25° (Figs. 21.16c, d and 21.17c, d) global HYCOM configurations are identical (including the initialization from climatology and the use of model years 9–10 after initialization), except for the horizontal resolution, friction/diffusion parameters tied to resolution, and the effects of resolution on the bottom topography. All three simulations use the same wind stress forcing as the HYCOM simulation in Sect. 21.3.3 with a weak AMOC, but they use a later version of HYCOM and a modification to salinity relaxation designed to increase the AMOC.

The mean over years 3–6 of the pivotal simulation yielded a realistic Gulf Stream pathway (Fig. 21.11c), but over time the simulation developed the overshoot pathway shown in the mean over years 11–13 in Fig. 21.16a. Due to the modification of the sea surface salinity relaxation, the salinity in the Gulf Stream and in pathways all the way to the Nordic Seas increased over time. As a result, the salinity and density of the Denmark Straits overflow into the subpolar Atlantic also increased. In addition, the strength of the AMOC increased from a mean of ~22 Sv over years 3–6 (Fig. 21.14c) to ~27 Sv over years 11–13 in the latitude range of interest (Fig. 21.17b). In the process the mean core speed of the Gulf Stream near separation increased from 1.72 to 2.15 m/s, making it the most inertial at separation of all the simulations considered and at the top end of observational values.

We know from Sect. 21.2 that the AMOC contributes to the demands of linear dynamics for an overshoot pathway, but why did that happen in the Atlantic HYCOM simulation and not in the MICOM simulation, which has a slightly stronger AMOC and a less inertial Gulf Stream near separation? Also, why did the two global HYCOM simulations (with less impact from modified salinity relaxation) develop an overshoot pathway with an AMOC of ~20 Sv and with only a 5% increase over earlier periods (e.g. Fig. 21.14d vs. Fig. 21.17d for 1/25° global HY-

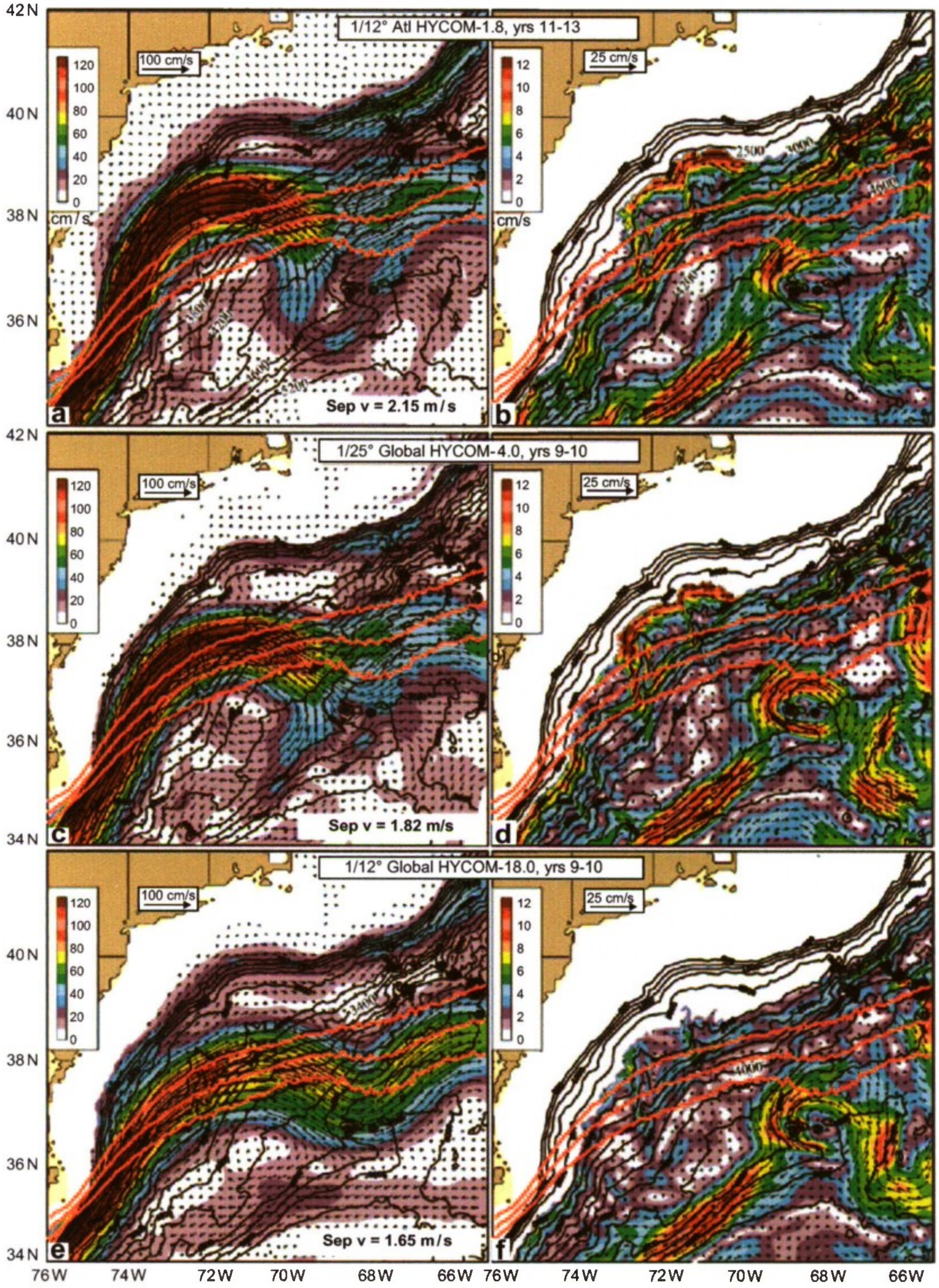

Fig. 21.16 Mean currents at ~25 m depth (**a**, **c**, **e**) and mean abyssal currents (**b**, **d**, **f**) from three simulations with a Gulf Stream pathway that overshoots the observed separation latitude, (**a**, **b**) 1/12° Atlantic HYCOM-1.8, years 11–13, (**c**, **d**) 1/25° global HYCOM-4.0, years 9–10, and (**e**, **f**) 1/12° global HYCOM-18.0, years 9–10 (Table 21.1). In all panels mean currents (*arrows*) are overlaid on their isotachs (*in color*) with contour intervals of 10 (1) cm/s for near surface (abyssal) currents and on depth contours. The reference current vector is 1 (0.25) m/s for near surface (abyssal) currents. The two global simulations are near twins designed to test the impact of increasing the horizontal resolution

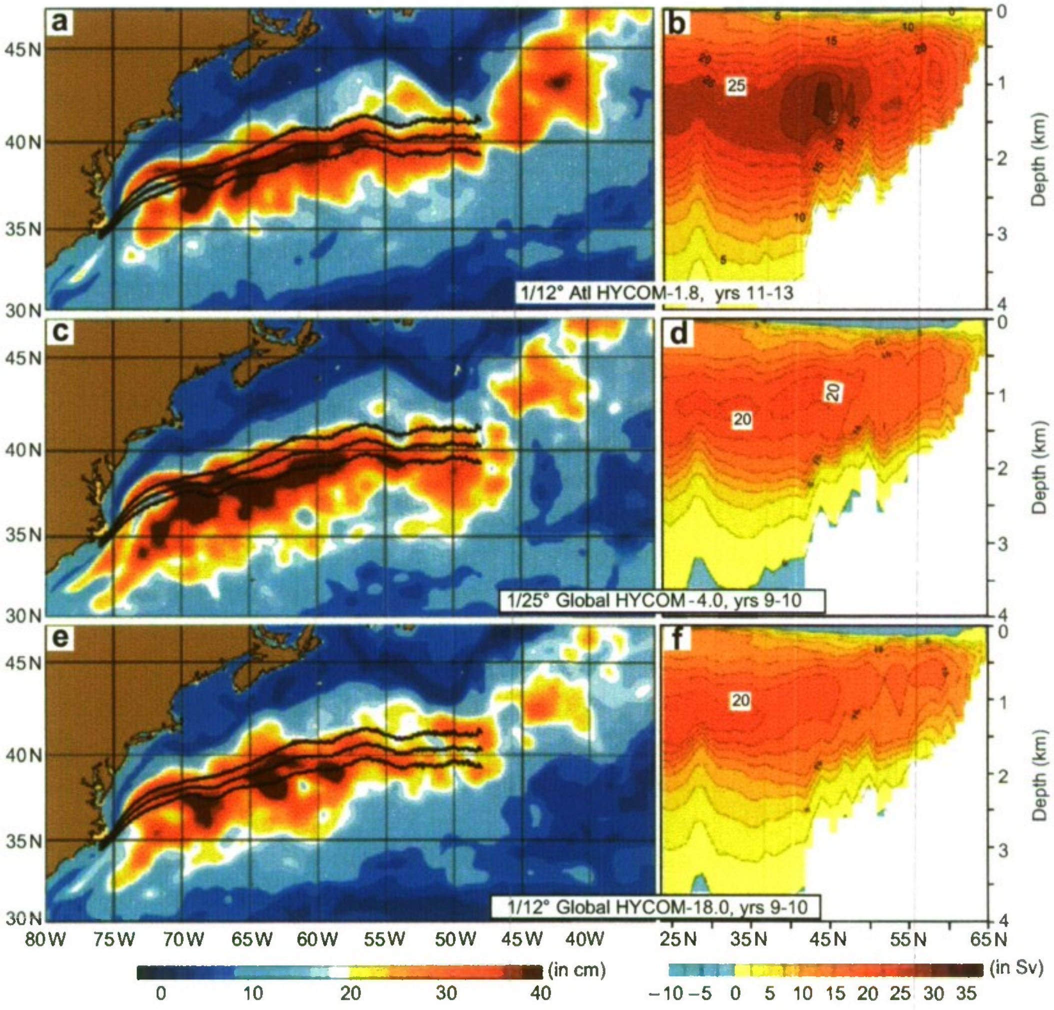

Fig. 21.17 SSH variability (**a**, **c**, **e**) and mean AMOC streamfunction (**b**, **d**, **f**) from the same simulations as Fig. 21.16

COM), when the overshoot did not occur (e.g., Fig. 21.11d vs. Fig. 21.16c for 1/25° global HYCOM)? The three HYCOM simulations with an overshoot pathway all used the ERA-40/QuikSCAT climatological wind stress forcing that gives a strong tendency for an overshoot pathway based on linear dynamics; see Sect. 21.3.1 and Fig. 21.10c. Further, the AMOC of the HYCOM simulations is relatively concentrated over depths of 2,000–3,000 m in the latitude range of Fig. 21.11, both before (Fig. 21.14c, d) and after (Fig. 21.17b, d, f) developing the overshoot pathway, while the AMOC from MICOM is more uniformly distributed with depth (Fig. 21.14a). Correspondingly, the DWBC in the HYCOM simulations is concentrated along shallower isobaths (Fig. 21.13c, d and Fig. 21.16b, d, f) than in the MICOM simulation (Fig. 21.13a). As discussed in Sect. 21.2, that places a greater burden on the eddy-driven abyssal circulation to generate the essential abyssal currents that cross under the Gulf Stream, either directly (Figs. 21.2d and 21.3d) or through interaction with the DWBC (Figs. 21.2a, e and 21.3a, e). To facilitate discernment of the relationships between near-surface currents, abyssal currents, and the topography, mean currents at the depth of the current core and mean abyssal currents are overlaid with topographic contours and the mean northwall frontal pathway in the same region for all three simulations (Fig. 21.16).

The northward penetration of the overshoot is greatest in the 1/12° Atlantic HYCOM simulation (Fig. 21.16a), as expected from the strength of the AMOC. In Fig. 16a the simulated Gulf Stream follows the shelf break and continental slope to a location east of 72°W, where a ridge in the topography exists in the depth range 2,200–2,800 m. The other two (Fig. 21.16c, e) reach that point over deeper isobaths of the continental slope, separated from the shelf break. At the location east of 72°W the main core of the current separates from the steeper part of the continental slope and the inshore portion continues along the shelf break and continental slope in all three simulations, although a large portion of the inshore flow does that farther up stream in Fig. 21.16e (1/12° global HYCOM). The source of this bifurcation is a strong southward abyssal current nearly perpendicular to the Gulf Stream along the eastern side of the ridge (Fig. 21.16b, d, f). Part of that current then becomes antiparallel to the Gulf Stream along the south side of the ridge. Since there is no ridge inshore of ~2,200 m, the inshore portion of the bifurcation continues along the shelf break. An additional portion on the inshore side of the stream joins the portion along the shelf break between 69° and 67°W in Fig. 21.16a, c, where the joining current flows nearly parallel to the isobaths and antiparallel to the underlying strong abyssal currents (Fig. 21.16b, d).

At the location where the main core of the Gulf Stream separates from the steeper continental slope in all three simulations, the underlying abyssal current also bifurcates (Fig. 21.16b, d, f). One branch continues westward along the continental slope until most of it crosses southward under the Gulf Stream along the western slope of a valley west of 72°W, while the second branch continues southward under the Gulf Stream east of 72°W, again along the western slope of a valley. In the process both abyssal currents cross isobaths from 2,600 to 3,600 m depth beneath the Gulf Stream, in accord with the theory of Hogg and Stommel (1985), before all (part) of them join a southwestward abyssal current along the 3,200–3,600 m isobaths that flows nearly antiparallel along the southeastern side of the simulated Gulf Stream in the Atlantic (global) simulations.

East of 71°W there is evidence that abyssal currents play a role in splitting the main jet, with the northern branch continuing eastward along 38–39°N and the southern branch forming a large mean meander in the 1/12° Atlantic (Fig. 21.16a, b) and 1/25° global HYCOM (Fig. 21.16c, d) simulations. In the 1/12° global HYCOM simulation there is mainly a simple mean meander centered near 68°W (Fig. 21.16e). In all three examples this is a region of high SSH variability with evidence of eddy generation on the south side of the stream (Fig. 21.17a, c, e) and high abyssal EKE (not shown). In addition, there is an eddy-driven abyssal gyre centered over a westward trough in the topography near 36.7°N, 68°W (Fig. 21.16b, d, f). In the 1/12° global HYCOM simulation (Fig. 21.16e, f) the Gulf Stream approaches the trough from the west at a slightly lower latitude than the other two simulations and the abyssal gyre is centered directly beneath the mean meander in a baroclinic relationship such that the east side of the gyre tends to advect the pathway northward, the northern and southern sides are antiparallel and parallel, and the western side tends to advect the pathway southward. In the other two simulations (Fig. 21.16a–d) the northern side of the abyssal gyre lies within the path of the approaching Gulf Stream and the western side of the abyssal gyre splits the jet, advecting the southern part southward while the northern side continues eastward.

21.3.5 Simulation with Premature Separation from the Western Boundary

The 1/12° Atlantic NEMO simulation exhibits premature separation from the western boundary near 34°N (Fig. 21.18a). Like the 1/12° Atlantic HYCOM simulation with an overshoot pathway in Sect. 21.3.4, the Gulf Stream core speed near separation is toward the high end of the observational evidence (1.9 m/s). However, in the latitude range of the separated jet, the AMOC (Fig. 21.18c) is weaker than in the MICOM simulation and the 1/12° Atlantic HYCOM overshoot simulation and similar to most of the other simulations with a realistic or overshoot pathway. The linear wind-driven contribution to the simulated Gulf Stream pathway again indicates a tendency for an overshoot pathway (Fig. 21.10a), but a tendency that is weaker than for the simulations in Sect. 21.3.4. In addition, most of the southward transport of the AMOC lies between ~1,500 and 3,000 m south of 43°N, a depth structure largely set by the southern boundary (not shown). Also, within the latitude range of Fig. 21.18a a relatively large amount of deep water formation occurs compared to the HYCOM and MICOM simulations.

In Fig. 21.18d the relationship between the mean abyssal circulation (below 2,800 m) and the simulated Gulf Stream pathway is obvious, a mean abyssal current crossing under the Gulf Stream where it separates from the western boundary. In the process the abyssal flow crosses the 3,300–4,400 m isobaths. The cross-under is fed by an abyssal current along the ~3,200–3,600 m isobaths as well as abyssal currents along continental slope isobaths shallower than 2,800 m. A similar abyssal current along the 3,200–3,600 m isobaths is seen in the 1/12° Atlantic HYCOM simulation (Fig. 21.16b), but in that case the current lies east of the overshooting Gulf Stream pathway. The 1/12° Atlantic NEMO simulation is missing abyssal currents along the 3,100 and 4,100–4,400 m isobaths that crossed under the Gulf Stream in the MICOM simulation (Fig. 21.13a). It is missing the latter near 68.5°W as a consequence of its shallow southward flow in the AMOC. In this example the simulated Gulf Stream pathway after separation parallels the underlying abyssal current eastward to ~65°W. There, an anticyclonic abyssal gyre splits off the southern edge of the model Gulf Stream to form part of the eastern boundary of a southern recirculation gyre. Between 71° and 70°W the northern edge of the model Gulf Stream is split off by the eastern edge of an elongated cyclonic abyssal gyre. The split-off current subsequently turns east-northeastward to become a

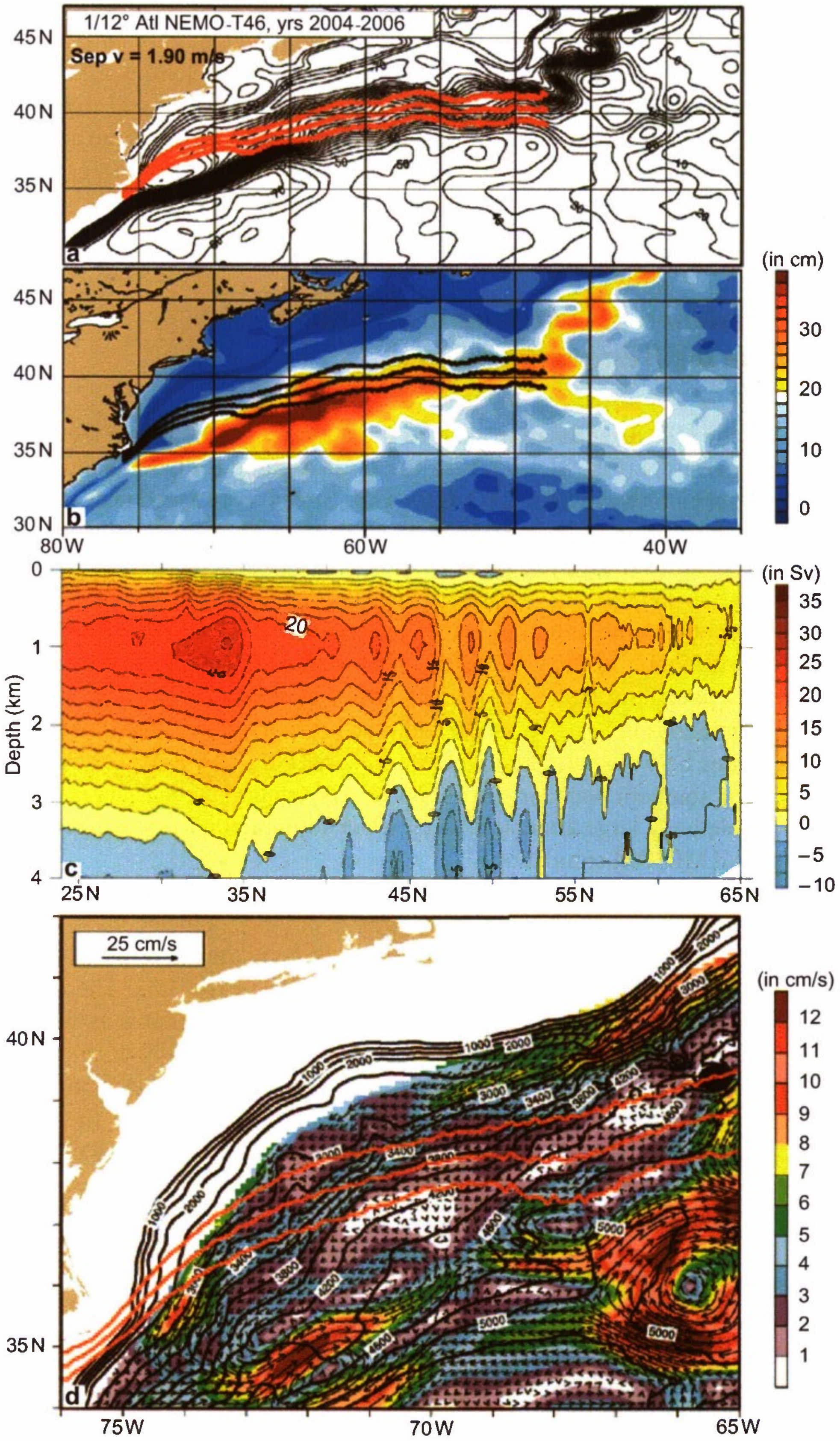

Fig. 21.18 Means from 1/12° Atlantic NEMO over 2004–2006 (Table 21.1), a simulation with premature separation from the western boundary: (**a**) SSH, (**b**) SSH variability, (**c**) AMOC streamfunction, and (**d**) abyssal currents, isotachs, and depth contours. Sep v = 1.9 m/s

northern branch of the Gulf Stream flowing antiparallel to the underlying abyssal currents.

21.3.6 Simulations with a Pathway Segment too far South After Separation at Cape Hatteras

The simulations in this section are characterized by a Gulf Stream pathway segment that is too far south after separation from the western boundary at the observed separation latitude, as seen in the mean SSH (Fig. 21.19) and the SSH variability (Fig. 21.20). The simulated Gulf Stream pathway in Fig. 21.19c actually exhibits premature separation (discussed in Sect. 21.3.5), but is included here because it is a near twin of the simulation in Fig. 21.19d. Figure 21.19a is a mean over years 4–6 from the same 1/12° global HYCOM simulation that developed an overshoot pathway in years 9–10 (Sect. 21.3.4, Fig. 21.16e). Figure 21.19b is from a 1/10° Atlantic simulation by the Los Alamos POP model. The simulations in Fig. 21.19c, d are from 1/12° global HYCOM later in a chain of simulations that included the one with a realistic Gulf Stream pathway and unrealistic dynamics (Sect. 21.3.3, Fig. 21.15a) and a weak AMOC (not shown). The interannually-forced simulations in Fig. 21.19c, d are nearly identical except that one includes external and internal tides with 8 tidal constituents (Arbic et al. 2010; Fig. 21.19d), while the other excludes tides (Fig. 21.19c), as do all the other simulations considered here.

Like the simulation with premature separation in Sect. 21.3.5 (Fig. 21.18a), all four of the simulations in Fig. 21.19 have abyssal current flow crossing to deeper depths under the Gulf Stream where it separates from the western boundary (Fig. 21.21), but slightly farther north in the simulations with separation at Cape Hatteras (Fig. 21.19a, b, d). In each case cross-under currents feed into an eddy-driven abyssal gyre centered near or slightly south of 35°N, 72°W over relatively flat topography, as in Fig. 21.18d (simulation with premature separation) and Fig. 21.15c (simulation with a realistic Gulf Stream pathway but unrealistic dynamics). In Fig. 21.15c this gyre is substantially weaker than the others. The abyssal gyres in Fig. 21.21 underlie a surface gyre along the southern edge of the Gulf Stream (Fig. 21.19) and are associated with high SSH variability (Fig. 21.20) and high abyssal EKE (not shown), evidence of strong baroclinic instability. In relation to the underlying abyssal currents, the subsequent pathway eastward to ~65°W in three of the simulations (Figs. 21.19a, b, d and 21.21a, b, d) is quite similar to that in the simulation with premature separation (Fig. 21.18). In Fig. 21.19c the Gulf Stream bifurcates near 69°W with the northern pathway becoming weak and diffuse in the mean and generally paralleling abyssal currents (Fig. 21.21c). The southern pathway shows a dip driven by converging abyssal currents near 71°W with the upper ocean current subsequently flowing antiparallel to the underlying abyssal current until the southern part is steered southward by an abyssal current near 68°W to form the eastern edge of a southern recirculation gyre lobe.

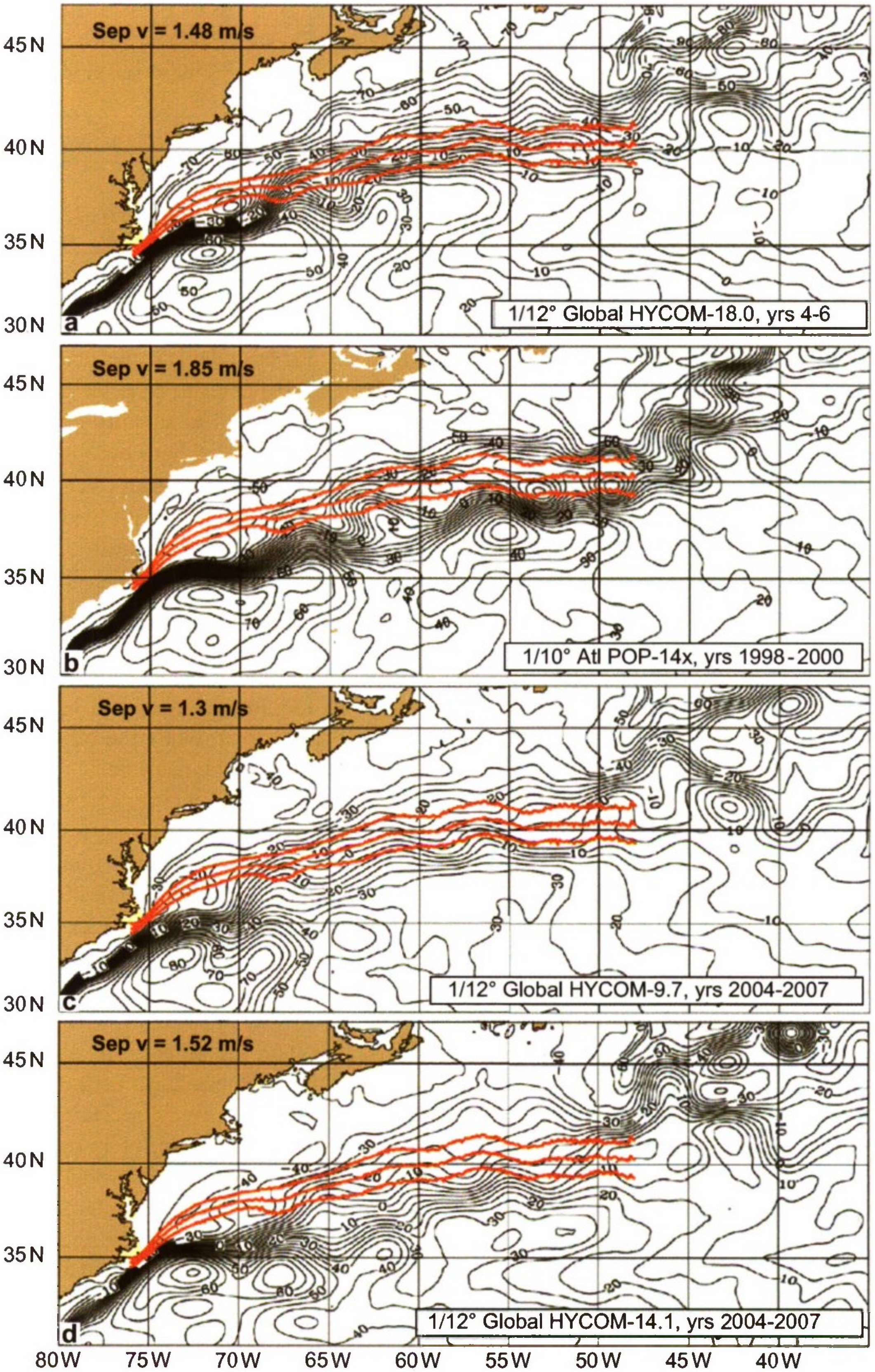

Fig. 21.19 Mean SSH from simulations with a Gulf Stream pathway segment too far south after separation from the western boundary. **a** 1/12° global HYCOM-18.0, years 4–6. **b** 1/10° Atlantic POP-14x, 1998–2000 discussed in Hecht et al. (2008). **c** 1/12° global HYCOM-9.7, 2004–2007, and **d** 1/12° global HYCOM-14.1, 2004–2007, a twin of (**c**) with the addition of external and internal tides. (See Table 21.1)

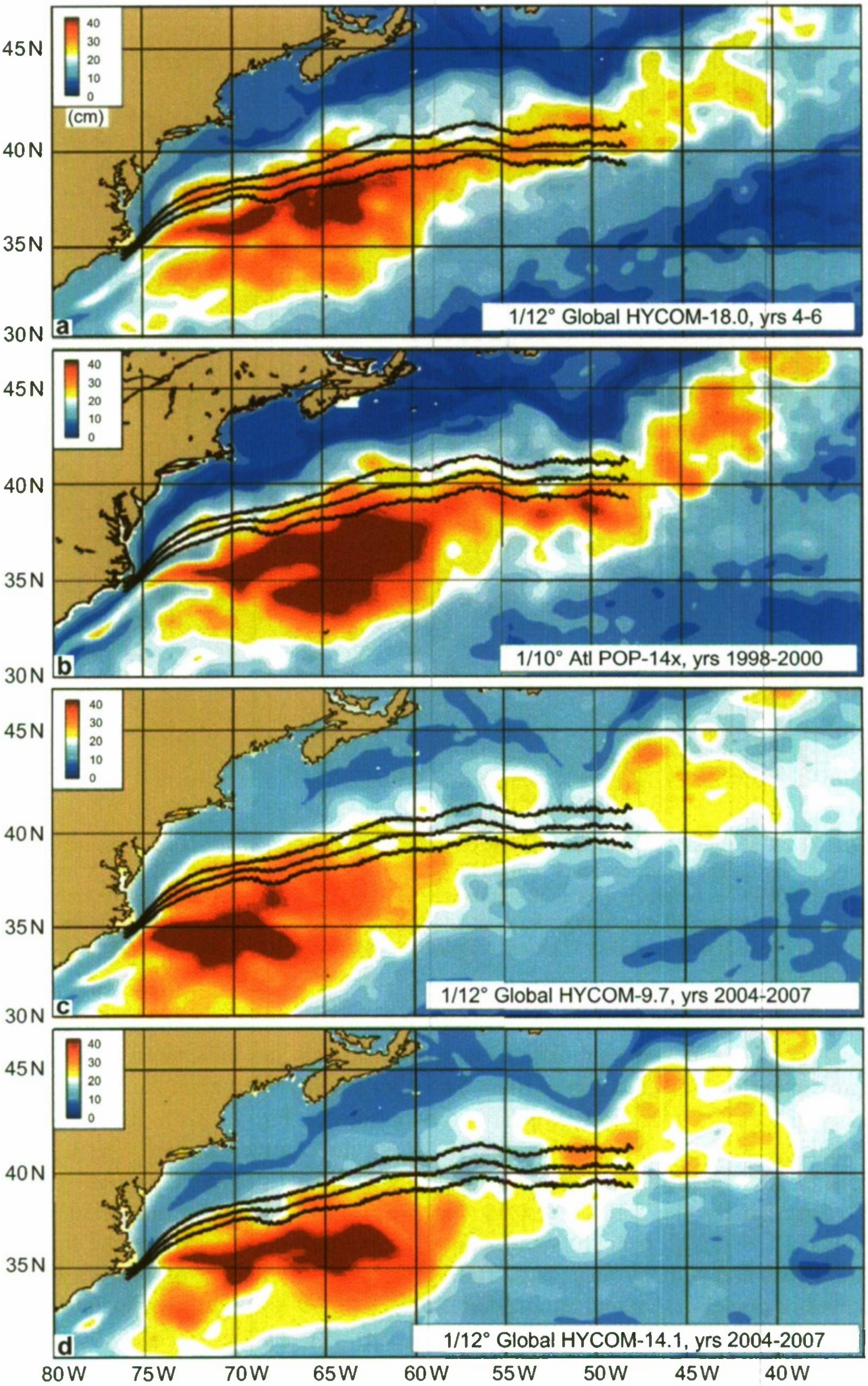

Fig. 21.20 SSH variability from the same four simulations as Fig. 21.19

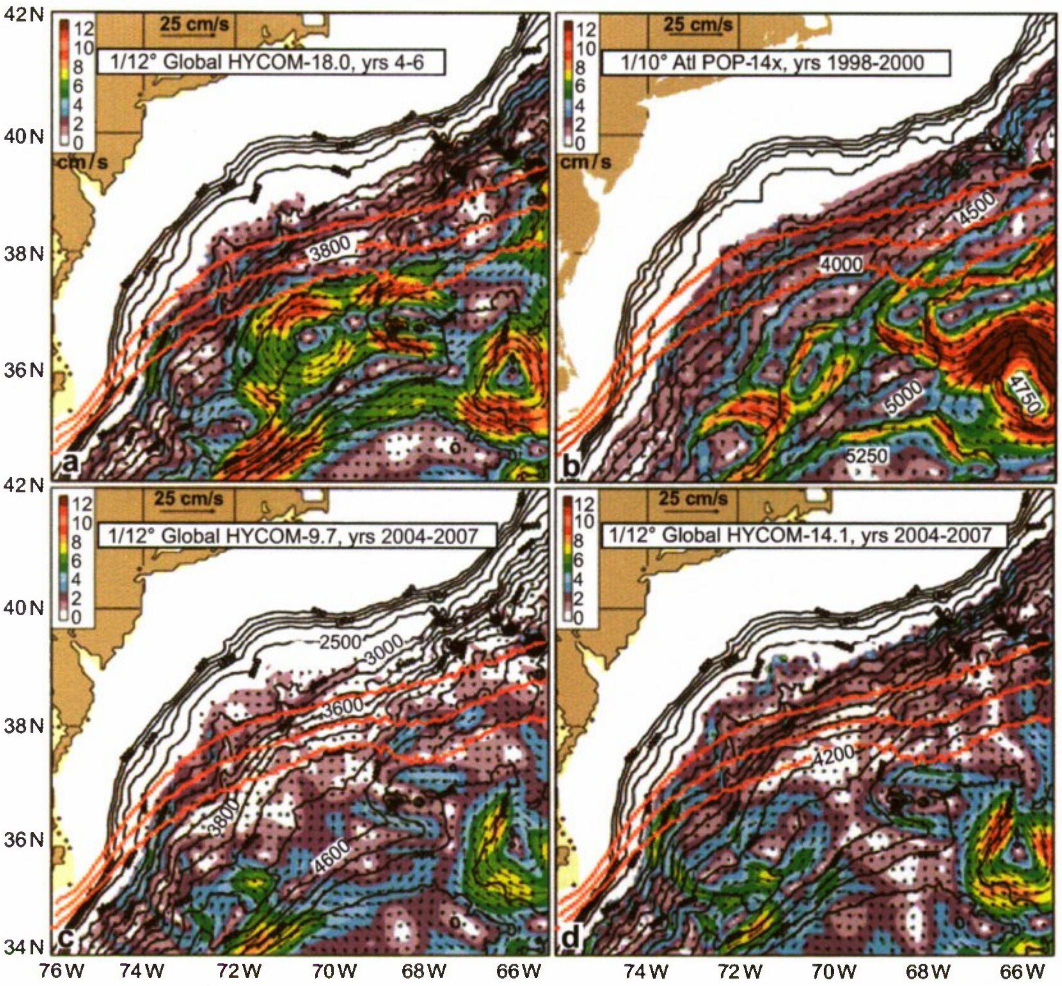

Fig. 21.21 Mean abyssal currents overlaid on isotachs and depth from the same four simulations as Fig. 21.19. The depth contours in the HYCOM simulations (**a**, **c**, **d**) are at 200 m intervals below 3,000 m as before, but the POP simulation (**b**) has full cell topography. Thus the bathymetric contours mark 250 m step boundaries at and below 3,000 m, not depths. Below 3,000 m the regions between step boundary contours are plateaus of constant depth, which are depth-labeled accordingly

A comparison of the simulations with and without tides indicates a modest improvement with the addition of tides. The tides slightly strengthen the AMOC and deepen the southward flow (Fig. 21.22d with tides vs. Fig. 21.22c). The result is a relatively weak but well-defined DWBC along the continental slope versus none east of 70°W in the simulation without tides within the depth range plotted.

Surprisingly, the 1/12° HYCOM (Figs. 21.19–21.22, panel a) and 1/10° POP (Figs. 21.19–21.22, panel b) simulations exhibit greater similarity than the simulations with and without tides (Figs. 21.19–21.22, panels c and d), despite the differences in model design and atmospheric forcing (linear wind-driven simulation for HYCOM in Fig. 21.10c and for POP in 21.10f). HYCOM is a hybrid coordinate ocean model on a C-grid with an isopycnal interior and partial step topography, while POP is a z-level model on a B-grid with full step topography, the only one

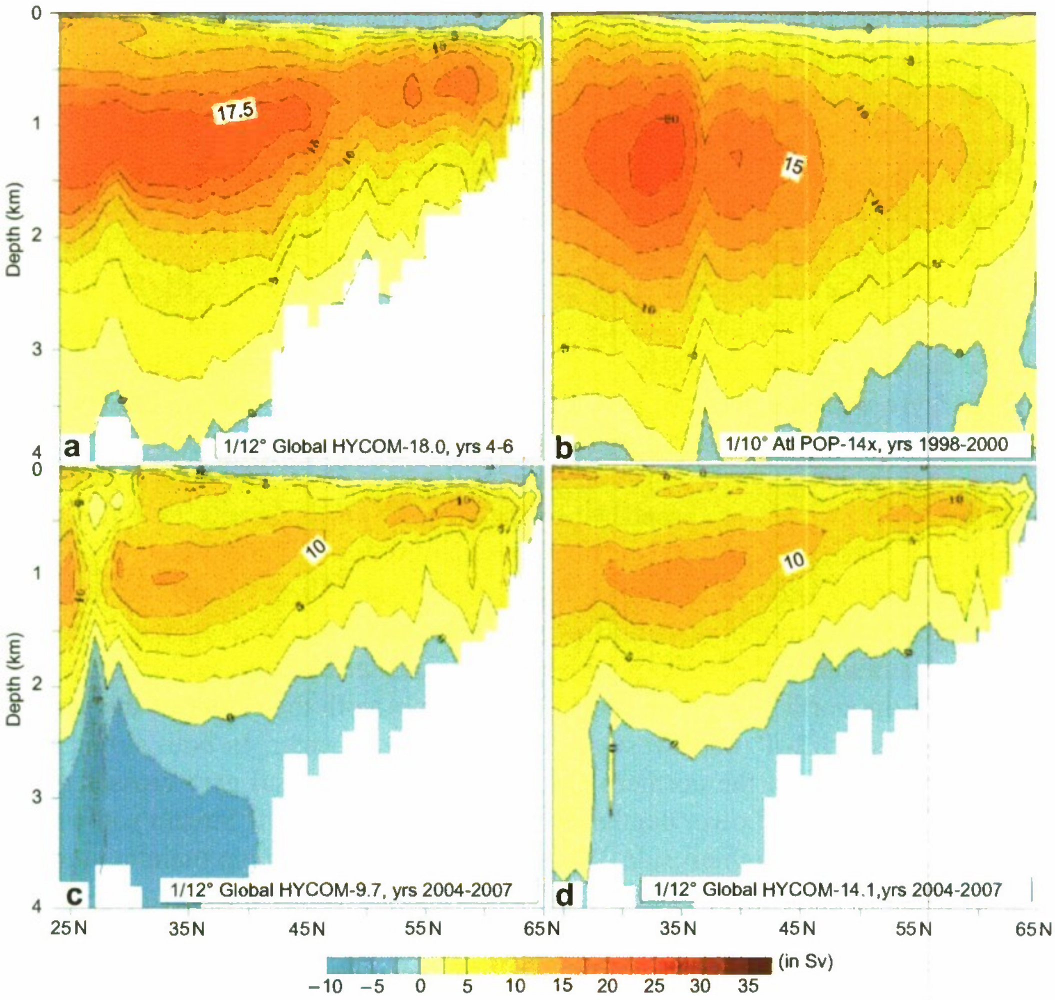

Fig. 21.22 Mean AMOC streamfunction from the same four simulations as Fig. 21.19

in this chapter with a B-grid or full step topography. In the other simulations the topographic contours are depth contours with a 200 m contour interval, while at and below 2,750 m the contours in the POP simulation mark the boundary between steps at 250 m intervals and the regions between contours are plateaus of constant depth. Despite these differences the mean Gulf Stream pathway within the segment of interest (Fig. 21.19a, b) and the mean abyssal circulation (Fig. 21.21a, b) are very similar, taking into account the tendency for abyssal currents to concentrate along the step boundaries in the full cell topography (Fig. 21.21b). The strength of the AMOC in the latitude range of Fig. 21.10 is similar, but the southward flow is shallower in HYCOM and there is more deep water formation in this latitude range in POP, as in NEMO, the other z-level model.

Most of the simulations depict a pair of eddy-driven cyclonic gyres (both observed, Figs. 21.5 and 21.6), the western one centered near 37°N, 71°W over sloping topography and the eastern one centered near 36.7°N, 68°W over a westward trough in the topography, the no tides simulation in Fig. 21.21c being a notable exception by lacking both. In the simulations with a realistic Gulf Stream pathway and realistic dynamics (Figs. 21.2a, c–e and 21.11), the western gyre lies directly beneath the Gulf Stream in association with abyssal current cross-unders along the northern and western sides (Figs. 21.3a, c, e, 21.4a, and 21.13), except in the simulation with no DWBC (Fig. 21.3d). The same is true for the eastern gyre in the subset of these simulations that exhibit the observed cross-under (Fig. 21.5) near 68.5 W (mean SSH in Figs. 21.2a, c–e and 21.11a; mean abyssal currents in Figs. 21.3a, c–e, 21.4a, and 21.13a). Here the corresponding abyssal gyres in HYCOM and POP (Fig. 21.21a and b, respectively) are substantially stronger than in the other simulations (except for the eastern gyre in comparison to the simulations with an overshoot pathway) and the gyre currents are strongest along the northern and southern sides of the gyres. In addition, the western gyres are displaced ~1° to the south-southeast, a distance less than the southward displacement of the Gulf Stream pathways. Although the mean Gulf Streams are broader than the mean abyssal currents, they generally follow along the southern sides of these abyssal gyres and the abyssal currents in both gyres cross isobaths to deeper depths where they flow toward the southern side of the stream, inhibiting its northward displacement to a more realistic latitude.

In each simulation the western gyre has an associated cyclonic upper ocean gyre adjacent to the north side of the model Gulf Stream with the center of the surface gyre displaced ~1/2–1° northwest of the abyssal gyre center. In both simulations the abyssal current on the northern side of the eastern abyssal gyre crosses under the Gulf Stream to shallower depths, broadening the mean Gulf Stream pathway to the north, while the southern side of the abyssal gyre acts to help maintain a more southern pathway. In the 1/12° global HYCOM simulation the western abyssal gyre weakens over time, the upper cyclonic gyre on the north side of the stream dissipates, and the year 8 mean exhibits a realistic mean pathway. However, by years 9–10 this abyssal gyre has moved westward and nearly dissipated (Fig. 21.16f) and the simulation has developed an overshoot pathway (Fig. 21.16e).

21.3.7 Gulf Stream Pathways and Variability Upstream of Separation at Cape Hatteras

Two main types of Gulf Stream variability are observed in the South Atlantic Bight (SAB) upstream of the separation point at Cape Hatteras, smaller and larger amplitude meanders, as illustrated in Plate 1 of Glenn and Ebbesmeyer (1994b). Compared to the larger meanders, the smaller ones are characterized by ~3× shorter event time scales, 2× faster propagation speeds (35–60 km/day), and a shore side meander amplitude that remains inshore of the 600 m isobath versus offshore of it for tens of kilometers (Bane and Dewar 1988). Both types of meander propagate northeastward from the vicinity of the Charleston Bump (Fig. 21.23) and often cyclonic eddies form on the inshore side of the meanders (Glenn and Ebbesmeyer 1994a, b). The small meanders are clearly illustrated by Xie et al. (2007, their Fig. 2) in a sequence of daily satellite SST snapshots over a 6-day period.

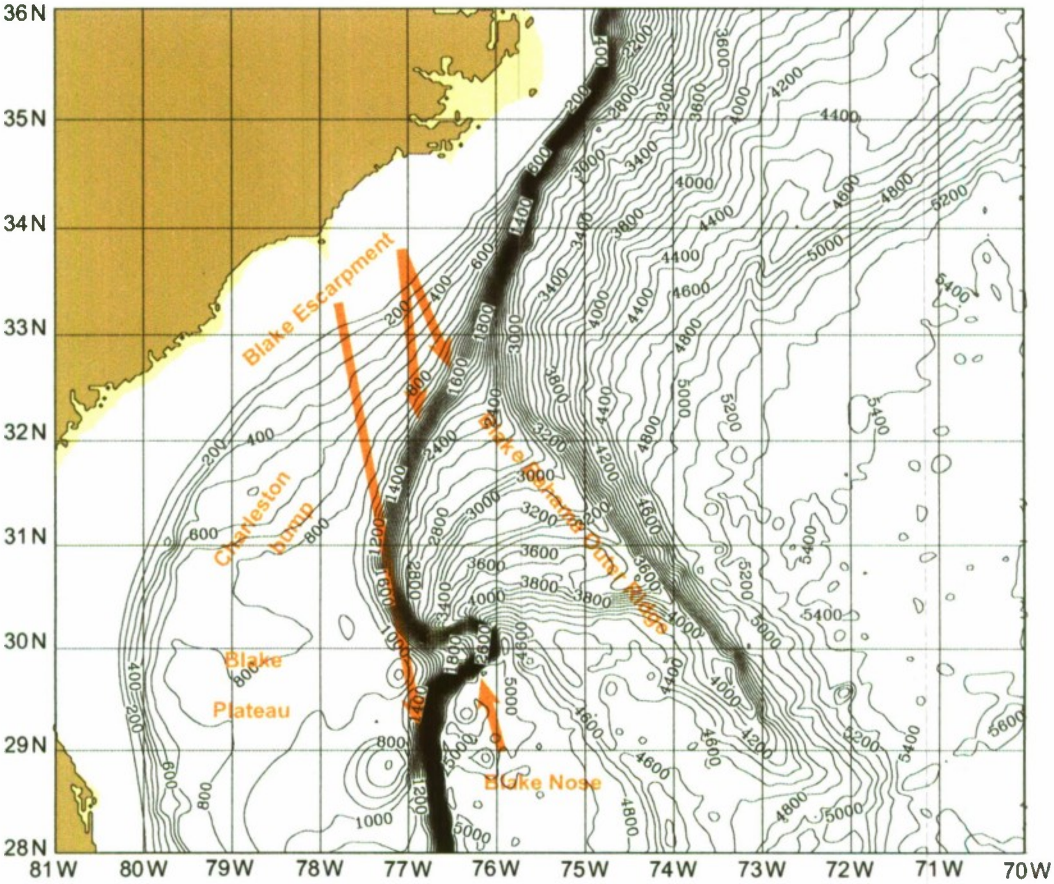

Fig. 21.23 Topographic map of the South Atlantic Bight (SAB). The Blake Bahama Outer Ridge, the Blake Escarpment, the Blake Nose, the Blake Plateau, and the Charleston bump are topographic features that influence the dynamics of the Gulf Stream and the DWBC. The topographic contour interval is 100 m

This variability has a 4–5 day time scale (Legeckis 1979; Glenn and Ebbesmeyer 1994b) and is a component of the observed SSH variability depicted in Fig. 21.8 as a narrow band beginning south of 32°N and extending along the Gulf Stream pathway past Cape Hatteras, a trajectory observed for individual eddy-meander features (Glenn and Ebbesmeyer 1994a, b). The SSH variability exceeds 20 cm near 32°N and is 15–20 cm along the Gulf Stream pathway downstream until larger variability occurs past the separation point. Such variability is seen in nearly every SSH variability panel in Sects. 21.3 and 21.4 except for simulations by 1/25° global HYCOM (e.g. Figs. 21.12d and 21.17b), where there is a slightly broader band of higher variability, and simulations where there is a broad band of much higher variability near the separation point (e.g. Figs. 21.15b and 21.20c). The observed variability has been attributed to barotropic and baroclinic instability, especially near the Charleston bump, based on observational evidence (Bane and Dewar 1988) and modeling studies. For example, Xie et al. (2007) investigated the effects of coastline curvature and the Charleston bump and found that both enhanced these Gulf Stream flow instabilities in the SAB.

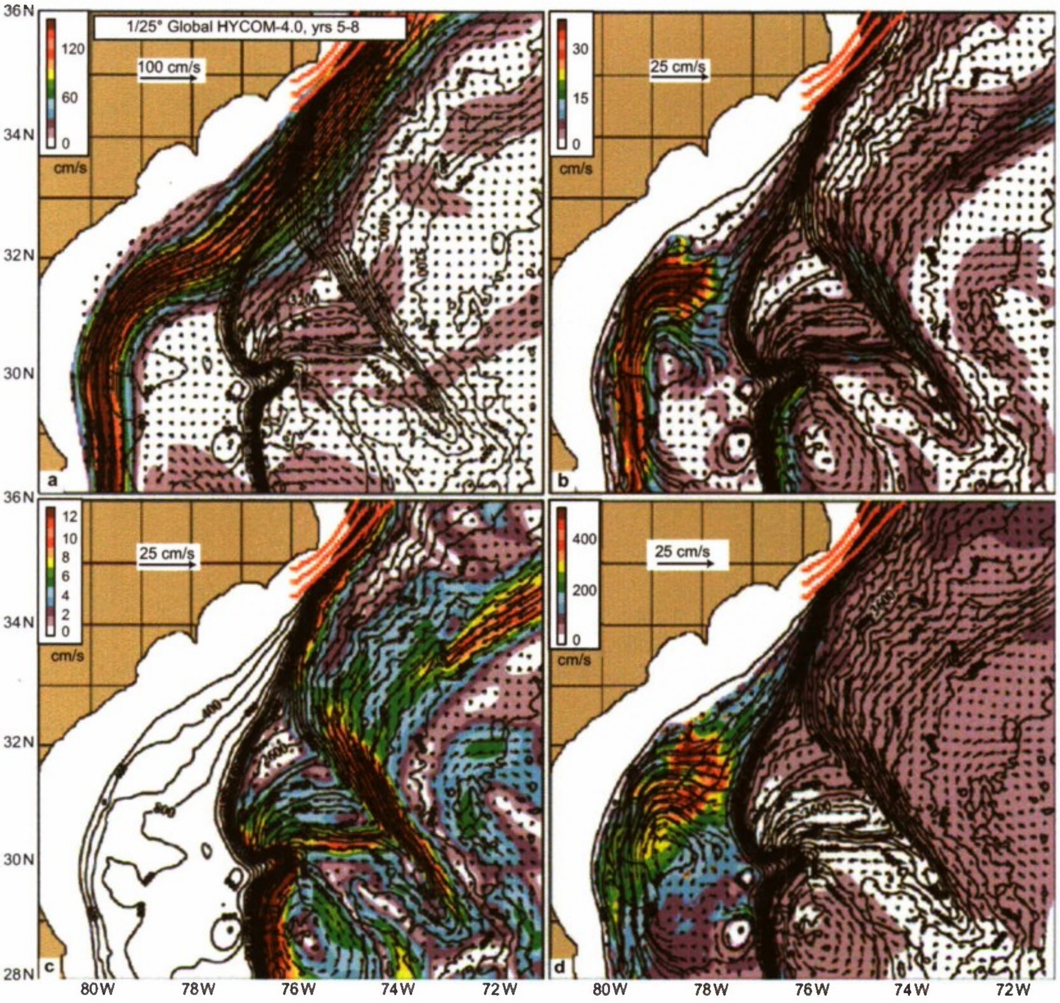

Fig. 21.24 **a–c** Mean currents (*arrows*) and isotachs (*in color*) overlaid on topographic contours in the SAB from 1/25° global HYCOM-4.0, years 5–8 (Table 21.1): **a** Near surface currents at ~25 m depth. **b** Depth average to the bottom starting from a depth of ~300 m near the inshore edge of the Gulf Stream and a depth of ~800 m seaward of the Gulf Stream in order to depict near bottom flow over the 400–850 m depth range of the Charleston bump and the Blake Plateau. **c** Depth average over ~2,000 m to the bottom to depict abyssal currents along the Blake Escarpment and over the Blake Bahama Outer Ridge, and **d** like **b** with isotachs replaced by EKE. The reference current vector lengths are 1 m/s in **a** and 0.25 m/s in **b–d**. The color contour intervals are 12 cm/s in (**a**), 3 cm/s in (**b**), 1 cm/s in (**c**), and 40 cm^2/s^2 in (**d**^{2}). The topographic contour interval is 200 m

The unrealistically high variability in 1/25° global HYCOM is driven by excessive flow instabilities over the Charleston bump and the adjacent Blake Plateau, which has nearly flat topography near 800 m depth (Fig. 21.23). Signatures of the relative strength of baroclinic instability are evident by comparing near bottom EKE and mean flow from 1/25° global HYCOM (EKE in Fig. 21.24d and mean flow in Fig. 21.24b) with corresponding results from a near twin 1/12° global HYCOM simulation (EKE in Fig. 21.25d and mean flow in Fig. 21.25b). The latter does not exhibit excessive SSH variability in the region (SSH variability from 1/25° global HYCOM in Fig. 21.12d versus 1/12° global HYCOM in Fig. 21.20a over the same model years used in Figs. 21.24

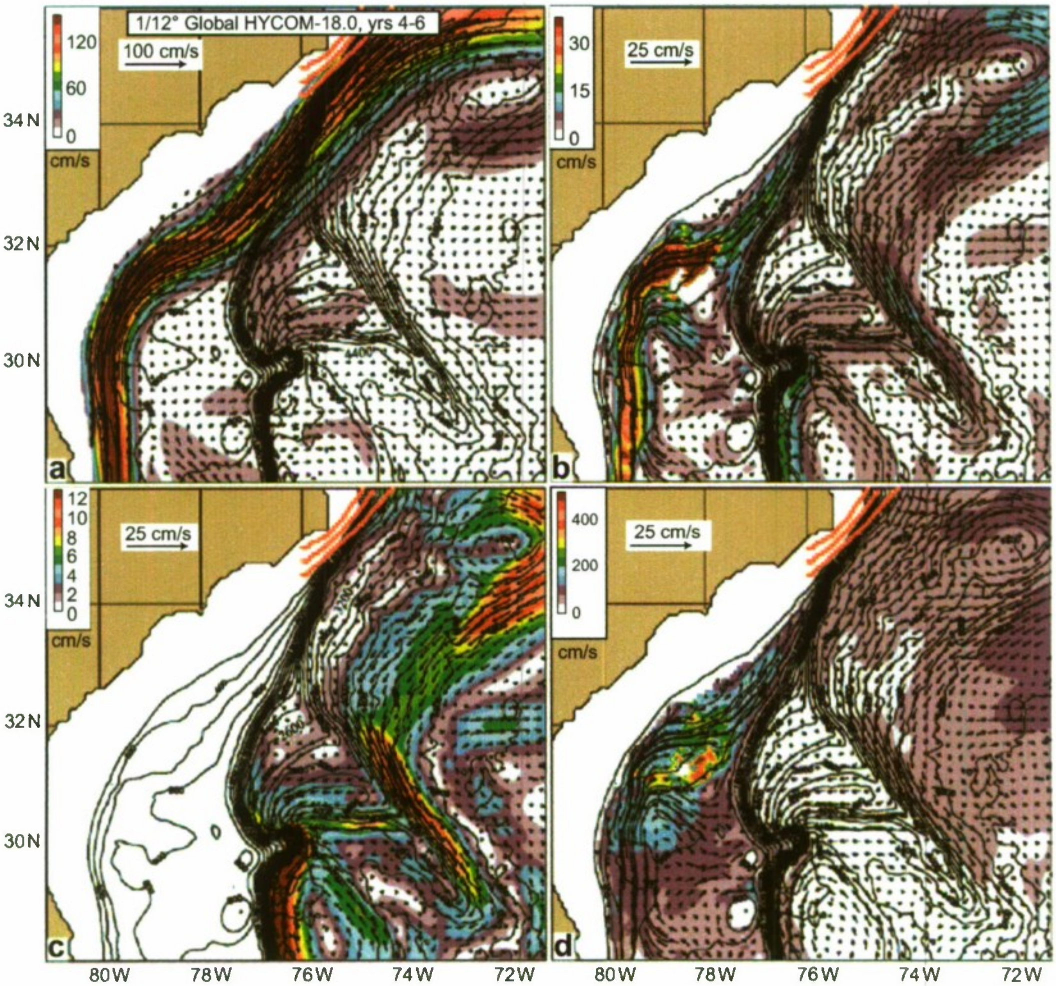

Fig. 21.25 Same as Fig. 21.24 except that results are from 1/12° global HYCOM-18.0, years 4–6 (Table 21.1)

and 21.25). The near bottom EKE is much higher in the 1/25° global HYCOM simulation and extends farther southward over the Blake Plateau. In addition, there is a closed eddy-driven bottom gyre not seen in the 1/12° simulation. Both the 1/12° and 1/25° simulations exhibit a small mean offshore meander immediately downstream of the Charleston bump where the inner edge of the mean currents temporarily follows a deeper isobath (400 m) (1/25° in Fig. 21.24a and 1/12° in Fig. 21.25a).

The second type of variability is larger amplitude meanders similar to that seen in Fig. 21.26a, c, but in observations (e.g., Bane and Dewar 1988; Glenn and Ebbesmeyer 1994b, their Plate 1; Legeckis et al. 2002, their Fig. 5) such features are transient on times scales up to a few months, whereas Fig. 21.26 depicts means over year 3 of the 1/25° global HYCOM simulation. Animations of SSH, used to monitor the simulated variability, also show the larger meanders occurring as transients in other years of the 1/25° simulation and in the near twin 1/12° simulation, where the amplitude is smaller. In addition, the animations show highly variable meandering in year 3 of the 1/25° simulation (Fig. 21.26b). These meanders tend to pause and

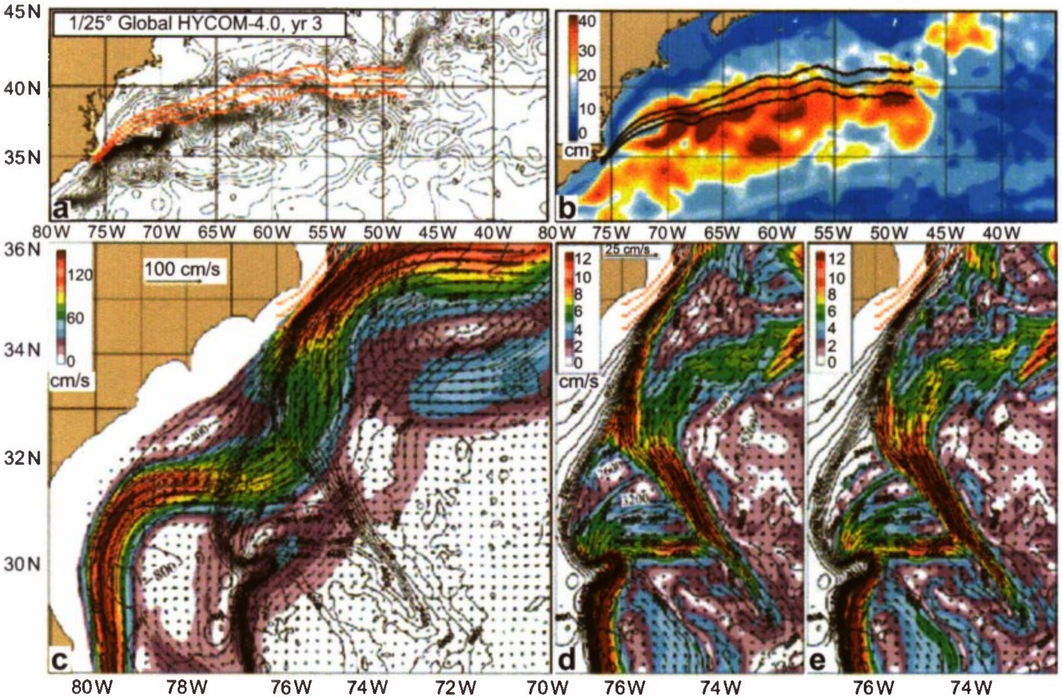

Fig. 21.26 Simulation of an unrealistic mean meander upstream of Gulf Stream separation from 1/25° global HYCOM-4.0, year 3 (Table 21.1): **a** Mean SSH. **b** SSH variability, and **c–e** Mean currents (*arrows*) and isotachs (*color*) overlaid on topographic contours in the SAB. **c** Near surface currents at ~25 m depth and **d**, **e** Depth averages from **d** ~2,000 m to the bottom and **e** ~3,000 m to the bottom. The color contour intervals are **a**, **b** 5 cm. **c** 12 cm/s, and **d**, **e** 1 cm/s

amplify between the northern end of the Charleston bump near 32°N and ~33°N in a region where the northern boundary of the Blake Bahama Outer Ridge separates from the Blake Escarpment near 2,000 m depth (Fig. 21.23).

Unrealistic mean meanders, such as seen in Fig. 21.26a, c, occasionally occur in simulations by a variety of ocean models, including the z-level Los Alamos POP model (Smith et al. 2000), the MICOM isopycnal model (Chassignet and Marshall 2008, their Fig. 9), NLOM (Hurlburt and Hogan 2008), and here HYCOM. They have been controlled by increasing coefficients of biharmonic dissipation (Smith et al. 2000; Chassignet and Marshall 2008) or by injecting the DWBC northern boundary inflow along deeper isobaths in simulations like those in Sect. 21.2. This type of unrealistic meander (e.g., Fig. 21.26a, c) occurs when there are strong mean abyssal currents along the 2,700–3,200 m isobaths where the Blake Bahama Outer Ridge separates from the Blake Escarpment. These currents flow southeastward along the north side of the Blake Bahama Outer Ridge near the ridge crest. In the process they cross under the Gulf Stream and advect it off shore (Fig. 21.26c–e). The cross-under to deeper depths facilitates the advection process because it allows the abyssal currents to better follow the north side of the deepening ridge crest, as can be seen by comparing Fig. 21.26d, e, the latter limited to deeper depths. Particularly, compare the current along the northeastern side of the ridge from the location where it separates from the Blake Escarpment to the 3,000 m isobath where part of the abyssal current turns southwestward from the ridge crest to the Blake Nose and flows along the 2,800–3,200 m isobaths, approximately antiparallel to the outer edge of the Gulf Stream. Here the 3,000 m isobath lies near the outer edge of the Gulf Stream mean flow that continues to the northeast. Note in comparison to the abyssal current responsible for offshore advection of the Gulf Stream, the corresponding current mean over years 5–8 from the same simulation (Fig. 21.24c) is much weaker and in the 1/12° simulation (Fig. 21.25c) it is nearly absent. Also note the Blake Nose is a junction where abyssal currents following a variety of pathways along different isobaths meet to form a strong DWBC flowing southward along the steep slope of the Blake Escarpment (Figs. 21.24c, 21.25c, and 21.26d, e).

The conduit for abyssal currents from the ocean interior, discussed in Sect. 21.2 and earlier subsections of Sect. 21.3, rejoins the abyssal flow along the continental slope near 33°N. Generally, this flow remains seaward of the Gulf Stream. However, in this case (Fig. 21.26c–e), it crosses under the offshore loop of the Gulf Stream simulation. As it flows southwestward on the north side of the loop, it crosses to shallower depths beneath the Gulf Stream and acts to advect its pathway shoreward, keeping it adjacent to the western boundary just upstream of separation at Cape Hatteras. This occurs not only because of the abyssal current pathway from the interior, but also because of the westward intrusion of relatively deep isobaths to the base of a very steep segment of the continental slope. Chassignet and Marshall (2008, their Fig. 9) also depict the mean Gulf Stream loop returning to the western boundary prior to separation. As the cross-under abyssal current continues to the south, the speed of the current greatly increases in a confluence along the steep northern slope of the Blake Bahama Outer Ridge, demonstrating the potential for even larger amplitude meanders with a lobe extending southeastward. That did not occur in the case of the loop simulated in Fig. 21.26a, c because the abyssal currents along the 2,800–3,200 m isobaths did not advect it far enough off shore for the deeper abyssal currents to continue the offshore advection process.

It has been suggested that the development of large amplitude meanders in the SAB is triggered by Gulf Stream interaction with cold core rings from the Sargasso Sea, rather than offshore deflections of the Gulf Stream at the Charleston bump (Glenn and Ebbesmeyer 1994b). The 10-year SSH animations from both the 1/12 and 1/25° global HYCOM simulations, discussed in this subsection, show such interactions occurring. Year 8 of 1/25° global HYCOM even demonstrates the generation of a strong modon when a strong anticyclonic eddy adjacent to the elbow of a large meander triggers the shedding of a cyclonic eddy from the elbow on the north side of the anticyclonic eddy. The modon subsequently propagated eastward to 62°W centered along ~28°N. A modon generated in a similar manner is illustrated near 27°N, 69°W in Hurlburt and Hogan (2000, their Fig. 4d). Although Gulf Stream—eddy interaction was involved in the development and evolution of some large meanders, many of them developed without such interaction. This result indicates that flow instabilities in the vicinity of the Charleston bump are sufficient to generate such meanders (near bottom EKE in Figs. 21.24d and 21.25d and near bottom mean currents in Figs. 21.24b and 21.25b over the Charleston bump and adjacent Blake Plateau), with a possible contribution from abyssal current advection of the Gulf Stream pathway where the north slope of the Blake Bahama Outer Ridge separates from the Blake Escarpment near 33°N.

21.4 Impact of Data Assimilation on Model Dynamics in the Gulf Stream Region

We can investigate the impact of data assimilation on the Gulf Stream pathway and dynamics using a set of near-twin experiments with the 1/12° global HYCOM. Each of these experiments starts from an initial state forced by ECMWF climatology for the surface momentum and heat. However, starting points for the two experiments are different. The first set of twin experiments starts from a spin up forced by an ERA-15 climatology, while the second set starts from a spin up forced by an ERA-40 climatology with the 10 m winds increased using QuikSCAT wind speed statistics (Kara et al. 2009). The interannual forced simulations use the Navy Operational Global Atmospheric Prediction System (NOGAPS) fluxes with an adjustment of the mean winds to the ECMWF climatology in the first experiment and in the second experiment with a scaling of the 10 m wind speeds using QuikSCAT wind speed statistics without the adjustment to the ECMWF climatology. For this discussion, the mean is taken over the last 3 years (2004–2006) for the first experiment and only one year (06/2007 to 05/2008) in the second experiment.

Two data assimilative hindcasts (data assimilative model runs not performed in real time) are used in this study. In both hindcasts, the data are assimilated via the Navy Coupled Ocean Data Assimilation system (NCODA, Cummings 2005) using a multivariate optimal interpolation. Both use the same atmospheric forcing as the corresponding non-assimilative simulation. The difference between the data assimilation in the two hindcasts is the treatment of the along-track altimetric sea surface height anomalies (SSHAs). The first hindcast, which will be designated as C-H assimilation, is a twin of the 4 year non-assimilative interannual forced simulation with the SSH updates extended into the ocean interior by adjusting the layer thickness, as proposed by Cooper and Haines (1996). The SSH updates are obtained (a) by adding the altimetric SSHAs to a model-based mean SSH and then (b) using NCODA to perform an SSH analysis with a model forecast as the first guess. For this purpose, the mean SSH from the ERA-15 forced climatological simulation, used to initialize the hindcast, is adjusted to the observed mean Gulf Stream pathway via a rubber-sheeting technique (Smedstad et al. 2003). The last three years of the corresponding simulation and hindcast are used for analysis. The second hindcast, which will be designated as MODAS assimilation, uses the Modular Ocean Data Assimilation System (MODAS, Fox et al. 2002, Barron et al. 2007) to extend the SSHA into the ocean interior via synthetic profiles of temperature and salinity, with the mean surface dynamic height coming from the MODAS climatology. It is a twin of the 2007–2008 simulation. Only the time period covering the last year of the 1.5 year hindcast is used for analysis. For more information on the 1/12° global HYCOM prediction system see Hurlburt et al. (2008a) and Chassignet et al. (2009).

21.4.1 Interannually Forced Simulation with a Weak Gulf Stream

The mean velocity in layer 6, ~25 m deep, for each of the four simulations is shown in Fig. 21.27 along with the 15 year mean IR northwall pathway. The interannual simulation, initialized from the ERA-15 spin up, generates a weak Gulf Stream (Fig. 21.27a). The Eulerian mean core speed south of the separation point is 1.1 m/s and it decreases rapidly to the east becoming <0.4 m/s near 72°W. The weak Gulf Stream is associated with weak mean abyssal currents, as shown in Fig. 21.28a. The key southward abyssal current at 72°W is weak with a speed <0.4 cm/s and displaced to the south. The observed key current at 68.5°W is absent as are two observed deep cyclonic gyres (Figs. 21.5 and 21.6). The strongest abyssal flows

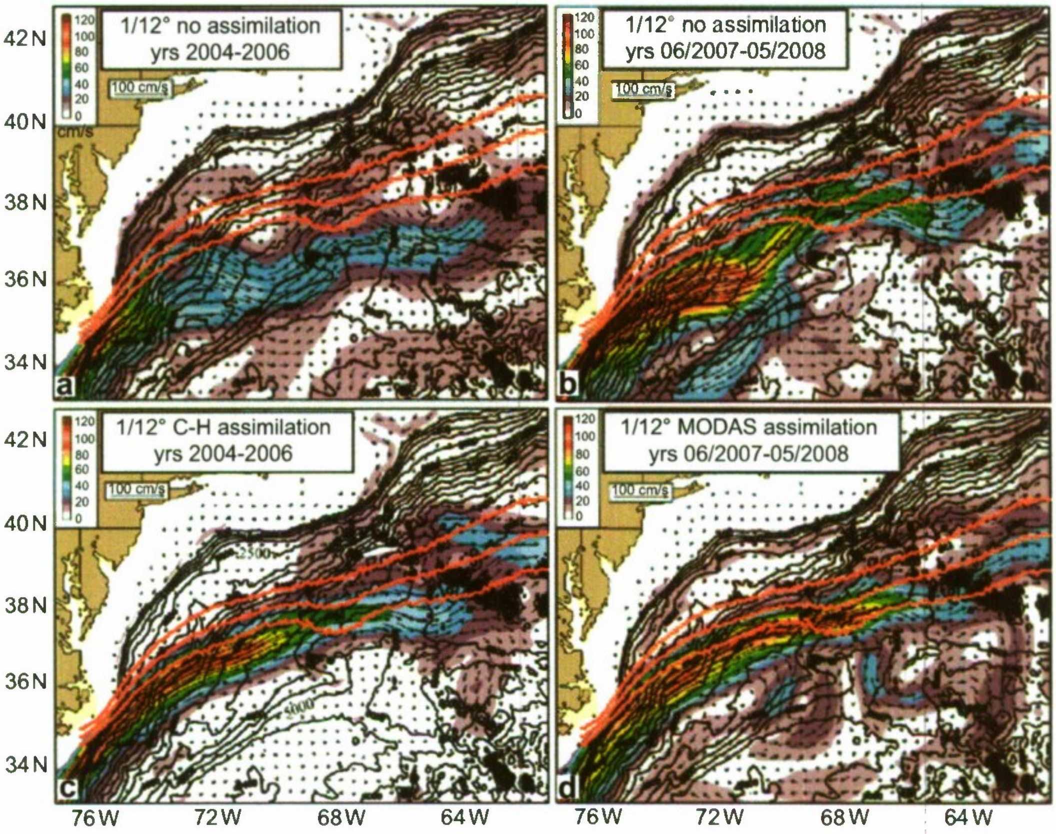

Fig. 21.27 Mean velocities in layer 6, ~25 m, with the 15-year mean Gulf Stream northwall pathway ±1σ by Cornillon and Sirkes overlaid in red and the bathymetry contoured at 200 (500) m intervals at depths >(<) 3,000 m from four 1/12° global HYCOM simulations or hindcasts: **a** Interannually forced weak Gulf Stream with separation velocity of 1.1 m/s, 12° global HYCOM-5.8. **b** Interannually forced stronger Gulf Stream with separation velocity of 1.4 m/s, 1/12° global HYCOM-19.0. **c** Cooper and Haines (1996) data assimilative twin, 1/12° global HYCOM-60.5, of the weak Gulf Stream simulation, and **d** MODAS synthetic temperature and salinity profile data assimilative twin, 1/12° global HYCOM-74.2, of the stronger Gulf Stream simulation (see Table 21.1)

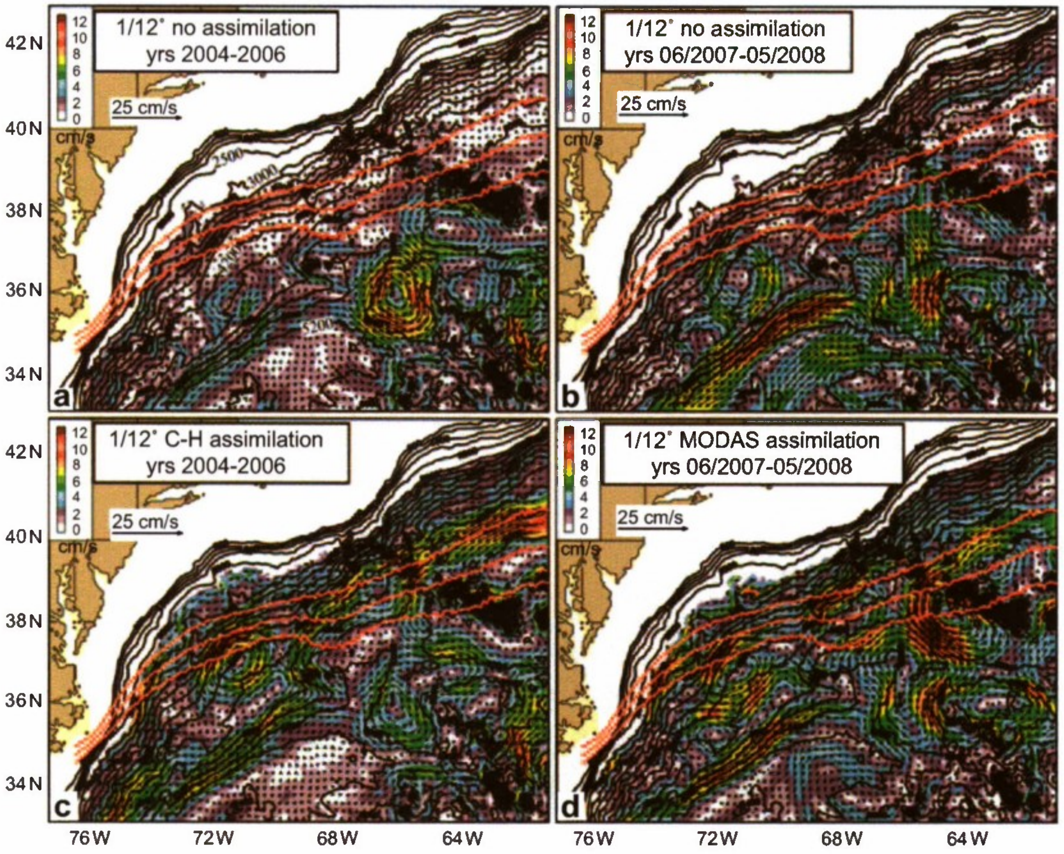

Fig. 21.28 Mean depth averaged velocities in layers 27 to 29, below ~3,000 m depth, with the 15-year mean Gulf Stream northwall pathway ±1σ by Cornillon and Sirkes overlaid in red and the bathymetry contoured at 200 (500) m intervals at depths >(<) 3,000 m from the same four 1/12° global HYCOM simulations or hindcasts as Fig. 21.27: **a** Interannually forced weak Gulf Stream with separation velocity of 1.1 m/s. **b** Interannually forced stronger Gulf Stream with separation velocity of 1.4 m/s. **c** Cooper and Haines (1996) data assimilation twin of the weak Gulf Stream and **d** MODAS synthetic temperature and salinity profile data assimilation twin of the stronger Gulf Stream

are found in an anticylonic gyre near (36°N, 66°W), which steers the Gulf Stream slightly northward. Near Cape Hatteras, the mean Gulf Stream shows two pathways, one path overshooting the separation point and clinging to the continental slope while another pathway with most of the flow turns almost due east. After separation, the mean pathway lies southward of the mean IR pathway.

The AMOC also is weak and shallow with a transport less than 11 Sv (Fig. 21.29a). Evidence for weak baroclinic instability can be found in (1) the large area of high SSH variability west of 70°W (Fig. 21.30a), (2) a weak southern recirculation gyre west of 70°W (Fig. 21.27a), (3) the eddy-driven mean abyssal gyre centered directly beneath the surface gyre over relatively flat topography (Fig. 21.28a) and (4) the associated deep EKE (not shown). The separating Gulf Stream pathway lies along the northern edge of the associated recirculation gyres. The location of the eddy-

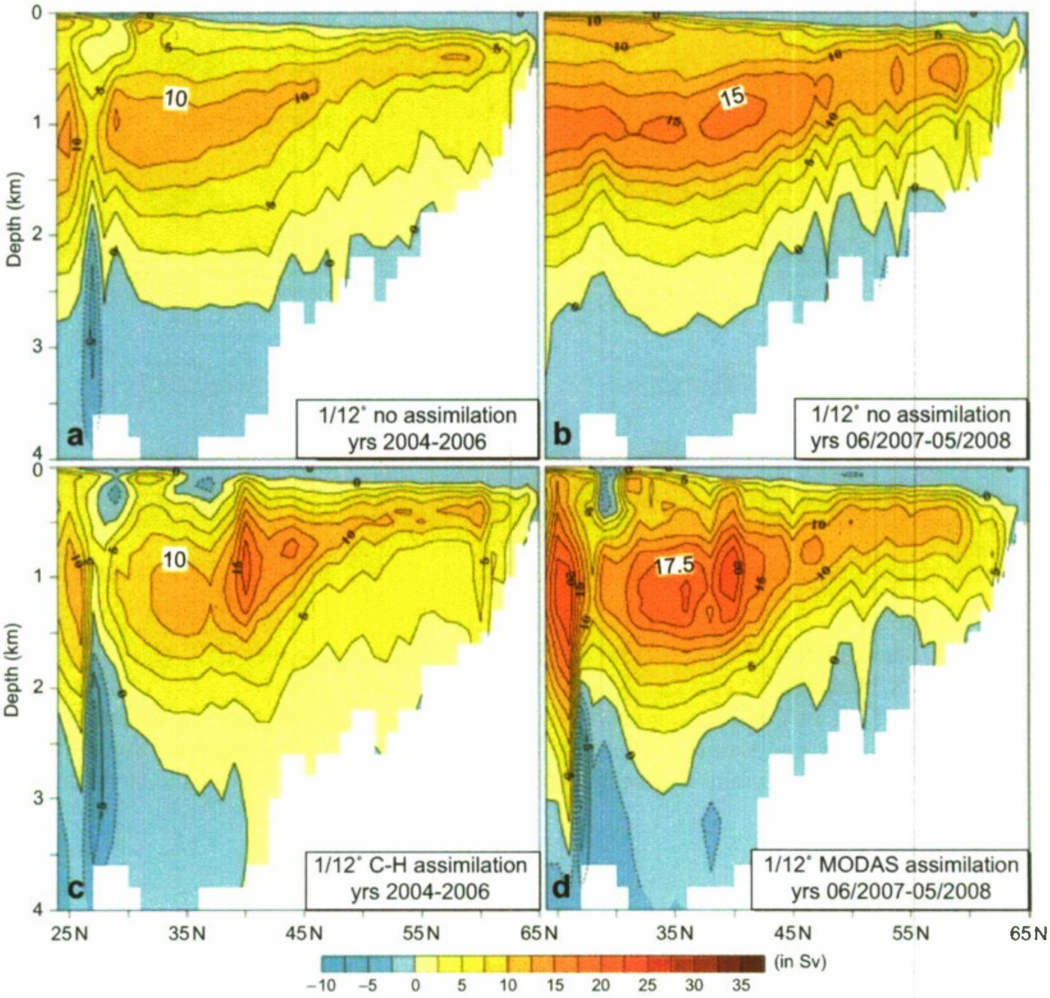

Fig. 21.29 AMOC streamfunction north of 24°N from the same four 1/12° global HYCOM simulations or hindcasts as Fig. 21.27: **a** Interannually forced weak Gulf Stream with separation velocity of 1.1 m/s. **b** Interannually forced stronger Gulf Stream with separation velocity of 1.4 m/s. **c** Cooper and Haines (1996) data assimilation twin of the weak Gulf Stream and **d** MODAS synthetic temperature and salinity profile data assimilation twin of the stronger Gulf Stream

driven mean abyssal gyre relative to the southern edge of the separating jet and the location of the northwestern most flat topography suggests a topographic role in the separating pathway driven by baroclinic instability of the separating jet.

21.4.2 Interannually Forced Simulation with a Stronger Gulf Stream

The interannual simulation using ERA-15 spin up and NOGAPS winds yields a too weak Gulf Stream. Kara et al. (2009) found that the QuikSCAT winds are highly

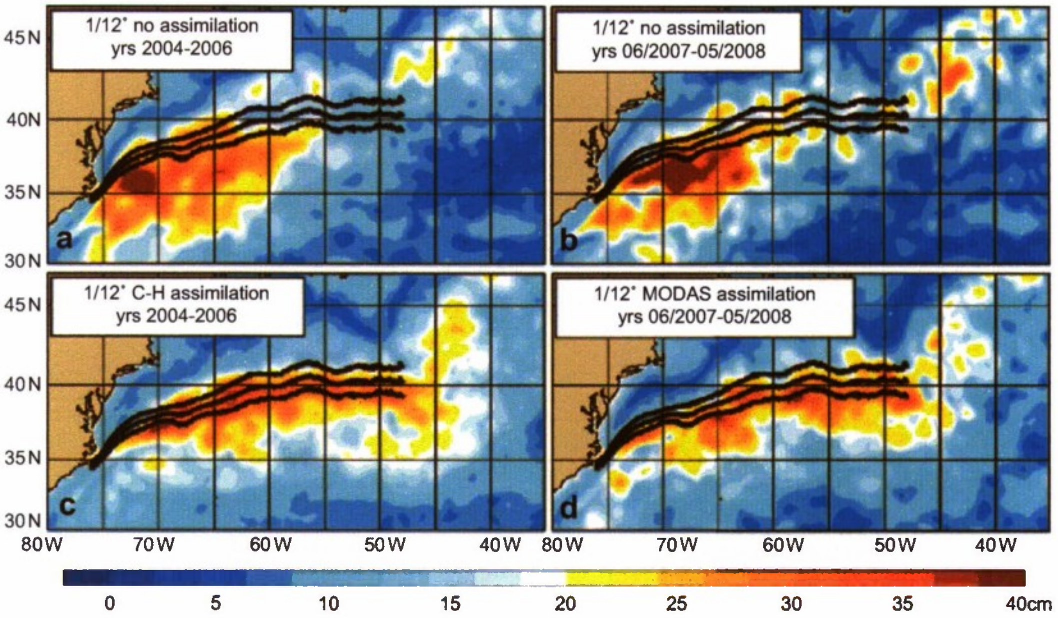

Fig. 21.30 Standard deviation of the sea surface height from the same four 1/12° global HYCOM simulations or hindcasts as Fig. 21.27: **a** Interannually forced weak Gulf Stream with separation velocity of 1.1 m/s. **b** Interannually forced stronger Gulf Stream with separation velocity of 1.4 m/s. **c** Cooper and Haines (1996) data assimilation twin of the weak Gulf Stream and **d** MODAS synthetic temperature and salinity profile data assimilation twin of the stronger Gulf Stream

correlated with the NOGAPS NWP winds, but that significant errors in the strength of the winds exist. Kara et al. propose a regression based correction for the NWP winds. This correction is applied to a new model spin up using the ERA-40 climatology to generate a new initial condition for an interannual forced simulation based upon regression corrected NOGAPS winds. Only 1 year from June 2007 to May 2008 is available for analysis. The mean Gulf Stream is stronger and the path much more realistic than the simulation described in Sect. 21.4.1 The core speed in layer 6 (~25 m) near the mean separation point is 1.4 m/s and remains greater than 1 m/s at 70°W, with the speed decreasing rapidly to the east of 70°W (Fig. 21.27b). A strong recirculation gyre is observed centered at (34.5°N, 72°W). The abyssal flow shown in Fig. 21.28b is stronger than the uncorrected NOGAPS forced simulation with temporal mean winds from ERA-15. The key abyssal current at 72°W and the associated cyclonic gyre are present but the key abyssal current near 68.5°W is absent. The eddy-driven abyssal circulation with speeds < 8 cm/s, flows under the Gulf Stream near 36°N, 72°W helping to steer the flow southward into the recirculation gyre, while the northward flow in the cyclonic abyssal gyre steers the Gulf Stream northward at 70°W. The AMOC is very shallow and relatively weak, with transport less than 16 Sv (Fig. 21.29b). The SSH variability in Fig. 21.30b shows a strong recirculation gyre, but little eddy activity east of 60°W. The pathway in this simulation is more realistic, but still inconsistent with the observed SSH variability and the relevant key abyssal currents, and the AMOC is relatively weak and shallow. This simulation is quite similar to one discussed in Sect. 21.3.3 with a realistic pathway but unrealistic dynamics.

21.4.3 Cooper-Haines Data Assimilation

The data assimilative hindcast starts from the end of the ERA-15 climatology simulation using NCODA to assimilate satellite SST, the SSH updates, and in situ temperature and salinity profiles, and also using C-H for downward projection of the SSH updates. The assimilation generates a mean Gulf Stream that follows the IR path from the coast out to 68°W, as seen in Fig. 21.27c. East of 68°W, the flow diverts southward of the IR path, turning sharply northward and splitting as the Stream crosses the New England Seamount Chain (NESC) at 64°W. The SSH variability shown in Fig. 21.30c reproduces all of the features found in the observed altimetric SSH variability shown in Fig. 21.8, which is an expected result since these data are assimilated. The Eulerian mean core speed of the Gulf Stream at the separation point near Cape Hatteras is relatively weak at only 1.1 m/s, which is about the same as the non-assimilative simulation. The assimilative Gulf Stream is much stronger to the east with Eulerian mean speeds of 0.8 m/s at 70°W and 0.6 m/s at 65°W.

A surprising result is the strong abyssal circulation in the hindcast shown in Fig. 21.28c. The key abyssal currents at 72°W and 68.5°W are present with strengths of 10 cm/s and 8 cm/s respectively. The southward flow at 72°W is associated with a cyclonic gyre. As a consequence of the C-H downward projection of the SSH updates, the AMOC is strengthened, with transport greater than 18 Sv, and the southward branch of the AMOC is stronger at deeper depths than in the non-assimilative simulation (Fig. 21.29c vs. 21.29a). The result is mean abyssal currents along deeper isobaths of the continental slope. Despite a weak Gulf Stream at Cape Hatteras, data assimilation generates a vigorous eddy field that drives a strong abyssal circulation. The eddy-driven contribution to the mean abyssal circulation is the result of vortex stretching and compression associated with the data-assimilative approximation to the observed meandering of the Gulf Stream and associated eddies. In Fig. 21.28c the stronger and deeper mean abyssal currents along the continental slope feed into the abyssal currents that cross under the Gulf Stream near 69° and 72°W and interact with the eddy-driven abyssal circulation. Although we can demonstrate that the data assimilative hindcast has a mean abyssal circulation in accord with available observational evidence and a theory for Gulf Stream pathway dynamics in this region that is also supported by the observational evidence, no observational evidence is available to determine whether or not the same is true for the time dependent evolution of the abyssal circulation. The results of Hurlburt (1986) suggest that this could be occurring. In a set of two-layer model experiments with the SSH field updated every 20 or 30 days from a non-assimilative control run, the abyssal circulation converged toward the time dependent abyssal circulation of the control run even in the most challenging examples with strong baroclinic-barotropic instability and a flat bottom.

21.4.4 MODAS Data Assimilation

The second data assimilative example starts on 1 June, 2007, taking its initial condition from the ERA-40 QuikSCAT scaled simulation. The assimilation is performed through NCODA with the SSHA extended into the ocean interior using synthetic profiles of temperature and salinity from MODAS. The mean Gulf Stream follows the IR path extremely well to the east past the NESC to 62°W, as shown in Fig. 21.27d. The Eulerian mean core speed near Cape Hatteras is weak, only 1.0 m/s. However, core speed is a maximum of 1.2 m/s at 72°W and exceeds 0.65 m/s at 65°W. The SSH variability reproduces the observed altimetric SSH variability (Fig. 21.30d). The eddy driven abyssal circulation is strong, with the key southward abyssal currents exceeding 10 cm/s. Each of the key currents is associated with a strong cyclonic gyre, as shown in Fig. 21.28d. The AMOC is the strongest, exceeding 20 Sv, and the southward branch extends the deepest of the four simulations or hindcasts (Fig. 21.29d). Assimilating the MODAS synthetic profiles appears to generate the most realistic Gulf Stream system with strong eddies along the entire path driving a strong abyssal circulation.

21.4.5 A Comparison of Model Forecasts to Hindcast States

The daily MODAS hindcasts (Sect. 21.4.4) from 48 different dates were used to initialize a 14 day forecast. The forecast skill of the HYCOM data assimilative model has been discussed in Hurlburt et al. (2008a, 2009). The assimilative model significantly beats persistence out to 14 days. However, the skill of the model is insignificant after about 10 days, with the median anomaly correlation between the forecast and the analysis for SSH dropping below 0.6 beyond 10 days in the Gulf Stream region. We can compare the effects of the model dynamics on the forecasts by using the differences between the forecast mean Gulf Stream and the analyses. In Fig. 21.31, the mean velocities in layer 6 (~25 m) and layers 27–29 (~3,000 m to the bottom) from 48 forecasts are shown. The 5 day forecast has appreciable skill with a median SSHA correlation of 0.8, but the 14-day forecast has little skill. In the forecasts, we find significant changes in the upper layer flow, but only modest changes in the abyssal circulation. The 5 day forecast still tracks the mean IR path west of the NESC (64°W), but the core speeds have decreased by approximately 0.1 m/s along the entire Stream. The core speeds in the 14 day forecast have decreased substantially with the speed at 72°W dropping below 0.8 m/s. The path of the Gulf Stream is deflected southward around 68.5°W, presumably steered southward by the strong southward abyssal current at 68.5°W. The AMOC (not shown) for the 14 day forecast is slightly weaker and shallower than either the 5 day forecast or analyses. The Gulf Stream in the forecasts is still inertial, with the variability driven by the instability of the flow. However, the dynamics of the model are insufficient to maintain a strong flow eastward to the NESC and the forecast Gulf Stream weakens

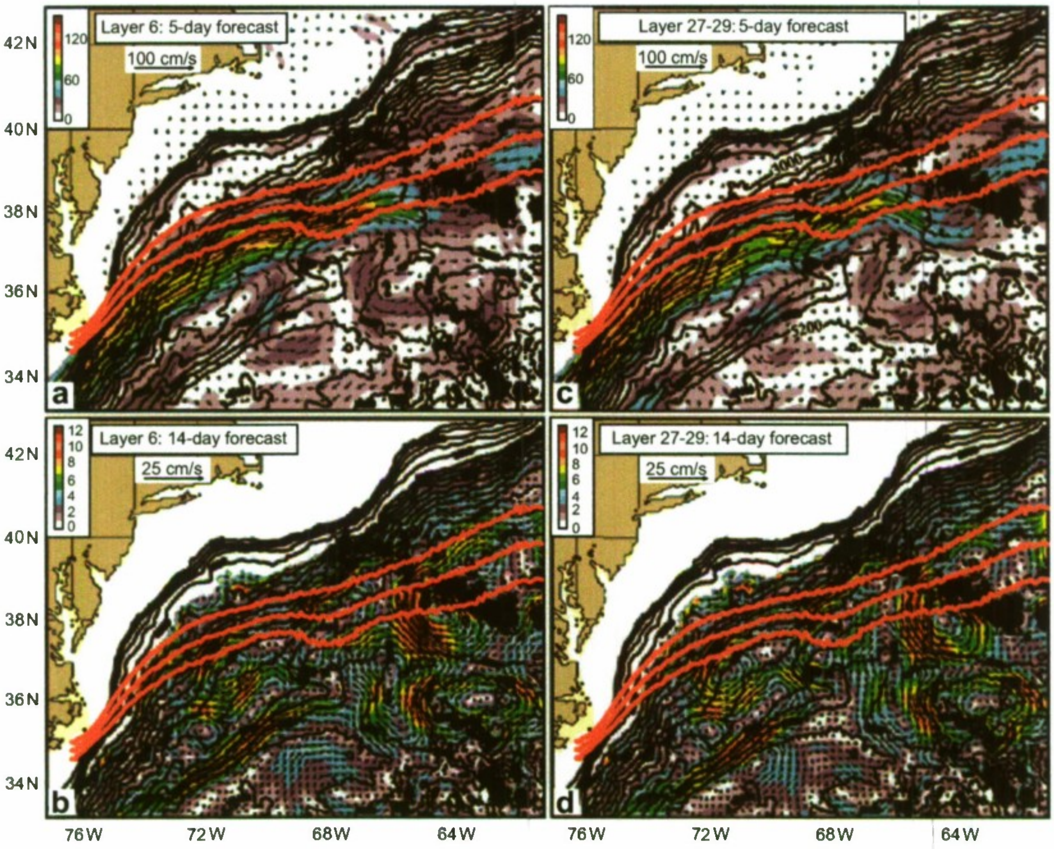

Fig. 21.31 The mean velocities for the forecasts starting from the state estimates of the MODAS data assimilation with the layer 6 (~25 m) velocities for the **a** 5-day forecast and the **b** 14-day forecast and the layer 27 to 29 (below ~3,000 m depth) velocities for the **c** 5-day forecast and the **d** 14-day forecast. The 15-year mean Gulf Stream northwall pathway ±1σ by Cornillon and Sirkes is overlaid in red and the bathymetry is contoured at 200 m intervals

over the 14 day period. The abyssal circulation appears to have a longer time scale showing little change in the mean over the 14 day forecast period. Thus, the steering by the abyssal currents helps to maintain a reasonable pathway, but the dynamics cannot maintain the strength of the Gulf Stream.

21.5 Summary and discussion

Dynamical understanding and evaluation of current systems simulated by eddy-resolving OGCMs is an essential step in the development of accurate models to aid in a greater understanding of the ocean circulation and to improve ocean weather and climate prediction. Here the Gulf Stream is the subject of investigation, including examples with and without data assimilation, because it is a major current system that is challenging to simulate and understand and because Gulf Stream simulations have demonstrated great sensitivity to small changes in simulation design, such as subgrid-scale parameterizations and parameter values. Several non-assimilative OGCMs of different design have yielded realistic simulations, as illustrated here, but consistently realistic results have not been obtained from any of them. Instead, these OGCMs have also demonstrated a variety of similar flaws.

Key aspects of Gulf Stream dynamics were identified using a simpler eddy-resolving model. The model is purely hydrodynamic with only five Lagrangian layers in the vertical, but includes sufficiently realistic boundary geometry, bathymetry, wind forcing, and AMOC to (1) simulate the dynamics of Gulf Stream separation and its pathway to the east, (2) permit detailed comparison with relevant observations, and (3) allow a detailed explanation of the dynamics (Sect. 21.2). In brief form, an eddy-driven abyssal current, typically augmented by the DWBC, the local topographic configuration, and a Gulf Stream feedback mechanism constrain the latitude of the Gulf Stream near 68.5°W. Between the western boundary and ~70°W the Gulf Stream pathway closely follows a CAV trajectory. Neither part of this explanation is sufficient alone. Constraint of the Gulf Stream latitude near 68.5°W is not a sufficient explanation of the pathway between the western boundary and ~69°W. However, without assistance from this constraint, Gulf Stream simulations with realistic speeds at the core of the current are not sufficiently inertial to overcome the linear solution demand for a pathway that overshoots the observed latitude (and a CAV trajectory).

The essential observational metrics are (a) agreement with the observed mean pathway, (b) agreement with the observed narrow band of high SSH variability between the western boundary and ~69°W to support the interpretation as a CAV trajectory, (c) realistic mean speed at the core of the current near separation from the western boundary (1.6–2.1 m/s), and (d) simulation of the key observed abyssal current near 68.5°W. Other observational and dynamical metrics are also useful. With the possible exception of a linear solution, starting with a simplified model is helpful but generally not a necessary step, as illustrated in the dynamical evaluation of OGCM simulations with several types of flawed dynamics.

The dynamics of simulations by four different eddy-resolving OGCMs (HYCOM, MICOM, NEMO, and POP) without data assimilation are evaluated in Sect. 21.3. The horizontal resolution and model domain range from 1/10° Atlantic to 1/25° global. Simulations by both the simplified model and the OGCMs demonstrate that it is possible to simulate a realistic Gulf Stream pathway with generally realistic dynamics without showing complete agreement with the relevant observational evidence, but with evidence of a possible sacrifice in simulation robustness, discussed later. In particular, three OGCM simulations yield a realistic Gulf Stream pathway, but do not simulate the key abyssal current near 68.5°W. Instead two mean abyssal currents that cross under the simulated Gulf Stream near 65.5 and 67.5°W perform essentially the same function at the appropriate latitude, but without the observational evidence to confirm or refute their existence. Another simulation has a realistic mean Gulf Stream pathway, but fails in relation to the other observational metrics and thus simulates a realistic pathway with unrealistic dynamics.

The remainder of Sect. 21.3 addressed dynamical evaluation of simulations with common types of flawed pathways upstream and downstream of Gulf Stream separation at Cape Hatteras. Downstream the simulations may have premature separation, pathway segments that are too far south west of roughly 67°W, or pathways that overshoot the observed latitude west of ~69°W. Upstream problems occur with unrealistic looping away from the coast and excessive small amplitude meandering that propagates downstream of Cape Hatteras and unrealistically increases the variability in the region within a few degrees after separation. The simulations demonstrate the greatest sensitivity to *differences in* AMOC strength and the depth structure of its southward abyssal flow, the abyssal currents in relation to the isobaths, the wind forcing, the inertial character of the separating jet, and the horizontal model resolution. In relation to pathway simulation skill, they demonstrate less sensitivity to *differences in* model design and model topography, even though there is great sensitivity to topographic features. The biggest problem occurs with the shallow vertical structure of the simulated AMOC southward abyssal flow and its relation to the isobaths because of its impact on the pathways of abyssal currents upstream and downstream of Gulf Stream separation. Upstream of separation, an unrealistically persistent Gulf Stream meander away from the coast can occur when strong mean abyssal currents follow isobaths in the depth range 2,700–3,200 m. Currents in that depth range separate from the Blake Escarpment and flow southeastward along the north slope of the Blake Bahama Outer Ridge near the ridge crest. In the process they cross under the Gulf Stream, advecting its pathway off shore, a problem occasionally seen in almost all of the models.

Downstream of Cape Hatteras, flow along particular, relatively deep isobaths is required to generate the key abyssal current near 68.5°W or the alternatives near 67.5 and 65.5°W. These abyssal currents are very weak or missing in the simulations with premature separation, a pathway segment with a southern bias, or a realistic pathway with unrealistic dynamics. The depth of the AMOC-related abyssal currents along the isobaths can directly affect the Gulf Stream pathway through advection but can also affect the stability properties of the simulated Gulf Stream and the interaction between AMOC-driven and eddy-driven abyssal currents. Thus the hypersensitivity of Gulf Stream simulations to small changes, such as subgrid-scale parameterizations and parameter values, can be traced to a hypersensitivity to the location of abyssal currents in relation to the isobaths and to the need for flow along particular isobaths in order to constrain the latitude of the Gulf Stream near 68°W. This sensitivity is aggravated by the tendency of ocean models to simulate an AMOC with a southward abyssal limb that is too shallow.

The simulations with a southern pathway bias exhibit abyssal currents, partly originating along isobaths shallower than 3,000 m, which cross under the simulated Gulf Stream to deeper depths at the separation point. They also depict an eddy-driven mean abyssal gyre centered near 72°W over a band of flat topography, a gyre that abuts the southern edge of the Gulf Stream. The simulations exhibit additional eddy-driven abyssal gyres farther to the east along the Gulf Stream segment with a southern bias. Very similar gyres occur in a 1/10° Atlantic POP simulation and one of the 1/12° global HYCOM simulations and quite different gyres in the 1/12° Atlantic NEMO and two other 1/12° global HYCOM simulations. The two strong cyclonic abyssal gyres along the north side of the Gulf Stream in the similar POP and HYCOM simulations also contribute to the southern pathway bias in those simulations. In all five simulations the Gulf Stream pathway follows the underlying eddy-driven abyssal currents for about 10° to the east, resulting in a mean Gulf Stream pathway that is strongly influenced by flow instabilities and thus a pathway that is dynamically very different than that observed.

The three OGCM simulations with an overshoot pathway (all by HYCOM) succumb to the demands of linear dynamics for a pathway with a northern bias with both the wind forcing and the AMOC contributing to that demand. The wind forcing product that forced the OGCM simulations with an overshoot pathway also yields the strongest tendency for an overshoot pathway based on linear dynamics. The simulation with the strongest overshoot has the second strongest AMOC and the most inertial Gulf Stream at the separation point (at the top end of observed speed). The strength of the AMOC in the other two overshoot simulations is typical, but the three simulations using the same model and wind forcing with a weak AMOC simulate a pathway with a southern bias or a realistic pathway with unrealistic dynamics. Although the overshoot simulations have abyssal current pathways that might constrain the Gulf Stream pathway, the 1/12° Atlantic MICOM simulation with a realistic Gulf Stream pathway has a much more robust abyssal current constraint on the Gulf Stream pathway in close agreement with observational evidence. It also has the strongest AMOC with a southward limb that extends deeper than in the three HYCOM simulations and a mean DWBC that includes observed strong flow along isobaths that feed into the key abyssal current near 68.5°W.

Bifurcations are a common occurrence in the Gulf Stream simulations and abyssal currents often play a role. Several of these roles are discussed in the section on overshoot pathways. In two of these simulations abyssal currents cause a major bifurcation of the Gulf Stream. More commonly they split off flow near the edge of the Gulf Stream and help define the eastern edge of a southern recirculation gyre. On the near-shore edge of the Gulf Stream an abyssal current constraint can also define a bifurcation between flow that separates from the shelf/slope and flow that becomes a shelf slope current. In cases where they create a bifurcation on the north side of the stream, often the result for the northern branch is a partial transition toward a pathway more consistent with linear dynamics, but a transition that can be limited by underlying abyssal currents.

Results from the simpler hydrodynamic model suggest that doubling the resolution from ~7 km to 3.5 km at mid-latitudes would reduce simulation sensitivity to the AMOC by increasing the inertial character of the simulated Gulf Stream and increasing the strength of the eddy-driven abyssal circulation. A comparison of the nearly twin 1/12 and 1/25° global HYCOM simulations yields some support for this finding. Each of these simulations was run for 10 years after initialization from climatology, an initial state used by all the OGCM simulations considered here. Starting in year 2, both develop a Gulf Stream pathway with a southern bias after separation from Cape Hatteras. Later both develop a realistic pathway, but ultimately both develop an overshoot pathway. However, the 1/12° simulation has a realistic mean pathway for only one year (year 8), while the 1/25° simulation has a realistic pathway for four years (years 5–8). Both have shallower southward flow in the

AMOC and a weaker abyssal current constraint on the Gulf Stream pathway than the MICOM simulation and with a 5% increase in the strength of the AMOC and especially conducive wind forcing, both ultimately develop an overshoot pathway.

Data assimilation has a strong impact on the Gulf Stream dynamics, especially on variables that are sparsely observed or, in some cases, not at all in real time (Sect. 21.4). Identical non-assimilative simulations are used as controls to help assess the impact of the data assimilation. Both of the control simulations have a mean Gulf Stream pathway with a southern bias and a weak AMOC with a southward limb that is too shallow. As a result they do not simulate flow along isobaths that yield observed abyssal currents (or their alternatives) that are relevant to a realistic Gulf Stream pathway. Two data-assimilative hindcast experiments (state estimates performed in arrears) were performed. A realistic mean Gulf Stream pathway is imposed by the mean sea surface height (SSH) that is added to the SSH anomalies from satellite altimeter track data, the key data type used to constrain the evolution of currents and eddies. The SSH updates are projected on to the stratified water column using two different techniques, Cooper-Haines in the first hindcast, synthetic temperature and salinity profiles in the second.

As expected, the data assimilation improves the SSH variability. The mean strength and pathway of the Gulf Stream are strongly constrained by the mean SSH added to the SSH anomalies from altimeter data, but the resulting mean Gulf Stream is too weak. In the ocean interior the data assimilation increases the strength of the AMOC and the depth range of its southward abyssal flow. A particularly salient result is the impact of the data assimilation on the mean abyssal currents, which are very different from the upper ocean currents and not observed in the assimilated data set. Both hindcasts depict the relevant abyssal currents seen in historical in situ observations, including the key abyssal current near 68.5°W and flow along the continental slope feeding into it as well as an observed cyclonic gyre farther to the west. These abyssal currents are well maintained in the mean of 48 14-day forecasts, although some weakening of an already weak Gulf Stream occurs and median forecast skill based on anomaly correlation >0.6 is only 10 days. The abyssal currents are generated via vortex stretching and compression when the assimilated SSH updates from altimeter data plus the mean SSH are projected downward. The data assimilation approximates the observed variations in the ocean features, such as current pathways and eddies, and in response the model dynamics interpolate and extrapolate the updates. The results indicate that in the process a more realistic AMOC generates more realistic abyssal currents along the continental slope and the representation of real variations in the Gulf Stream and related eddies in the upper ocean produces a model response that simulates flow instabilities well enough to generate realistic eddy-driven mean abyssal currents and maintain them in 14-day forecasts.

Acknowledgements The project US Global Ocean Data Assimilation Experiment (GODAE): Global Ocean Prediction with the HYbrid Coordinate Ocean Model (HYCOM), funded under the National Ocean Partnership Program (NOPP); the 6.1 project Global Remote Littoral Forcing via Deep Water Pathways, funded by the Office of Naval Research (ONR) under program element 601153N; and grants of computer time from the US Defense Department High Performance Computing Modernization Program. Alan Wallcraft is in charge of developing and maintaining the standard version of HYCOM and Ole Martin Smedstad the data assimilative experiments. The European high-resolution global ocean model was developed in France by Mercator Océan with the financial support of the European MERSEA integrated project for the development, validation, and exploitation of the system and from the Région Midi Pyrénées, which financed a dedicated computer for this project. The mean Gulf Stream northwall pathway, based on satellite infrared imagery, is an unpublished analysis performed by Peter Cornillon (University of Rhode Island) and Ziv Sirkes (deceased) for the ONR project Data Assimilation and Model Evaluation Experiment–North Atlantic Basin (DAMEE–NAB).

References

Arbic BK, Wallcraft AJ, Metzger EJ (2010) Concurrent simulation of the eddying general circulation and tides in a global ocean model. Ocean Model 32:175–187

Bane JM Jr, Dewar WK (1988) Gulf Stream bimodality and variability downstream of the Charleston bump. J Geophys Res 93(C6):6695–6710

Barnier B, Madec G, Penduff T, Molines JM, Treguier AM, Le Sommer J, Beckmann A, Biastoch A, Böning C, Dengg J, Derval C, Durand E, Gulev S, Remy E, Talandier C, Theeten S, Maltrud M, McClean J, De Cuevas B (2006) Impact of partial steps and momentum advection schemes in a global ocean circulation model at eddy-permitting resolution. Ocean Dyn 56:543–567. doi:10.1007/s10236-006-0082-1

Barron CN, Smedstad LF, Dastugue JM, Smedstad OM (2007) Evaluation of ocean models using observed and simulated drifter trajectories: impact of sea surface height on synthetic profiles for data assimilation. J Geophys Res 112:C07019. doi:10.1029/2006JC002982

Bleck R (2002) An oceanic general circulation model framed in hybrid isopycnic-cartesian coordinates. Ocean Model 37:55–88

Bleck R, Smith L (1990) A wind-driven isopycnic coordinate model of the north and equatorial Atlantic Ocean. 1. Model development and supporting experiments. J Geophys Res 95:3273–3285

Bower AS, Hunt HD (2000) Lagrangian observations of the deep western boundary current in the North Atlantic Ocean. Part II. The Gulf stream—deep western boundary current crossover. J Phys Oceanogr 30:784–804

Bryan FO, Hecht MW, Smith RD (2007) Resolution convergence and sensitivity studies with North Atlantic circulation models. Part I: the western boundary current system. Ocean Model 16:141–159

Chassignet EP, Marshall DP (2008) Gulf Stream separation in numerical ocean models. In: Hecht M, Hasumi H (eds) Ocean modeling in an eddying regime, geophysical monograph 177. American Geophysical Union, Washington

Chassignet EP, Hurlburt HE, Metzger EJ, Smedstad OM, Cummings JA, Halliwell GR, Bleck R, Baraille R, Wallcraft AJ, Lozano C, Tolman HL, Srinivasan A, Hankin S, Cornillon P, Weisberg R, Barth A, He R, Werner F, Wilkin J (2009) US GODAE: global ocean prediction with the HYbrid Coordinate Ocean Model (HYCOM). Oceanography 22:64–75

Cooper M, Haines KA (1996) Altimetric assimilation with water property conservation. J Geophys Res 24:1059–1077

Cummings JA (2005) Operational multivariate ocean data assimilation. Quart J R Meteor Soc 131:3583–3604

Fox DN, Teague WJ, Barron CN, Carnes MR, Lee CM (2002) The modular ocean data analysis system (MODAS). J Atmos Ocean Technol 19:240–252

Gibson JK, Kallberg P, Uppala S, Hernandez A, Nomura A, Serrano E (1999) ERA ECMWF reanalysis project report series 1. ERA-15 description, version 2. European Centre for Medium-Range Weather Forecasts, Reading

Glenn SM, Ebbesmeyer CC (1994a) The structure and propagation of a Gulf Stream frontal eddy along the North Carolina shelf break. J Geophys Res 99(C3):5029–5046

Glenn SM, Ebbesmeyer CC (1994b) Observations of Gulf Stream frontal eddies in the vicinity of Cape Hatteras. J Geophys Res 99(C3):5047–5055

Godfrey JS (1989) A Sverdrup model of the depth-integrated flow for the world ocean allowing for island circulations. Geophys Astrophys Fluid Dyn 45:89–112

Gordon AL, Giulivi CF, Lee CM, Furey HH, Bower A, Talley L (2002) Japan/East Sea thermocline eddies. J Phys Oceanogr 32:1960–1974

Halkin D, Rossby HT (1985) The structure and transport of the Gulf Stream at 73°W. J Phys Oceanogr 15:1439–1452

Haltiner GJ, Martin FL (1957) Dynamical and Physical Meteorology. McGraw-Hill, New York

Hecht MW, Smith RD (2008) Towards a physical understanding of the North Atlantic: a review of model studies in an eddying regime. In: Hecht M, Hasumi H (eds) Ocean modeling in an eddying regime, geophysical monograph 177. American Geophysical Union, Washington

Hecht MW, Petersen MR, Wingate BA, Hunke E, Maltrud ME (2008) Lateral mixing in the eddying regime and a new broad-ranging formulation. In: Hecht M, Hasumi H (eds) Ocean modeling in an eddying regime, geophysical monograph 177. American Geophysical Union, Washington

Hellerman S, Rosenstein M (1983) Normal monthly wind stress over the world ocean with error estimates. J Phys Oceanogr 13:1093–1104

Hogan PJ, Hurlburt HE (2006) Why do intrathermocline eddies form in the Japan/East Sea? A modeling perspective. Oceanography 19:134–143

Hogg NG, Stommel H (1985) On the relation between the deep circulation and the Gulf Stream. Deep-Sea Res 32:1181–1193

Hurlburt HE (1986) Dynamic transfer of simulated altimeter data into subsurface information by a numerical ocean model. J Geophys Res 91(C2):2372–2400

Hurlburt HE, Hogan PJ (2000) Impact of 1/8° to 1/64° resolution on Gulf Stream model-data comparisons in basin-scale subtropical Atlantic Ocean models. Dyn Atmos Ocean 32:283–329

Hurlburt HE, Hogan PJ (2008) The Gulf Stream pathway and the impacts of the eddy-driven abyssal circulation and the Deep Western Boundary Current. Dyn Atmos Ocean 45:71–101

Hurlburt HE, Thompson JD (1980) A numerical study of Loop Current intrusions and eddy shedding. J Phys Oceanogr 10:1611–1651

Hurlburt HE, Thompson JD (1982) The dynamics of the Loop Current and shed eddies in a numerical model of the Gulf of Mexico. In: Nihoul JCJ (ed) Hydrodynamics of semi-enclosed seas. Elsevier, Amsterdam

Hurlburt HE, Wallcraft AJ, Schmitz WJ Jr, Hogan PJ, Metzger EJ (1996) Dynamics of the Kuroshio/Oyashio current system using eddy-resolving models of the North Pacific Ocean. J Geophys Res 101(C1):941–976

Hurlburt HE, Chassignet EP, Cummings JA, Kara AB, Metzger EJ, Shriver JF, Smedstad OM, Wallcraft AJ, Barron CN (2008a) Eddy-resolving global ocean prediction. In: Hecht M, Hasumi H (eds) Ocean modeling in an eddying regime, geophysical monograph 177. American Geophysical Union, Washington

Hurlburt HE, Metzger EJ, Hogan PJ, Tilburg CE, Shriver JF (2008b) Steering of upper ocean currents and fronts by the topographically constrained abyssal circulation. Dyn Atmos Ocean 45:102–134. doi:10.1016/j.dynatmoce.2008.06.003

Hurlburt HE, Brassington GB, Drillet Y, Kamachi M, Benkiran M, Bourdallé-Badie R, Chassignet EP, Jacobs GA, Le Galloudec O, Lellouche JM, Metzger EJ, Oke PR, Pugh TF, Schiller A, Smedstad OM, Tranchant B, Tsujino H, Usui N, Wallcraft AJ (2009) High-resolution global and basin-scale ocean analyses and forecasts. Oceanography 22:110–127

Johns WE, Shay TJ, Bane JM, Watts DR (1995) Gulf Stream structure, transport, and recirculation near 68°W. J Geophys Res 100:817–838

Joyce TM, Wunsch C, Pierce SD (1986) Synoptic Gulf Stream velocity profiles through simultaneous inversion of hydrographic and acoustic Doppler data. J Geophys Res 91:7573–7585

Kallberg P, Simmons A, Uppala S, Fuentes M (2004) ERA-40 project report series: 17. The ERA-40 archive. ECMWF. Reading

Kara AB, Hurlburt HE, Wallcraft AJ (2005) Stability-dependent exchange coefficients for air-sea fluxes. J Atmos Ocean Technol 22:1080–1094

Kara AB, Wallcraft AJ, Martin PJ, Pauley RL (2009) Optimizing surface winds using QuikSCAT measurements in the Mediterranean Sea during 2000–2006. J Mar Sys 78:119–131

Large WG and Pond S (1981) Open ocean momentum flux measurements in moderate to strong winds. J Phys Oceanogr 11(3):324–336

Lee H (1997) A Gulf Stream synthetic geoid for the TOPEX altimeter. MS Thesis Rutgers University, New Brunswick

Lee T, Cornillon P (1996) Propagation of Gulf Stream meanders between 74° and 70°W. J Phys Oceanogr 26:205–224

Legeckis R, Brown CW, Chang PS (2002) Geostationary satellites reveal motions of ocean surface fronts. J Mar Sys 37:3–15

Legeckis RV (1979) Satellite observations of the influence of bottom topography on the seaward deflection of the Gulf Stream off Charleston, South Carolina. J Phys Oceanogr 9:483–497

Madec G (2008) NEMO ocean engine. Report 27 ISSN No 1288–1619. Institute Pierre-Simon Laplace (IPSL), France

Munk WH (1950) On the wind-driven ocean circulation. J Met 7:79–93

Paiva AM, Hargrove JT, Chassignet EP, Bleck R (1999) Turbulent behavior of a fine mesh (1/12°) numerical simulation of the North Atlantic. J Mar Sys 21:307–320

Pickart RS (1994) Interaction of the Gulf Stream and Deep Western Boundary Current where they cross. J Geophys Res 99:25155–25164

Pickart RS, Watts DR (1990) Deep Western Boundary Current variability at Cape Hatteras. J Mar Res 48:765–791

Reid RO (1972) A simple dynamic model of the Loop Current. In: Capurro LRA, Reid JL (eds) Contributions on the Physical Oceanography of the Gulf of Mexico. Gulf Publishing Co, Houston

Rosmond TE, Teixeira J, Peng M, Hogan TF, Pauley R (2002) Navy operational global atmospheric prediction system (NOGAPS): forcing for ocean models. Oceanography 15(1):99–108

Rossby CG (1940) Planetary flow patterns in the atmosphere. Quart J R Meteor Soc 66:68–87

Rossby T, Flagg CN, Donohue K (2005) Interannual variations in upper-ocean transport by the Gulf Stream and adjacent waters between New Jersey and Bermuda. J Mar Res 63:203–226

Schmitz WJ Jr (1996) On the world ocean circulation: Volume I. Some global features/North Atlantic circulation. Technical Report WHOI-96–03 Woods Hole Oceanographic Institution, Woods Hole

Schmitz WJ Jr, McCartney MS (1993) On the North Atlantic circulation. Rev Geophys 31:29–49

Shriver JF, Hurlburt HE, Smedstad OM, Wallcraft AJ, Rhodes RC (2007) 1/32° real-time global ocean prediction and value-added over 1/16° resolution. J Mar Sys 65:3–26

Smedstad OM, Hurlburt HE, Metzger EJ, Rhodes RC, Shriver JF, Wallcraft AJ, Kara AB (2003) An operational eddy resolving 1/16° global ocean nowcast/forecast system. J Mar Sys 40–41:341–361

Smith RD, Maltrud ME, Bryan FO, Hecht MW (2000) Numerical simulation of the North Atlantic Ocean at 1/10°. J Phys Oceanogr 30:1532–1561

Sverdrup HU (1947) Wind-driven currents in a baroclinic ocean—with application to the equatorial currents of the eastern Pacific. Proc Natl Acad Sci U S A 33:318–326

Thompson JD, Schmitz WJ Jr (1989) A regional primitive-equation model of the Gulf Stream: design and initial experiments. J Phys Oceanogr 19:791–814

Townsend TL, Hurlburt HE, Hogan PJ (2000) Modeled Sverdrup flow in the North Atlantic from 11 different wind stress climatologies. Dyn Atmos Ocean 32:373–417

Tsujino H, Usui N, Nakano H (2006) Dynamics of Kuroshio path variations in a high-resolution general circulation model. J Geophys Res. doi:10.1029/2005JC003118

Usui N, Tsujino H, Fujii Y (2006) Short-range prediction experiments of the Kuroshio path variabilities south of Japan. Ocean Dyn 56:607–623

Usui N, Tsujino H, Fujii Y, Kamachi M (2008a) Generation of a trigger meander for the 2004 Kuroshio large meander. J Geophys Res. doi:10.1029/2007JC004266

Usui N, Tsujino H, Nakano H, Fujii Y (2008b) Formation process of the Kuroshio large meander in 2004. J Geophys Res. doi:10.1029/2007JC004675

Watts DR, Tracey KL, Bane JM, Shay TJ (1995) Gulf Stream path and thermocline structure near 74°W and 68°W. J Geophys Res 100:18291–18312

Xie L, Liu X, Pietrafesa LJ (2007) Effect of bathymetric curvature on Gulf Stream instability in the vicinity of the Charleston Bump. J Phys Oceanogr 37(3):452–475